

Studies on Endothermic Fuels for Aerospace Application: Preparation, Characterization, and Kinetic Analysis

THESIS

Submitted in partial fulfillment
of the requirements for the degree of
DOCTOR OF PHILOSOPHY

by

VUCHURU KALYAN

ID. No. 2018PHXF0041H

Under the Supervision of
Prof. Srikanta Dinda



BITS Pilani

Pilani | Dubai | Goa | Hyderabad

BIRLA INSTITUTE OF TECHNOLOGY AND SCIENCE, PILANI

2024



Birla Institute of Technology & Science, Pilani
Hyderabad Campus

CERTIFICATE

This is to certify that the thesis entitled "**Studies on Endothermic Fuels for Aerospace Application: Preparation, Characterization, and Kinetic Analysis**" and submitted by **VUCHURU KALYAN** (ID. No. **2018PHXF0041H**) for award of Ph.D. of the institute embodies original work done by him under my supervision.

Signature of the supervisor : 


Name in capital letters : **SRIKANTA DINDA**

Designation : Professor

Date : **20-04-2024**

Declaration

The research work embodied in this thesis entitled "**Studies on Endothermic Fuels for Aerospace Application: Preparation, Characterization, and Kinetic Analysis**" has been carried out by me under the supervision Prof. Srikanta Dinda, Department of Chemical Engineering, BITS-Pilani Hyderabad Campus, India. This work is original and has not been submitted in part or full for any degree to this or any other university.

Signature: 

Name: VUCHURU KALYAN

Date: 20-04-2024

Acknowledgments

This research work was carried out between August 2018 and December 2023 in the Chemical Engineering Department of Birla Institute of Technology and Science – Pilani, Hyderabad Campus. I am grateful to Birla Institute of Technology and Science – Pilani, India, for giving me the opportunity and also providing the necessary facilities and support to carry out the research work.

I take this opportunity to express my respect and sincere gratitude toward my research supervisor – **Prof. Srikanta Dinda**, for giving me an opportunity to work with him on the wonderful research area of *endothermic fuel development*. I am indebted to **Prof. Dinda** for his valuable guidance and for instilling in me a relentless quest for perfection. He gave me the freedom to work independently and encouraged me to develop my skills in experimentation, reporting, and communicating my findings regularly and in a time-bound manner.

I express my heartfelt gratitude toward **Prof. Inkollu Sreedhar** (Head of the Department), for providing the necessary laboratory and departmental facilities. At this juncture, I must gratefully acknowledge the help and support willingly provided by Doctoral Advisory Committee members – **Prof. D. Purnima** (Department of Chemical Engineering), and **Dr. Satyapaul A. Singh** (Department of Chemical Engineering) for their insightful comments, suggestions, and encouragement during my research work. Also, thankful to **Prof. Vikranth Kumar Surasani** (In-charge, Central computing laboratory) for providing the necessary support. My sincere thanks to all the faculty members of the Department of Chemical Engineering for extending their support during different phases of my research work.

I would like to extend my sincere thanks to all my departmental colleagues for sharing their experiences helping me understand some common problems and relieving stress. I would like to extend my thanks to **Dr. Sundaraiah Konda** (former Ph.D. student) and **Mr. N. Madhavaiah** (Ph.D. student) for their active support in participating in experimental work. I am thankful to **Mr. M. Khan, Mr. Appala Reddy P., Mr. Somi Reddy P. and Mr. Bhaskara Raju N.**, and, laboratory staff members, for their willing assistance in my experimental work. I take the opportunity to thank each and every individual who has helped me directly or indirectly in the completion of my work. I would also like to acknowledge my senior Ph.D. colleagues **Dr. Appala Naidu U., Dr. Premanath, Dr. Varun Y., Dr. Anirudha R., Dr. Pradeep P., and Mr. Suresh K.**, for helping me in formatting my Ph.D. thesis.

Finally, I express my deepest gratitude towards my parents Late **Smt. Bramarambha Vuchuru** and **Mr. Uday Kumar Vuchuru**. I am thankful to my wife **Mrs. Sakshi Kalyan Vuchuru** for bearing the long waiting during my Ph.D. work. I thank everyone for their immense moral support, sacrifice, patience, and unfettered encouragement through all stages of my work. Thanks to all my Family Members, and Friends, for their encouragement and emotional support.

*Birla Institute of Technology and Science – Pilani,
Hyderabad Campus, Hyderabad, India*

Vuchuru Kalyan
2024

Studies on Endothermic Fuels for Aerospace Application: Preparation, Characterization, and Kinetic Analysis

A supersonic/hypersonic engine above Mach-5 speeds requires active cooling to dissipate the heat load generated during propellant combustion. The thermal management of a supersonic engine under supercritical conditions is a critical task. Typically, the combustor wall temperature in a supersonic missile can exceed 800 °C without onboard active cooling. For any hypersonic vehicle, liquid hydrocarbon fuel is preferred as a propellant due to its ease of storage, low vapor pressure compared to H₂ and CH₄, operability, and handling. In the current study, the feasibility of hydrocarbon fuel as an onboard regenerative coolant was examined. An experimental setup was designed and fabricated to perform the thermal cracking experiments under elevated temperature and pressure conditions. A tubular flow reactor was heated externally by a direct power source to measure the heat sink capability of hydrocarbon fuels. The research investigated the thermal cracking characteristics of various hydrocarbon fuels under supercritical conditions, and the research outcomes are presented in graphical or tabular forms in this thesis.

In the work, three single-component hydrocarbons, namely n-heptane, methylcyclohexane (MCH), and toluene, were considered for thermal cracking studies to establish a standard operating procedure and to understand the effect of hydrocarbon structure on cracking characteristics. All three compounds comprise seven carbon atoms (C₇ hydrocarbon) but with different bond connectivity. n-Heptane is a straight-chain alkane, MCH is a cycloalkane, and toluene is an aromatic compound. The cracking experiments were carried out for a temperature range of 500-700 °C and under 55 bar pressure to examine the fuel conversion, coke deposition, and heat sink capability of the hydrocarbons. At a temperature of 700 °C, the cracking conversion of n-heptane, MCH, and toluene are 31%, 20%, and 2.5%, respectively, and the coke deposition rates of the three fuels are 19.1, 12.9, and 4.5 mg/min, respectively. The chemical heat sink of n-heptane is 987 kJ/kg, about 18% higher than the cycloalkane, i.e., MCH. The experimental data showed good agreement for the first-order rate kinetic model. The first-order rate constant lies in the range of 0.01 to 0.6 (1/s), and the apparent activation energy for the cracking reaction of MCH and n-heptane is 93 kJ/mol and 62 kJ/mol, respectively.

Abstract

The cracking characteristic of a multi-component hydrocarbon fuel (HCF-1) having a boiling range and specific gravity of 131-238 °C and 0.79, respectively, was examined for a temperature, pressure, and space-time range of 550-680 °C, 25-55 bar, and 2.8 to 8.5 s, respectively. The impact of reactor temperature, pressure, and space-time on fuel conversion, coke deposition, heat sinks, and product distributions was thoroughly investigated. At a temperature of 680 °C and under 55 bar pressure, the HCF-1 exhibited a fuel conversion of 10.5 wt.%, a coke deposition rate of 7 mg/min, and a chemical heat sink capacity of 805 kJ/kg. The fuel conversion, coke deposition, and heat sink capacity increased by about 2.9 times, 2 times, and 9% as the reactor pressure increased from 25 to 55 bar. The olefin-to-alkane mole ratio in the gaseous products decreased with the increase in temperature and pressure. At 650 °C and 55 bar, the fuel conversion and chemical heat sink capacity of the fuel increased by 2.4-time (from 7.6% to 18.3%) and 1.8-time (from 634 kJ/kg to 1144 kJ/kg), respectively, as the space-time value increased from 2.8 s to 8.5 s. The kinetic analysis showed that the cracking follows a first-order kinetics with a rate constant range of 0.01 to 0.15 (1/s), and the apparent activation energy is about 125 kJ/mol. The thesis also includes a brief investigation of coke morphology. A SEM analysis confirmed the formation of both amorphous and filamentous coke during the supercritical cracking of the fuel.

The suitability of homogeneous initiators on thermal cracking characteristics was examined with a multi-component fuel (HCF-2) having a boiling range and specific gravity of 149-224 °C and 0.795 respectively. A comprehensive investigation was conducted to assess the effectiveness of two initiators, namely triethylamine (TEA) and di-tert-butyl-peroxide (DTBP). The experiments were conducted at 650 °C, under 55 bar, and a 50 mL/min feed flow rate. For 1 wt.% of initiator loading, the fuel conversion increased by 8.6% and 6.1% with TEA and DTBP, respectively. In the presence of initiators, the chemical heat sink and coke deposition increased by about 80-100 kJ/kg and 2.5 mg/min, respectively. The analysis of liquid products revealed that alkyl benzenes (C₁ to C₅ alkyl benzene) can act as coke precursors in enhancing the coke deposits.

Abstract

Furthermore, a Coke predictive model was developed to estimate the coke deposition rate for thermal cracking reactions. Numerical investigations were performed considering a narrow cut of kerosene range fuels such as n-dodecane, RP-3, and HF-1 to find the concentration of coking precursors like light olefins and aromatics. A predictive coke model was developed based on the precursor concentration, fuel property, and operating parameters. FLUENT 21 software with the finite volume method was used in numerical simulation. The SIMPLEC algorithm coupled with pressure and velocity parameters into the FLUENT. Product distribution and transport properties were estimated using the shear stress transport k- ω turbulence model. The developed Coke model was validated experimentally by conducting experiments with h-heptane. The model predicted coke value showed a good agreement (< 25% deviation) with the experimental results. From the comprehensive investigation, it can be said that thermal management of hypersonic vehicles can be achieved by employing hydrocarbon fuels with about 15-30% cracking conversion. A multi-component fuel may be more desirable than a single-component fuel because of distributed cracking over a long range of fuel transfer lines. The distributed cracking is mainly due to different lengths of hydrocarbons and each of them having different cracking temperature. The investigation revealed that cyclic hydrocarbons are more stable than straight-chain hydrocarbons. Kerosene range hydrocarbons can provide a sufficient cooling effect in regenerative cooling. Though an initiator helps in enhancing the heat sink capability, coke formation can be a critical issue in selecting an appropriate fuel. A suitable coke additive may be useful to decelerate the coke formation rate during the pyrolysis process. Therefore, the present research may be helpful in understanding the cracking phenomena under a supercritical environment and in identifying an appropriate fuel for hypersonic applications.

Keywords: *Hydrocarbon fuel, Thermal cracking, Supercritical conditions, Chemical heat sink, Coke formation, Initiator. Coke model.*

CONTENTS	Page No.
List of Tables	i-ii
List of Figures	iii-v
List of Abbreviations	vi-vii
INTRODUCTION	1-10
1.1. Introduction to Air-Breathing Engines	1
1.2. Thermal Management of Air-Breathing Engines	2
1.3. Endothermic Fuel	3
1.4. Gaps Noted in Existing Research	7
1.5. Objective of Present Research	7
1.6. Summary of Thesis	8
LITERATURE ON ENDOTHERMIC FUEL DEVELOPMENT	11-30
2.1 Introduction to Literature Review on Endothermic fuel	11
2.2 Physico-Chemical Characteristics of Hydrocarbon Fuels	12
2.3 Thermal Cracking Characteristics of Hydrocarbon Fuels	14
2.4 Influence of Catalyst on Supercritical Cracking of Hydrocarbon Fuels	16
2.5 Coke Deposition During Thermal Cracking of Hydrocarbon Fuels	19
2.6 Suitability of Initiators to Enhance Endothermicity	21
2.7 Influences of Pressure on Cracking Characteristics	24
2.8 Numerical Simulations on Supercritical Hydrocarbon Cracking	25
2.9 Summary of Review	28
2.10 Gaps/Limitation noted on Endothermic Fuel Development	29
MATERIALS, EXPERIMENTAL, AND CHARECTERIZATION	31-42
DETAILS	
3.1 Materials	31
3.2 Experimental Setup and Procedure Details	33
3.3 Numerical Simulation on Thermal Cracking of Hydrocarbons	35
3.4 Characterization Techniques Used in Present Research	37

3.4.1.	GC and GC-MS analysis	37
3.4.2.	Micro GC analysis	38
3.4.3.	Scanning electron microscope (SEM) analysis	38
3.4.4.	ASTM D86 distillation characteristics	38
3.4.5.	Moisture content analysis	39
3.4.6.	Aniline point analysis	39
3.4.7.	Calorific value analysis	40
3.4.8.	Coke analysis	40
3.4.9.	Mass balance analysis	41
3.4.10	Repeatability and Uncertainty	42
INVESTIGATION OF CRACKING CHARACTERISTICS OF SINGLE- COMPONENT HYDROCARBONS UNDER SUPERCRITICAL CONDITIONS		43-64
4.1	Introduction	43
4.2.	Materials, Experimental Procedure, and Characterization Techniques	44
4.3.	Results and Discussion	45
4.3.1.	Physico-chemical properties of n-heptane, MCH, and toluene	45
4.3.2.	Effect of temperature on cracking percentage of n-heptane, MCH, and toluene	46
4.3.3.	Effect of temperature on coke deposition of n-heptane, MCH, and toluene	49
4.3.4.	Effect of temperature on gas composition	50
4.3.5.	Effect of temperature on liquid product composition	53
4.3.6.	Probable mechanism of n-heptane and MCH cracking	56
4.3.7.	Effect of temperature on heat sink characteristics of n-heptane, MCH, and toluene	57
4.3.8.	Analysis of kinetic parameters	61
4.4.	Conclusion	64

THERMAL CRACKING AND HEAT SINK CHARACTERISTICS OF MULTI-COMPONENT HYDROCARBON FUELS UNDER SUPERCRITICAL CONDITIONS **65-90**

5.1	Introduction	65
5.2.	Materials and Experimental Details	66
5.2.1.	Materials	66
5.2.2.	Experimental setup and procedure	66
5.2.3.	Characterization of feed and product properties	67
5.3.	Results and Discussion	68
5.3.1.	Influence of temperature on cracking characteristics of HCF-1	69
5.3.1.1.	Effect of temperature on fuel cracking and coke deposition	69
5.3.1.2.	Effect of temperature on cracked-gas composition	72
5.3.1.3.	Effect of temperature on heat sink capacity of HCF-1 fuel	76
5.3.3.	Pressure effect on cracking characteristics of HCF-1 Fuel	81
5.3.3.1.	Effect of pressure on cracking percentage, coke deposition, and heat sink	81
5.3.3.2.	Effect of pressure on product gas composition	83
5.3.3.	Effect of space-time on cracking percentage, coke deposition, and heat sink.	84
5.3.4.	Analysis of coke morphology	86
5.3.5.	Estimation of kinetic rate constant and activation energy	88
5.4.	Conclusion	89

EFFICAY OF INITIATORS ON THE CRACKING CHARACTERISTICS OF HYDROCARBON FUEL UNDER SUPERCRITICAL CONDITIONS **91-104**

6.1	Introduction	91
6.2	Materials and Methods	92
6.2.1.	Materials	92
6.2.2.	Experimental setup and procedure	92
6.3.	Results and Discussion	92

6.3.1.	Characterization of HCF-2 fuel	92
6.3.2.	Influence of initiators on supercritical characteristics of HCF-2	94
6.3.2.1.	Effect of initiator on fuel cracking percentage and coke deposition	95
6.3.2.2.	Effect of initiator on gas composition and heat sink	101
6.3.2.3.	Effect of initiator loading on fuel cracking percentage, coke deposition, and heat sink.	103
6.4	Conclusion	104
 DEVELOPMENT OF COKE MODEL OF HYDROCARBON FUELS UNDER SUPERCRITICAL CONDITIONS		105-138
7.1	Introduction	105
7.2	Methodology Adopted for Numerical Simulations and its Validation.	107
7.2.1.	Computational setup used for numerical simulation	107
7.2.2.	Governing equations	108
7.2.3.	Simulation setup	110
7.2.4.	Experimental details for validation of simulation results	114
7.3	Results and Discussion	114
7.3.1.	Numerical analysis	114
7.3.2.	Analysis of experimental results for n-heptane cracking	127
7.3.2.1.	Effect of temperature on cracking percentage, coke, and product distribution	127
7.3.2.2.	Heat sink capacities of n-heptane	129
7.3.3.	Development of predictive coke model and its validation	129
7.3.3.1.	Validation of coke model	135
7.4.	Conclusion	138
 SUMMARY AND CONCLUSIONS OF PRESENT RESEARCH		139-144
8.1.	Summary and Conclusions	139
 SCOPE OF FUTURE STUDIES		145

BIBLIOGRAPHY

146-157

List of Publications Based on Present Research

Biography of Student and Supervisors

LIST OF TABLES		Page No.
Table 1.1	Properties of various Jet fuels	6
Table 2.1	Distillation characteristics of JP-7, JP-8, RP-3, JP-900, and Jet fuels	13
Table 2.2	Properties of JP-7, JP-8, RP-1, RP-3, and JP-900 fuels	13
Table 2.3	Total and endothermic heat sink values of various fuels	16
Table 2.4	Heat sink capacity of hydrocarbon fuels with various catalysts	18
Table 2.5	Influence of initiators on fuel conversion and heat sink capacities	23
Table 2.6	Summary of numerical simulations of hydrocarbon fuel cracking studies	27
Table 3.1	Properties of hydrocarbon fuels	31
Table 3.2:	Temperature and pressure program used for Micro-GC	38
Table 4.1	Properties of n-heptane, MCH, and toluene	46
Table 4.2	$T_{0.5\%}$, $T_{95\%}$, and T_{avg} , values of feed and products	47
Table 4.3	Heat loss values at different temperatures under 55 bar pressure	58
Table 4.4	Heat sink and cracking percentage values of n-heptane and MCH	60
Table 4.5	Residence time values at different temperatures under 55 bar pressure	62
Table 5.1	Physico-chemical properties of HCF-1 fuel	68
Table 5.2	Properties of surrogate components obtained from NIST database	70
Table 5.3	ASTM D86 distillation results of HCF-1 feed and liquid products	78
Table 5.4	Heat loss quantity at different temperatures under 55 bar pressure	79
Table 5.5	Endothermic heat sink capacity of various fuels	80
Table 5.6:	Effect of space-time on cracking percentage, gas composition, coke deposition, and heat sink capacity of HCF-1 at 650 °C and 55 bar	86
Table 5.7:	Values of first-order rate constant (k_1) at different temperatures	88
Table 6.1	Physico-chemical properties of HCF-2 fuel	93
Table 6.2	Effect of initiator on cracking percentage, coke deposition, and heat sinks	103
Table 7.1	Fuels and operating parameters used in numerical simulation	111
Table 7.2	Physico-chemical properties of various fuels	112
Table 7.3	Kinetic parameters used in simulation studies	113

List of Tables

Table 7.4	Variation in composition of various species along the reactor length for nine different cases.	120
Table 7.5	Fuels and parameters used in developing coke model	134
Table 7.6	Validation of coke model with experimental results	137
Table 8.1	Properties of various hydrocarbon fuels	142
Table 8.2	Cracking percentage, heat sink, and coke deposition for various fuels	143
Table 8.3	Effect of pressure on conversion, coke deposition, and heat sinks	143
Table 8.4:	Effect of initiator loading on cracking percentage, coke depositions, and heat sinks	143

LIST OF FIGURES		Page No.
Fig. 1.1	Schematic of ramjet engine	2
Fig. 1.2	Schematic of scramjet engine	2
Fig. 1.3	Heat sink requirement vs. Mach number	3
Fig. 1.4	Enthalpy vs. temperature data of JP-7 fuel	4
Fig. 1.5	A flow diagram of overall thesis work	10
Fig. 2.1	Coke deposition rate of various hydrocarbon fuels	20
Fig. 3.1	Flow diagram of hydrocarbons considered for experimental studies	32
Fig. 3.2	A schematic (top) of test setup and a zoomed view of reactor section (bottom)	34
Fig. 3.3	Photograph of experimental setup	34
Fig. 3.4	A Schematic of thermal cracking of hydrocarbon in a flow reactor	36
Fig. 3.5	A schematic of thermal cracking of hydrocarbon in a flow reactor	37
Fig. 3.6	Scheme of computational domain considered in numerical	38
Fig. 4.1	ASTM D86 results of the feed and liquid products obtained at different temperatures for a) n-Heptane, b) MCH, and c) Toluene	48
Fig. 4.2	Effect of temperature on cracking percentage of n-heptane, MCH, and toluene.	48
Fig. 4.3	Effect of temperature on coke deposition of n-heptane, MCH, and toluene	50
Fig. 4.4	Variation of a) H ₂ , b) C ₁ , c) C ₂ , d) C ₃ , e) C ₄ , f) C ₂ ⁻ , g) C ₃ ⁻ , h) C ₄ ⁻ compositions, i) olefin-to-alkane ratio, and j) H ₂ -to-C ₁ ratio in the product gas at different temperatures	52-53
Fig. 4.5	Retention time of selected hydrocarbons	54
Fig. 4.6	Chromatograms of a) n-heptane, b) MCH, and c) toluene-derived samples	55
Fig. 4.7	Effect of temperature on a) heat input, and b) total heat sink values of n-heptane, MCH, and toluene	59
Fig. 4.8	Variation in k ₁ or k ₂ with reactor temperature	62
Fig. 4.9	Variation in k ₁ with temperatures for different values of volume expansion parameter for a) n-heptane, and b) MCH	63

List of Figures

Fig. 4.10	Arrhenius plots for a) n-heptane, and b) MCH	64
Fig. 5.1	ASTM D86 distillation characteristic curve of HCF-1 fuel	67
Fig. 5.2	GCMS chromatogram of HCF-1 feed	68
Fig. 5.3	Effect of temperature on a) cracking percentage, and b) coke deposition rate	70
Fig. 5.4	Effect of temperature on the gas composition and olefin-to-alkane ratio	74
Fig. 5.5	Variation of energy loss and power input with temperature for toluene feed	78
Fig. 5.6	Effect of temperature on heat sink capacities of HCF-1 fuel	80
Fig. 5.7	Composition in feed and liquid product obtained at 650 °C and 55 bar	81
Fig. 5.8	Effect of pressure on a) cracking percentage, b) coke deposition rate at 650 °C	82
Fig. 5.9	Effect of pressure on energy input and heat sink capacities of HCF-1 at 650 °C.	83
Fig. 5.10	Effect of pressure on a) gaseous product distribution, b) olefin-to-alkane ratio	84
Fig. 5.11	SEM images of coke sample obtained at 650 °C for a) 200 μm, b) 10 μm, c) 1 μm, and d) 0.5 μm magnification	87
Fig. 5.12	a) Variation of first-order rate constant with temperature, b) Arrhenius plots	89
Fig. 6.1	a) GC-MS chromatogram, b) Carbon number-wise composition, (c) P, N, and A composition among C ₁₀ to C ₁₃ hydrocarbons of feed HCF-2 fuel	94
Fig. 6.2	Effect of TEA and DTBP on a) fuel cracking %, b) coke deposition rate	96
Fig. 6.3	GC-MS chromatogram of HCF-2 derived product a) without initiator, b) with TEA, and c) with DTBP	98-99
Fig. 6.4	Variation in a) alkyl-benzene concentration, b) olefinic-bond containing aromatics concentration, c) alkane-to-aromatic ratio, and d) alkane-to-cycloalkane ratio, in feed and liquid products	101
Fig. 6.5	Influence of initiators on a) gas composition, b) heat sink capacities	103
Fig. 7.1	A representation of thermal cracking of hydrocarbon in a flow reactor	108

List of Figures

Fig. 7.2	Scheme of computational domain considered in numerical analysis	108
Fig. 7.3	Schematic of experimental setup used in present work	114
Fig. 7.4	Variation in a) wall and fluid temperature, b) specific heat capacity, c) thermal conductivity, d) fluid viscosity, and e) fluid density, along reactor length for n-dodecane at 650 °C and 40 bar	116
Fig. 7.5	Variation of various components along reactor length obtained from numerical simulation a) H ₂ and lighter paraffins, b) lighter olefins, c) cyclo-compounds, d) n-dodecane	118
Fig. 7.6	Temperature profiles for all ten different cases	119
Fig. 7.7	Concentration profile of a) ethylene, b) propylene, c) toluene d) n-propyl benzene for different cases for different hydrocarbons	126
Fig. 7.8	Effect of temperature on a) ASTM D86 distillation characteristics of cracked products, b) n-heptane cracking percentage	127
Fig. 7.9	Effect of temperature on a) coke deposition rate, b) components distribution in gaseous products, c) olefin-to-paraffin ratio, d) components distribution in liquid products	129
Fig. 7.10	Effect of temperature on a) energy loss, b) heat sink capacity of n-heptane	130
Fig. 7.11	Variation in a) reactor temperature, b) H ₂ and lighter paraffins, c) lighter olefins, d) major components in liquid fractions, along reactor length.	131
Fig. 7.12	a) Pareto plot of experimental and model predicted coking rates, b) comparison of present predictive model and Arrhenius equation-based coke model	136

Abbreviations

avg.	Average
FBP	Final Boiling Point
FID	Flame Ionization Detector
GC-MS	Gas Chromatography-Mass Spectroscopy
HCF	Hydrocarbon fuel
IBP	Initial Boiling Point
MCH	Methylcyclohexane
MJ	Mega Joule
NDIR	Non-dispersive infrared
PAH	Polycyclic Aromatic Hydrocarbons
PONA	Paraffinic Olefinic Naphthenic Aromatic
SEM	Scanning Electron Microscopy
SG	Specific gravity
TCD	Thermal Conductivity Detector
TEA	Triethylamine
vol.	Volume
C_0	Initial concentration
c_p	Specific heat capacity
E_a	Activation energy
H	Enthalpy
h	Specific enthalpy
I	Current
k	Rate constant
k_1	First-order rate constant
k_2	Second-order rate constant
m	Mass flow rate
M_w	Molecular weight
P	Reactor pressure
P_c	Critical pressure of fuel

Abbreviations

Q	Energy per unit time
q	Energy per unit mass
T	Temperature
t	Residence time
T_c	Critical temperature of fuel
u	Velocity of fuel
V	Voltage
v	Volumetric flow rate
V_R	Reactor volume
x	Fractional conversion
z	Compressibility factor
ε	Volume expansion factor

Chapter-1

Introduction

Introduction

1.1. Introduction to Air-breathing Engines

Over the last three decades, scientists and researchers from around the world have shown interest in developing air-breathing hypersonic technology, especially in the field of spacecraft applications. Hypersonic vehicles have attracted significant attention due to achievable speeds higher than Mach-5. Air-breathing engines function by the intake of atmospheric oxygen, which acts as an oxidizer during fuel combustion. These engines can provide several advantages over the conventional rocket systems. The advantage can be attributed to increased fuel consumption efficiency, thereby facilitating extended operational ranges. A scramjet engine is an air-breathing engine with potential uses in hypersonic cruise missiles, high-speed rockets, and air-breathing boosters.

Two types of engines, namely ramjet and scramjet engines, mainly work on the principle of sonic combustion. The working mechanisms of fuel combustion of Ramjet and Scramjet engines are slightly different. A ramjet engine utilizes the ramming effect to compress and slacken the speed of air molecules. Fig. 1.1 illustrates the primary components of a typical ramjet engine, which include an air inlet section, diffuser, fuel injectors, combustor, flame holder, and exhaust nozzle. The compression of air begins at the inlet and is then directed toward the combustor via a diffuser at a lower velocity. This leads to the generation of ram-induced pressure and heat for combustion. The nozzle directs the hot combustion gas through the exhaust cone for developing thrust.

For supersonic combustion, fuel is ignited at supersonic ($> \text{Mach-1}$) speeds. A scramjet engine, as depicted in Fig. 1.2, is an air-breathing engine designed for hypersonic ($> \text{Mach-5}$) speeds. In a conventional ramjet engine, the incoming airflow undergoes deceleration to achieve subsonic velocities before entering the ignition zone. Whereas for a scramjet engine, the burning of fuel and air occurs at supersonic velocities. Scramjets rely on the kinetic energy of the hypersonic jet stream to compress the incoming air and act as an oxidizer for the combustion of fuel to generate thrust. Though the concept seems simple, the practical implementation of scramjet engines requires significant tests due to the technological challenges. A hypersonic vehicle encounters significant drag force during its travel through the earth atmosphere. Additionally, the temperature of the engine assembly can exceed $600\text{ }^{\circ}\text{C}$. In order to sustain

combustion within the supersonic flow regime, fuel injection, mixing with air, and ignition processes should occur within a second.

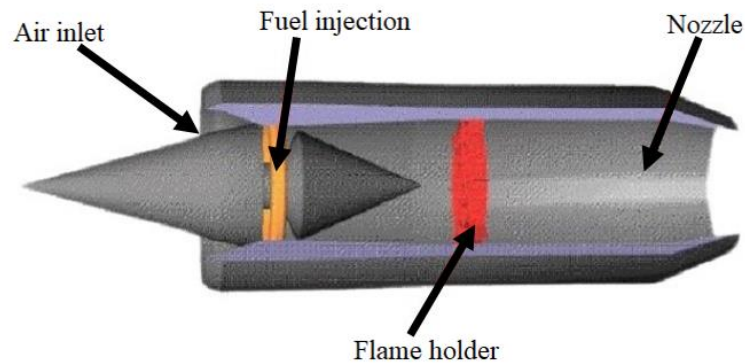


Fig. 1.1: Schematic of ramjet engine (www.grc.nasa.gov).

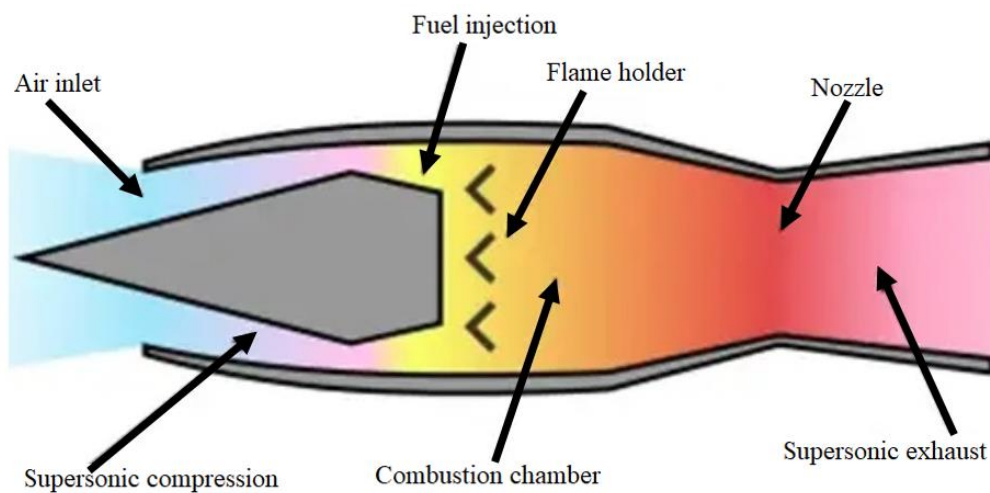


Fig. 1.2: Schematic of scramjet engine (www.isro.gov.in).

1.2. Thermal Management of Air-breathing Engines

The development of high-speed engines involves expertise in the area of thermal management. The increase in local temperature can pose thermal degradation of engine structure during flight. The advancements in materials may provide passive cooling techniques, but the inclusion of a separate cooling system on aircraft introduces excess weight. In order to restrict additional weight for passive cooling techniques, a regenerative cooling technique is preferred. Cryogenic fuels, such as liquid methane and hydrogen, have the ability to act as coolants in regenerative cooling. However, due to their low densities, they require huge storage facilities

within the vehicle. The additional facility constraints in terms of economics, logistics, operations, and safety. The concept of regenerative cooling involves the implementation of an onboard fuel as a coolant. The cooling or heat sink requirements depend on the flight speed, as depicted in Fig. 1.3. The heat sink capacity of a fuel is defined as ‘the amount of energy absorbed by the fuel’ at a particular operating condition. It is generally expressed as kilojoules of energy per kilogram of feed fuel. A vehicle with Mach-5 speed requires fuel with a heat sink capacity of about 1900 kJ/kg of fuel (Lander et al. (2012)). Hence, thermal management in a high-speed engine poses a significant challenge. For example, the X-51 wave-rider and other similar demonstrative flights are designed to operate with a fuel-to-air ratio of about 0.06, which significantly increases heat loads. Thus, the development of scramjet engines involves significant challenges with regard to thermal management.

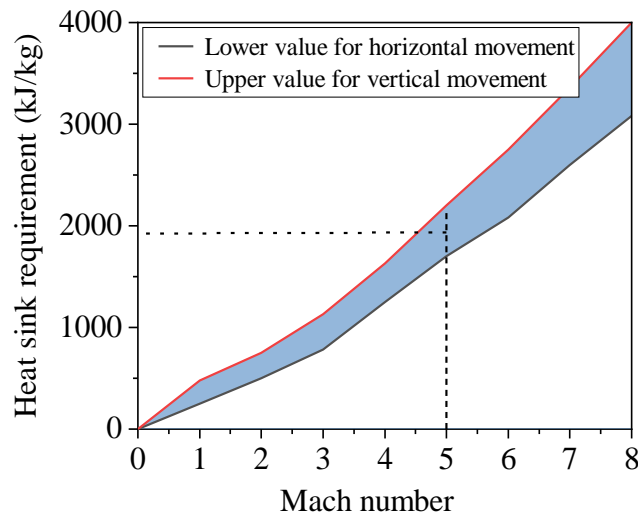


Fig. 1.3: Heat sink requirement vs. Mach number (Lander et al. (2012)).

1.3. Endothermic Fuel

The suitability of the scramjet engine for generating propulsion in hypersonic air-breathing vehicles has been discussed by Buncker et al. (2018) and Edwards (2006). The heat generated in a scramjet engine requires effective cooling. The aptness of onboard hydrocarbon fuels for cooling the engine structure has been reported by many researchers (Li et al. (2018), Jin et al. (2017), Gascoin et al. (2010)). It has been reported that the sensible heat sink capacity of the majority of hydrocarbon fuels lies in the range of 1400-1700 kJ/kg for a temperature range of 500-600 °C (Edward 2003). Hence, the sensible heat sink alone is inadequate to satisfy the

cooling requirement of hypersonic vehicles, according to the data furnished in Fig 1.3. However, the heat sink capacity of a fuel can be enhanced by allowing it to undergo endothermic cracking reactions. When an onboard fuel circulates through cooling channels around the combustion chamber, it can undergo decomposition reactions and enhance the heat sink capacity of the fuel. The additional amount of heat absorbed by the fuel for its cracking is often called a ‘chemical heat sink’. The overall heat sink is the summation of sensible heat sink and chemical heat sink. During the cracking process, hydrocarbon fuel undergoes decomposition reactions at elevated temperatures. Based on the experimental investigation, it is reported that the cracked products are also beneficial in enhancing the efficiency of combustion (Feng et al. (2018), Ma et al. (2016)). Edwards et al. (2012) estimated the heat sink capability of JP-7 fuel at different temperatures under 62 bar reactor pressure, as illustrated in Fig. 1.4.

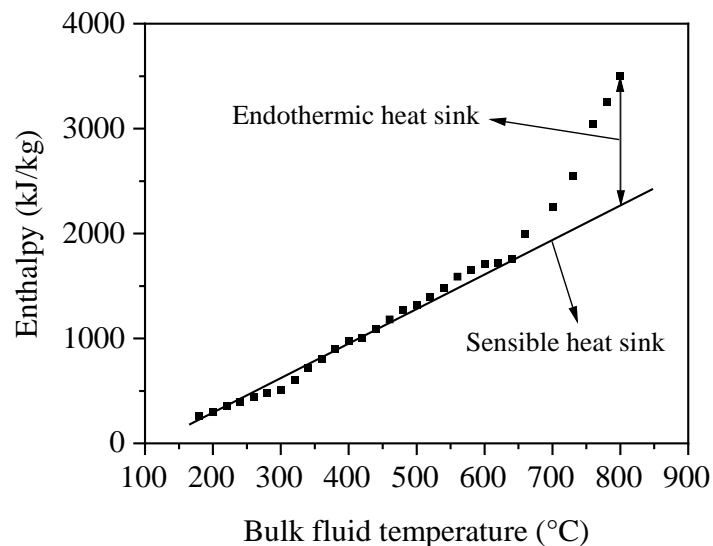


Fig. 1.4: Enthalpy vs. temperature data of JP-7 fuel (Edwards et al. (2012)).

To satisfy cooling requirements by an endothermic fuel, the fuel should comprise a carbon number range between C_9 to C_{14} hydrocarbons and should be capable of undergoing cracking reactions with less tendency towards coke formation during the cracking process (Edwards (2003)). Also, the fuel should possess a higher calorific value and lower viscosity for better fluid flow and combustion efficiency. Various fuels, such as JP-7, JP-8, RP-1, and RP-3, are widely used in supersonic vehicles because of their better combustion, lower coke deposition rates, and high energy density. The suitability of other fuels, such as n-dodecane, JP-4, JP-10, RJ-4, and RJ-5, has been studied by researchers for their potential application in hypersonic

systems (Burdette et al. (2012). Table 1.1 presents a summary of the various properties of different hydrocarbon fuels. The rate of thermal cracking reactions can be improved by adding additives or initiators to the fuel Wickham et al. (2001). At lower temperatures, the initiators are helpful in facilitating the initiation of the cracking reaction. The heat sink capability of a fuel depends on operating temperature, pressure, fuel residence time, fuel composition, and extent of cracking. A comprehensive survey of the impact of these variables on heat sinks has been addressed in Chapter-2 of this thesis.

Table 1.1: Properties of various jet fuels

Fuel name	JP-5 ^a	JP-7 ^{b,c}	JP-8 ^d	JP-9 ^{a,e}	JP-10 ^{a,e}	RJ-4 ^e	RP-1 ^d
Chemical formula	C ₁₀ H ₁₉	C ₁₂ H ₂₅	C ₁₁ H ₂₁	C _{10.6} H _{16.2}	C ₁₀ H ₁₆	C ₁₂ H ₂₀	C ₁₂ H ₂₃
Molecular weight	139	169	153	143	136	164	167
Specific gravity	0.83	0.79	0.81	0.94	0.94	0.94	0.81
Kinematic viscosity (cSt)	17	-	-	24	19	60	-
Freezing point (°C)	< -48	< -44	< -51	< -54	< -79	< -40	< -48
Flashpoint (°C)	65	60	53	-	54	65	57
Heating value (MJ/kg)	41.9	43.9	43.1	42.1	42.1	41.5	43.3
Boiling range (°C)	196-213	206-239	183-248	190	187.2	-	196-241
Average boiling temperature (°C)	205	222	220	-	-	-	212
Paraffin (%), ± 0.5	53	45	41	-	-	-	32
Cycloparaffin (%), ± 0.5	31	50	42	100	99	99	29
Aromatic (%), ± 0.5	17	4	17	-	-	-	5

^aBurdette et al. (2012), ^bEdwards (2003), ^cLovestead et al. (2009), ^dBruno et al. (2006), ^eSmith et al. (1981)

1.4. Gaps Noted in Existing Research

- Although a reasonable number of investigations have been reported by researchers on the thermal cracking behavior of various fuels under supercritical temperature and pressure conditions, the primary emphasis was on fuel conversion and heat sink capacity improvement (Edward et al. (2012), Yue et al. (2014), Jin et al. (2017), Li et al. (2018), Sun et al. (2019)). Articles on coke deposition studies under a supercritical environment are limited in numbers.
- In most of the fuel cracking investigations, cracking experiments were carried out below 45 bar pressure and a temperature range of 500-600 °C (Huang et al. (2004), Jia et al. (2019), Zhou et al. (2017), Jiang et al. (2013), Gua et al. (2019), Liu et al. (2019)). The heat sink capacity obtained for the temperature range may be sufficient for the cooling requirements up to Mach-5 speed vehicles. Cooling requirements will increase with vehicle speed. Hence, the heat sink offered by a fuel at 600 °C may not be enough to cool the scramjet engine above Mach-5 speeds. The heat sink capacity of hydrocarbon fuels above 600 °C and 50 bar pressure has been reported by a few scientists and only for two or three fuels (Xu et al. (2015), Pan et al. (2020), Wang et al. (2021)).
- While numerous studies have reported the cracking and heat sink characteristics of different hydrocarbons, comprehensive details regarding fuel conversion, product composition, and coke deposition rates are not provided in a single place. As a result, establishing correlations between operating parameters and cracking behavior becomes a challenge.
- Furthermore, most of the literature does not provide any information on heat loss, which is crucial in estimating heat sink values.
- In more than 90% of the investigations, scientists have focussed only on reactor-containing coke and have not provided insights about carry-away or bulk-flow coke. The total amount of coke should be a combination of both reactor-containing coke and carry-away coke.
- Although a few studies (Wang et al. (2008), Liu et al. (2009), Chakraborty et al. (2012)) have reported about the use of initiators in enhancing fuel conversion, details regarding the feed and product characterization and the impact of initiators on coking are often lacking.

1.5. Objectives of Present Research

A hypersonic engine produces substantial heat loads on its structure above Mach-5 speeds. Due to space constraints, hypersonic jets face problems in accommodating an additional

amount of coolant solely for the purpose of engine cooling. A possible solution to address this issue is the utilization of onboard fuel as a regenerative coolant, in addition to power generation for its movement. The primary objective of the present study is to develop low-cost hydrocarbon fuels that can offer sufficient heat sink capacity to cool the engine structure effectively at hypersonic velocities.

- Designing an appropriate test setup capable of conducting pyrolysis experiments up to a temperature of 750 °C and 60 bar pressure.
- Establishing a standard procedure for measurement and analysis of various characteristics and parameters, like heat sink capacity, cracking percentage, heat loss, and coke deposition, by conducting pyrolysis experiments with single component hydrocarbons.
- Conducting pyrolysis experiments using both single-component and multicomponent hydrocarbon fuels to gain insights into the cracking phenomenon under supercritical environments and estimate cracking percentage, heat sink capacity, and coke deposition.
- Investigating the influence of operating parameters, such as temperature, pressure, and fuel residence time, on cracking percentage, endothermicity, and coke deposition rate.
- Understanding the impact of homogeneous initiators on fuel endothermicity and coking rate at different temperatures.
- Developing a coke model to predict the coke deposition rate for the thermal cracking of hydrocarbon fuels and its validation with experimental results.

1.6. Summary of Thesis

The primary objective of this research is to investigate the pyrolysis behavior of different hydrocarbon fuels at supercritical conditions and to determine the fuel cracking percentage, heat sink, and coke deposition rates. Furthermore, the suitability of homogeneous initiators in improving the heat sink capacities of the fuels. The entire research work has been carefully organized into distinct chapters, and each chapter is dedicated to a specific aspect of the investigation.

Chapter-2 of this thesis deals with literature analysis on endothermic fuels. The chapter highlights the characteristics of multiple hydrocarbon fuels and a comparative analysis of their endothermic capacities, cracking conversion, and coke deposition rates across a wide range of operational conditions. In order to enhance clarity, the chapter has been divided into multiple

sub-sections, each addressing a distinct issue that is relevant to the research. This chapter aims to provide a comprehensive understanding of the current state of knowledge regarding endothermic fuels.

Chapter-3 of this thesis focuses on illustrating the procedures and methodology adopted in various analyses and experiments in the present study. This section provides a detailed description of the experimental and numerical setup, including information regarding the specifications and configurations of the equipment used. Additionally, a thorough clarification of the processes and mathematical equations necessary for understanding the various approaches and methods of characterization is explained.

Chapter-4 of the thesis includes the investigation of heat sink capacity, cracking efficiency, and coke deposition rate of three single-component hydrocarbons. In this regard, three types of C₇ hydrocarbons, namely n-heptane, methylcyclohexane, and toluene, were chosen due to their low cost and easy availability. The aim of this study was to conduct a comparative analysis of the cracking characteristics of a straight-chain hydrocarbon, cyclic hydrocarbon, and aromatic hydrocarbon of the same carbon number.

Chapter-5 of this thesis focuses on the investigation of cracking characteristics of a kerosene range multicomponent hydrocarbon fuel, namely HCF-1, under supercritical conditions. The physicochemical characteristics of the fuel are mentioned in Chapter 5. The chapter highlights the effect of temperature, pressure, and residence time on the cracking propensity of the HCF-1 fuel. The research presented in this chapter provides a comprehensive understanding of the cracking characteristics of a multi-component fuel in terms of cracking percentage, heat sink capacity, and coke deposition rates.

Chapter-6 of the thesis demonstrates the suitability of homogeneous initiators in enhancing the cracking behavior of hydrocarbon fuel. To investigate the efficacy of initiators on endothermicity and coke deposition rate, two different initiators, namely tri-ethylamine (TEA) and di-tert-butylperoxide (DTBP), were considered in work, and the pyrolysis experiments were performed with HCF-2 fuel. The study demonstrated that the initiator has an overall improvement in performance on the heat sink capacity.

Chapter-7 of this thesis presents the development of a Coke model using numerical simulations. Numerical simulation was performed to obtain the concentration profiles of coke-

forming precursors. FLUENT 21 software with the finite volume method was used in numerical simulation. The SIMPLEC algorithm coupled with pressure and velocity solver was used in the FLUENT software. Product distribution and transport properties were estimated using the shear stress transport $k-\omega$ turbulence model. The aptness of the model was verified experimentally by performing experiments with n-heptane.

Chapter 8 includes the overall conclusion of the thesis. This chapter summarizes, in what way the present research bridged some of the research gaps identified at the beginning of the research work.

Fig. 1.5 depicts the major objectives of the present research and the chapter-wise link between the objective and research outcomes.

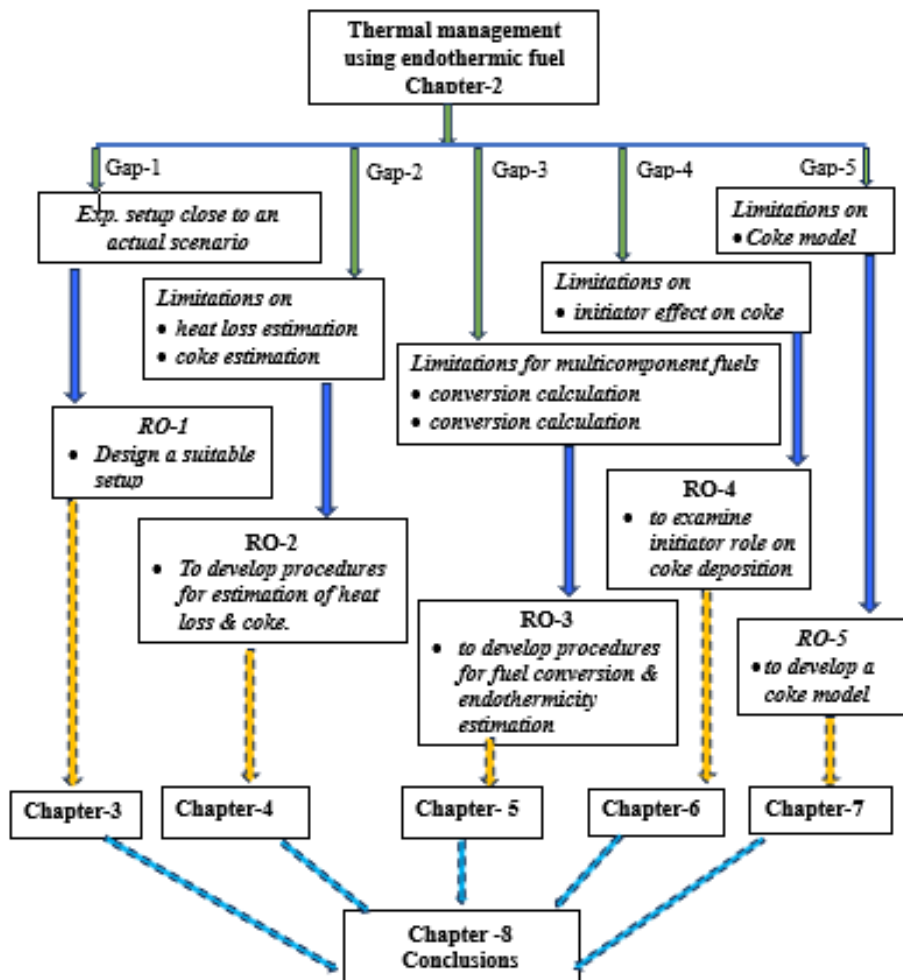


Fig. 1.5: A flow diagram of overall thesis work. (RO: research objective)

Chapter-2

Literature on Endothermic Fuel Development

Literature on Endothermic Fuel Development

2.1. Introduction to Endothermic Fuel

The advancement of a hypersonic air-breathing vehicle depends on the capabilities of a supersonic combustion ramjet (SCRAMJET) engine for its propulsion. Hypersonic engines are designed to operate above Mach-5 speeds. With an increase in Mach number, the temperature of the compressed ram air increases and may exceed the thermal design limits. Hence, a scramjet engine requires considerable cooling at hypersonic speeds. A multi-component hydrocarbon fuel having higher specific gravity, higher energy density, higher heat capacity, lower coke propensity, and lower viscosity can be an appropriate fuel as a substitute of solid or gaseous propellants, for managing the thermal load in an onboard hypersonic engine. Hydrocarbon fuels can serve as substitutes for solid propellants and hypergolic fuels. One potential method for cooling the engine is the use of onboard fuel for regenerative cooling. It is widely acknowledged among the research community that the implementation of active and spontaneous cooling may offer benefits compared to relying solely on passive cooling or thermal protection materials. The regenerative cooling of the engine structure can be achieved by circulating the onboard liquid fuel around the combustion chamber. During the flow of fuel through the cooling channels, the fuel will experience an upsurge in temperature, and beyond certain temperatures, the fuel starts an endothermic cracking reaction. An effective use of endothermic heat sinks during pyrolysis reactions is essential to satisfy the cooling needs of a hypersonic engine. However, the accumulation of coke deposits as a consequence of fuel cracking is unavoidable and poses a challenge for regenerative cooling.

In this context, the investigation of the cracking behavior of hydrocarbon fuels at high temperatures and pressures has garnered significant attention in numerous studies. To examine the suitability of hydrocarbon fuels, cracking studies have been conducted using a tubular reactor with a diameter of less than 5 mm. Also, the majority of the research has been conducted with JP-8, RP-1, RP-3, JP-7, JP-900, JP-10, n-heptane, n-decane, and n-dodecane hydrocarbon fuels. A comprehensive review and analysis of investigations related to endothermic fuels has been performed and summarized. The entire analysis is divided into six categories: (i) physicochemical characteristics of various endothermic fuels, (ii) pyrolysis studies of endothermic fuels, (iii) influence of initiators in enhancing the endothermicity of hydrocarbon

fuels, (iv) coking aspects of the cracking process, (v) impact of additives on coke suppression, and (vi) development of a coke prediction model.

2.2. Physico-chemical Characteristics of Hydrocarbon Fuels

Jet propellants like JP-7, JP-8, RP-1, and RP-3 are commonly used in supersonic applications due to their high energy density, good combustion quality, and low coke deposition. Many research groups have also studied the aptness of JP-7 and JP-8 equivalent fuels for hypersonic applications. Smith et al. (2007) and Lovestead et al. (2009) examined the boiling properties and other characteristics of several jet fuels. The distillation characteristics of various jet fuels are shown in Table 2.1. Based on the distillation data, it can be said that the JP-7 fuel contains more amounts of heavier hydrocarbons than the JP-8 fuel. Song et al. (1993) performed a comparative analysis between JP-8 and JP-8C fuels. The JP-8C is a coal-derived fuel, whereas the JP-8 is a petroleum-derived fuel. The density of JP-8C is higher compared to JP-8 fuel, and it consists of over 75 wt.% cycloalkanes and 20 wt.% aromatics. It is also reported that at 450 °C, the coal-derived JP-8C fuel demonstrated better thermal stability than the petroleum-derived JP-8 fuel.

Balster et al. (2008) examined the suitability of JP-900 fuel for supersonic applications. The fuel was prepared by mixing equal amounts of coal-derived refined chemical oil (RCO) and petroleum-derived light cycle oil (LCO). The specific gravity of the JP-900 fuel is 0.87. The concentration of polar molecules in JP-900 is significantly lower (around 22 mg/L) compared to Jet fuels (100 to 600 mg/L). Upon comparable test conditions, the coke deposition rate of the JP-900 fuel was one-tenth of the JP-8 fuel. JP-10 is a single-component synthetic fuel with 99% tri-cyclodecane content (Li et al. (2019)). The calorific value of the fuel is about 39 MJ/kg. The average boiling point of the fuel is 192 °C. The impact of aromatic content in fuel was investigated by DeBlase et al. (2018). It is reported that at higher temperatures, low molecular weight aromatics and their methyl substitution derivatives can enhance the propensity of polycyclic aromatic hydrocarbons (PAHs) formation, which serve as precursors for coke deposition. Table 2.1 shows a comparison of the distillation properties of several jet fuels. The average boiling point temperature of JP-7, JP-8, RP-1, RP-3, and JP-900 fuels are 219°C, 199°C, 203.7°C, 207.3°C, and 205.1 respectively.

Table 2.2 presents a summary of various parameters associated with different types of Jet fuels. The paraffin content is higher in JP-7 than in JP-8 fuel, and the aromatic concentration

in JP-8 is nearly four times higher than in JP-7 fuel. Though the density of RP-1 and RP-3 fuels are almost the same, the paraffin and naphthene contents are significantly different. The data are useful in analyzing thermal cracking characteristics at elevated temperatures.

Table 2.1: Distillation characteristics of JP-7, JP-8, RP-3, JP-900, and Jet fuels*

Fuel name	JP-7 ^a	JP-8 ^b	RP-1 ^c	RP-3 ^d	JP-900 ^b	Jet fuel ^c
Distillate (vol.%)	Temperature (°C)					
5	206	175	197	180	191	160
10	208	179	199	184	195	170
20	211	185	202	189	197	195
30	213	186	205	193	199	205
40	215	194	209	198	202	212
50	218	200	212	203	206	220
60	221	204	217	209	211	228
70	226	212	222	215	217	237
80	232	219	228	224	228	242
90	239	-	241	237	-	257

*Values are extracted from distillation curves with a maximum deviation of ± 0.5 °C.

^aLovestead et al. (2009), ^bSmith et al. (2007), ^cBurno et al. (2006), ^dWu et al. (2019), ^eSaggese et al. (2019)

Table 2.2: Properties of JP-7, JP-8, RP-1, RP-3, and JP-900 fuels

Fuel name	JP-7 ^a	JP-8 ^{b,c}	RP-1 ^{d,e}	RP-3 ^{f,g}	JP-900 ^{b,c}
Paraffin (vol.%)	45.0	40.8	36.8	52.2	1.3
Mono-cycloparaffins (vol.%)	35.0	30.3	37.0	33.8	32.2
Di-cycloparaffins (vol.%)	15.0	11.4	16.0	6.0	63.1
Alkylbenzenes (vol.%)	3.0	16.8	8.9	5.1	3.3
Naphthalenes (vol.%)	1.0	0.3	0.9	1.5	0.0
Total sulfur (wt.%)	0.1	0.3	0.05	0.2	-
°API gravity	47.1	37.0	44.2	44.8	32.1
Boiling range (°C)	206-239	175-238	197-241	180-237	191-243

^aLovestead et al. (2009); ^bSmith et al. (2007); ^cBalster et al. (2008); ^dLisa et al. (2008); ^eHubert et al. (2009); ^fMa et al. (2016); ^gBishop et al. (2019); ^hSobel et al. (1995)

2.3. Thermal Cracking Characteristics of Hydrocarbon Fuels

Numerous researchers have proposed the suitability of hydrocarbon fuels as a way to improve thermal management in supersonic/hypersonic engines. Multiple methods, such as thermal cracking, catalytic cracking, depolymerization, and dehydrogenation, are used in hydrocarbon fuel cracking. The thesis focuses on the thermal cracking of hydrocarbon fuels. The thermal cracking process involves the decomposition of heavier hydrocarbon compounds into lighter hydrocarbon molecules. The formation of smaller molecules contributes to the quality of combustion. However, the heat sink capability of a fuel depends on both the fuel cracking percentage and the composition of products.

Heinrich et al. (2001) studied the cracking of Norpar-12 and n-dodecane to estimate the heat sink capacity of the fuels. Cracking experiments were conducted in a tubular reactor for a temperature and pressure range of 627 to 727 °C and 25 to 35 bar, respectively. At a temperature of 647 °C, the estimated values of heat sink capacity of Norpar-12 and n-dodecane are 2750 and 2590 kJ/kg, respectively. Jackson et al. (2004) examined the heat sink capacity of JP-7 fuel. The estimated value of heat sink capacity is about 4000 kJ/kg at a condition of 700° C and 24 bar pressure. Huang et al. (2004) examined the thermal cracking characteristics of n-octane and JP-7 fuels. The experiments were conducted at 23.4 bar pressure and a temperature range of 700 to 815 °C. The heat sink values for the n-octane and JP-7 fuels are 3279 and 3233 kJ/kg, respectively.

Chakraborty et al. (2009) investigated the cracking behavior of n-heptane under subcritical and supercritical pressure for a temperature range of 640 to 680 °C. The increase in pressure from 7.9 bar to 29.3 bar yields a 9% increment in heptane conversion. The increase in pressure enhanced the yield of alkanes and reduced the yield of lower olefins. Zhang et al. (2018) emphasized the mechanism of thermal cracking reactions. At high temperatures (> 550 °C), olefins can undergo bimolecular reactions to form cycloalkenes. The bimolecular addition reaction may reduce the heat sink capacity of a fuel. It is reported that fuel-containing cyclic compounds may undergo isomerization reactions to form active precursors for coke formation under a supercritical environment. Jiang et al. (2013) used a flow reactor to evaluate the heat sink capacity of HF-1 fuel with a boiling range of 169-236 °C. At 680 °C and 50 bar pressure, the heat sink capacity of the fuel is approximately 3045 kJ/kg. The heat sink capacity of n-decane at 667 °C and 40 bar pressure is estimated to be 2700 kJ/kg (Zhu et al. (2014)). Pan et al. (2020)

carried out pyrolysis studies of JP-10 fuel using a tubular flow reactor. The heat sink value of the fuel is 2600 kJ/kg at a temperature of 730 °C, 45 bar pressure.

Operating parameters such as temperature, pressure, and residence time play a crucial role in a thermal cracking process. To understand the cracking characteristics, the products obtained from a cracking reaction need to be quantified properly. The chemical composition and thermo-physical properties of fluids throughout the reactor must be assessed accurately. In some studies, surrogate compounds have been used as a substitute for a kerosene range fuel to simplify the complexity and gain a mechanistic understanding of pyrolysis reactions. To calculate the sensible heat sink value of a hydrocarbon fuel, most researchers assumed that the fluid composition remains constant within the reactor zone. The endothermic/chemical heat sink was estimated by subtracting the sensible heat sink from the total heat sink. Many researchers used the following expressions (Eq. 2.1-2.4) to estimate the endothermic heat sink of different fuels.

$$Q_{heat\ sink} = Q_{input} - Q_{loss} \quad \text{Eq. (2.1)}$$

$$Q_{input} = V \times I \quad \text{Eq. (2.2)}$$

$$H(T_{exit}) - H(T_{inlet}) = \Delta H_{sensible} \quad \text{Eq. (2.3)}$$

$$H_{endothermic} = \frac{Q_{heat\ sink}}{m} - \Delta H_{sensible} \quad \text{Eq. (2.4)}$$

where, Q = energy per unit time, V = voltage, I = current, H = enthalpy, and m = mass flow rate.

Table 2.3 presents a comprehensive overview of the heat sink capacity of various fuels under different temperature and pressure conditions. The heat sink capacity of different fuels varies between 2500 kJ/kg and 3200 kJ/kg for a temperature range of 600 °C to 750 °C. Whereas the chemical heat sink capacity for various fuels varies between 500 kJ/kg and 1200 kJ/kg. The heat sink capacity of hydrocarbon fuels is influenced by several factors such as fuel composition, hydrocarbon type, fuel flow rate, and operating temperature and pressure. The statistics indicate that, in most cases, the total heat sink capacity is approximately three to four times greater than the chemical heat sink value.

Table 2.3. Fuel conversion, coke and heat sink values of various fuels

Fuel	Temp (°C)	Pressure (bar)	Conversion %	Coke deposition (mg/min)	Total heat sink (kJ/kg)	Chemical heat sink (kJ/kg)	References
n-dodecane	727	35	88	-	2590	-	Heinrich et al. (2001)
JP-7	700	23.4	-	0.93	3233	988	Huang et al. (2002)
JP-7	815	23.4	-	-	3791	1186	Huang et al. (2004)
n-octane	700	23.4	-	-	3023	953	Huang et al. (2004)
JP-8	700	23.4	-	-	2954	802	Huang et al. (2004)
HF-1	680	50	88	-	3045	1000	Jiang et al. (2013)
n-decane	667	40	22	-	2700	550	Zhu et al. (2014)
RP-3	750	60	85	-	3250	740	Jin et al. (2017)
JP-10	730	45	88	5.78	2600	-	Pan et al. (2020)
JP-10	725	40	60	161.6	2850	-	Li et al. (2022)
n-decane	614	30	5	-	-	300	Feng et al. (2023)
n-decane	652	30	90	55.7	-	-	Cheng et al. (2024)
n-dodecane	700	55	25	28	2577	559	Nalabala et al. (2024)

2.4. Influence of Catalyst on Supercritical Cracking of Hydrocarbon Fuels

Catalytic cracking of hydrocarbons is generally used to improve the cracking rate and selectivity of desired products. The selection of catalyst depends on hydrocarbon type and specific objective. Although many studies are available on the catalytic cracking of hydrocarbons, only some are related to supercritical catalytic cracking on endothermic fuels. Heinrich et al. (2001) have studied the cracking of n-dodecane fuel in the presence of a Zeolite catalyst. The studies for catalyst and catalyst-free cases at 827 °C and with a fuel flow rate of 800 mL/min in a flow reactor. The reactor (length =1400 mm and Inner diameter = 5 mm) was coated with a Zeolite catalyst. The chemical heat sink capacity of the fuel with and without a catalyst is 2758 kJ/kg and 2593 kJ/kg, respectively. Zhang et al. (2002) studied the catalytic cracking of NNJ-150 fuel (a mixture of C9 to C17 hydrocarbons) in Ag and La-impregnated USHY and HZSM catalysts. In the presence of catalysts, the fuel cracking percentage increased by more than two-fold compared to the thermal cracking reaction at 500 °C and 35 bar pressure. Huang et al. (2002) studied the supercritical cracking of JP-7, JP-10, and n-octane fuels over a

=====

zeolite-coated tubular reactor. The coke deposition rate of JP-7, JP-10, and n-octane was 0.94, 0.88, and 0.43 mg/min, and the chemical heat sink was 1074, 823, and 409 kJ/kg, respectively, at 723 °C and 41 bar pressure. Gokulakrishnan et al. (2011) have developed a gas-phase kinetic model for the catalytic cracking of *n*-octane fuel under supercritical conditions under the influence of Zeolite catalyst. The developed model was used to predict the n-octane cracking products under different operating conditions, and the model showed a close fit between the estimated and experimental results.

Huang et al. (2018) studied the pyrolysis of JP-10 fuel over Zeolite-Y in a fixed-bed reactor. At 477 °C, 60 bar, and with a feed flow rate of 1.2 mL/min, the chemical heat sink capacity of the fuel is 21 kJ/kg. It is reported that the product distribution pattern for the catalytic cracking was significantly different from thermal cracking. Gao et al. (2019) studied the suitability of Ni-doped Al₂O₃ catalyst for the suppression of coke during the cracking of RP-3 fuel. The experiments were conducted at 680 °C and 30 bar pressure using a flow reactor. The study claims that the catalytic steam reforming improved chemical heat sink capacity by 750 kJ/kg of RP-3 fuel. It is also reported that there was a decrease in coke deposition from 3.55 mg/min to 0.54 mg/min. However, the individual effect of steam and catalyst on heat sink capacity and coke deposition is not reported.

A summary of the endothermic heat sink capacity of various fuels in the presence of different catalysts is shown in Table 2.4. A catalytic system can offer an extra cushion to increase the operating temperature due to the low value of coke yield and can improve the endothermicity of fuels. Though a catalyst can enhance the conversion and heat sink of fuels, their demonstration in capillary channels could be a significant challenge in designing an active cooling system for a hypersonic engine.

Table 2.4: Heat sink capacity of hydrocarbon fuels with various catalysts

Fuel	Catalyst type	Temp. (°C)	Pressure (bar)	Total heat sink (kJ/kg)	Chemical heat sink (kJ/kg)	Coke deposition (mg/min)	References
n-dodecane	-	727	35	-	2090	-	Heinrich et al. (2001)
n-dodecane	Zeolite	727	35	-	2196	-	Heinrich et al. (2001)
n-dodecane	-	827	35	-	2593	-	Heinrich et al. (2001)
n-dodecane	Zeolite	827	35	-	2758	-	Heinrich et al. (2001)
JP-7	Zeolite	723	41	3414	1074	0.94	Huang et al. (2002)
JP-10	Zeolite	696	41	2605	541	0.88	Huang et al. (2002)
n-octane	Zeolite	650	41	2493	309	0.43	Huang et al. (2002)
JP-10	-	687	60	2228		-	Huang et al. (2018)
RP-3	-	600	30	2300	400	1.03	Gao et al. (2019)
RP-3	Ni/Al ₂ O ₃	600	30	2480	480	0.12	Gao et al. (2019)
RP-3	-	680	30	3400	1000	3.55	Gao et al. (2019)
RP-3	Ni/Al ₂ O ₃	680	30	4000	1750	0.54	Gao et al. (2019)

2.5. Coke Deposition During Thermal Cracking of Hydrocarbon Fuels

Coke formation is an undesirable outcome that occurs during the decomposition of hydrocarbon fuels. Coke deposition inside a fuel line may lead to engine failure by blocking the fuel flow line. Hence, coking is a critical concern for hydrocarbons in scramjet engines. Typically, unsaturated and cyclic hydrocarbons (i.e., C_nH_{2n} , C_nH_{2n-2} , C_nH_n) are prone to form coke precursors. The amount of coke formation depends on several factors, such as operating temperature, pressure, hydrocarbon composition, dissolved oxygen level, presence of sulfur compounds in fuel, and the metallurgy of the fuel transfer line. Generally, gum formation starts at relatively lower temperatures for straight-chain alkanes than for branched-chain hydrocarbons. Once the gum formation initiates, it increases exponentially with the reactions involving alkenes and aromatic compounds. Zhu et al. (2008) have studied the coking phenomena of RP-3 fuel pyrolysis under supercritical conditions using a tubular reactor. The coke deposition rate was found to be about 1.5 mg/min at 470 °C and 50 bar. The study furthermore revealed that the aromatic percentage in the liquid product increased by more than 2.5-fold (from 8.9% to 23.9%) compared to the aromatic content in the feed. Gascoïn et al. (2008) investigated the pyrolysis of n-decane in a flow reactor. At a temperature of 852 °C, pressure of 60 bar, and a flow rate of 4.1 mL/min, the coke deposition was 20 mg/min.

Yang et al. (2012) studied the suitability of alumina coating to suppress metal-catalyzed oxidative coking of China RP-3 fuel. The chemical vapor deposition (CVD) technique was used to coat the alumina on the metallic (SS-321) surface. The thickness of the alumina coating varied in the range of 318 nm to 1280 nm. The cracking experiment was carried out at 720 °C, under 50 bar pressure, with a flow rate of 75 mL/min, and for a duration of 30 min. The coke deposition rates for bare tube, 505 nm, and 1280 nm alumina-coated tubes were 32.9 mg/min, 13.79 mg/min, and 10.3 mg/min, respectively. Tang et al. (2014) have investigated the suitability of titanium oxide (TiO_2) coating on the coke propensity of n-hexane fuel. The inner surface of the SS-304 tube was coated with TiO_2 using a CVD technique. The pyrolysis was carried out at a temperature of 600 °C, pressure of 33 bar, and a flow rate of 40 mL/min. The study revealed that coke formation reduced by about 76% (from 0.056 mg/min to 0.013 mg/min) with a 6-micron thickness of TiO_2 coating. Gong et al. (2015) examined the efficacy of Al_2O_3 coating on the coke propensity of MCRI-1 (mainly consisting of C_{12} - C_{16} hydrocarbons) fuel using a tubular flow reactor. The decomposition study was carried out. It is reported that at 800 °C and 40 bar

pressure, the run time of the reactor increased by 3-fold with 165 nm thickness of alumina coating compared to a bare tube.

Wickham et al. (2016) studied the coke deposition phenomena of RP-2 fuel (boiling point range is 205-263 °C (Lisa et al. (2008)) under a high heat flux environment. It is reported that the exposure of fuel to a heat flux of 3200 W/cm² for a duration of three minutes resulted in about a 0.013-micron thick layer of coke deposition. Jin et al. (2017) studied the effect of pressure on the coke yield of RP-3 fuel. The coke yield increased 1.7 times when pressure increased from 7 bar to 35 bar at 650 °C. It is reported that at lower pressure (<15 bar), the contribution of filamentous coke was more than amorphous coke, and an opposite behavior was noted at higher pressures. Development of coke deposits on the reactor surface can occur *via* two major pathways: i) oxidative /filamentous coking and ii) cracking/pyrolytic coking. Heterogeneous species like sulfur, nitrogen, etc., can initiate coke formation with the dissolved oxygen present in the fuel (Gascoin et al. (2010), Xie et al. (2009)). Pyrolytic coke deposition occurs at high temperatures (> 450 °C), and the amount of coke depends on the extent of cracking conversion. Fig 2.1 shows a comparison of the coke deposition rate of various fuels under different operating conditions.

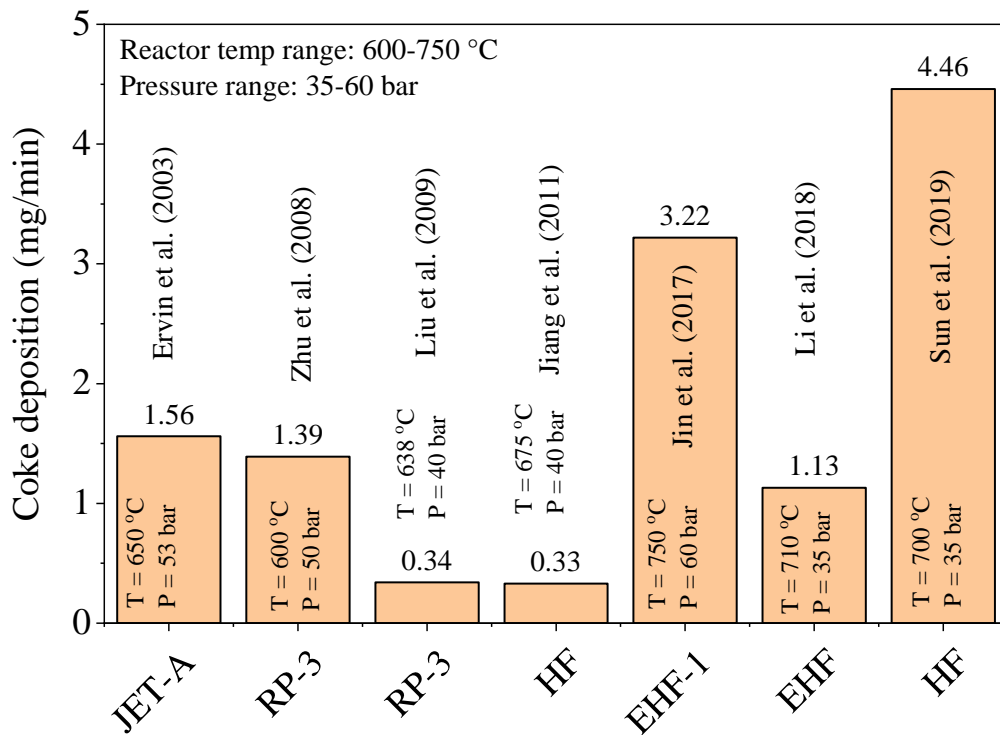


Fig. 2.1: Coke deposition rate of various hydrocarbon fuels.

2.6. Suitability of Initiators to Enhance Endothermicity

The cracking conversion and endothermicity of hydrocarbons can be increased with an increase in temperature but lead to more coke deposition. To mitigate this limitation, the aptness of initiators to improve the endothermicity of fuels at lower temperatures has been examined by several authors. Nitrogen, oxygen, and phosphorus-containing organic initiators have weak bonds between atoms and can be used in thermal cracking reactions to enhance the reaction rate. In many cases, when a reaction proceeds via a free-radical mechanism pathway, the initiation step is slower than the propagation and termination steps. Hence, organic molecules having weak bonds are usually used as initiators. The addition of initiators to the hydrocarbon fuels can initiate the cracking reaction by generating radicals (i.e., from initiators). These radicals having unpaired electrons, are very active and tend to stabilize by abstracting electrons from feed hydrocarbon molecules, thus forming higher alkyl radicals (from feed hydrocarbons). The presence of 1 wt. % of di-tert-butyl peroxide enhanced the fuel cracking percentage of heavy oil by 55% at 430 °C and 50 bar pressure (Chang et al. (2003)). Wickham et al. (2002, 2008) have examined the effect of diphenyl selenide (DPS) on the heat sink capacity of n-heptane, JP-7, and n-decane fuels. At 575 °C and 38 bar, with the addition of 8 wt.% DPS, the heat sink capacity of n-heptane enhanced by 18%. Similarly, at 600 °C, the addition of 4% DPS enhanced the heat sink capacity of n-decane and JP-7 fuels by 7.6% and 6.7%, respectively. Wang et al. (2006) studied the suitability of triethylamine (TEA) on the cracking performance of n-heptane. At 600 °C and 35 bar pressure, the heptane conversion increased by about 1.7 times (from 7.5% to 12.5%) in the presence of 5.5 wt.% of triethylamine. Wang et al. (2008) investigated the suitability of tributylamine (TBA) to improve the heat sink capacity of n-heptane. In the presence of 10 wt.% of TBA, the cracking percentage of n-heptane increased by about 12%, and the energy input increased by about 3 times with respect to the initiator-free case at 650 °C and under atmospheric pressure. Though the effect of the initiator on cracking percentage and energy intake is reported explicitly, no details about the variation in coke yield and selectivity of products are reported.

Liu et al. (2009) studied the suitability of nitropropane (NP) and triethylamine (TEA) on the cracking performance of dodecane. At 638 °C, 40 bar pressure, and with 4 wt.% loading of NP and TEA, the cracking percentage of the fuel increased by about 2.5% and 3.4%, respectively. In the presence of an initiator, the alkene-to-alkane ratio decreased in the liquid product,

=====

possibly due to an increased rate of bimolecular hydrogen abstraction reactions. Chakraborty et al. (2012) studied the effect of di-tertbutyl peroxide (DTBP), diisopropylamine (DIPA), and triethylamine (TEA) on the cracking behavior of n-heptane. In the presence of 3 wt.% of TEA, the cracking percentage of heptane increased by 10% (from 38% to 48%) at a reactor condition of 540 °C temperature and 30 bar pressure. Though the author mentioned the benefits of initiators on fuel conversion and selectivity of lighter olefins (e.g., ethylene and butene), no information on coke yield and heat sink capacity is mentioned. Han et al. (2023) studied the influence of nitropropane as an initiator on the cracking performance of n-decane fuel in a tubular flow reactor. The study demonstrated that the addition of 2 % nitropropane enhanced the selectivity of alkenes (C₃-C₉) by 5% at 627 °C under 30 bar pressure. The addition of an initiator enhanced the cracking percentage of n-decane by 10.5% (from 17.5% to 28%).

A summary of the consequence of different initiators on cracking characteristics of hydrocarbon fuels is tabulated in Table 2.5. Though most of the initiators performed well in enhancing the conversion and endothermicity, the extent of improvement depends on the type of initiator, the concentration of the initiators, and the operating conditions.

Table 2.5: Influence of initiators on fuel conversion and heat sink capacities

Fuel	Temp (°C)	Pressure (bar)	Initiator name	Initiator loading (wt.%)	Total heat sink (kJ/kg)	Conv. (%)	Coke deposition (mg/min)	References
n-dodecane	638	40	-	-	-	35	0.21	Liu et al. (2009)
n-dodecane	638	40	NP	4	-	38	0.50	Liu et al. (2009)
n-dodecane	638	40	TEA	4	-	37	0.30	Liu et al. (2009)
n-heptane	600	35	-	-	-	8	-	Wang et. (2008)
n-heptane	600	35	TEA	10	-	12	-	Wang et. (2008)
JP-7	600	38	-	-	2170	36	-	Wickham et al. (2008)
JP-7	600	38	DPS	4	2230	44	-	Wickham et al. (2008)
n-heptane	575	38	-	-	1880	5	-	Wickham et al. (2002)
n-heptane	575	38	DPS	8	2209	32	-	Wickham et al. (2002)
n-decane	600	38	-	-	2212	28	-	Wickham et al. (2008)
n-decane	600	38	DPS	4	2440	49	-	Wickham et al. (2008)
n-heptane	540	30	-	-	-	38	-	Chakraborty et al. (2012)
n-heptane	540	30	TEA	3	-	48	-	Chakraborty et al. (2012)
n-decane	627	30	-	-	-	17	-	Han et al. (2023)
n-decane	627	30	NM	2	-	28	-	Han et al. (2023)

DPS: diphenylselenide; NP: nitropropane; NM: nitromethane; TEA: triethylamine; TBA: tributylamine

2.7. Influence of Pressure on Cracking Characteristics

The section highlights the influences of pressure on the cracking characteristics of hydrocarbon fuel under subcritical and supercritical conditions. Xing et al. (2008) studied the cracking phenomena of JP-10 fuel under subcritical and supercritical conditions. At 610 °C with a flow rate of 2 mL/min, the cracking percentage of JP-10 increased marginally ($\approx 1.2\%$) as the reactor pressure was raised from 27 bar to 38 bar. The selectivity of ethylene in the cracked products decreased, but the selectivity of methane, ethane, and propane increased with reactor pressure. The increase in pressure Hou et al. (2013) studied the influence of pressure on the thermal cracking behavior of China-3 fuel using a tubular reactor. The study reported that the overall heat sink capacity of the fuel decreased from 2850 kJ/kg to 2800 kJ/kg as the reactor pressure increased from 10 bar to 30 bar for a fixed temperature of 590 °C.

Jin et al. (2017) studied the effect of pressure on the cracking of EHF fuel using a silica-coated tubular reactor. The fuel cracking percentage, coke deposition rate, and total heat sink increased by 1.2 times (from 58% to 70%), 30% (from 2.5 mg/min to 3.22 mg/min), and 4.8% (from 3100 kJ/kg to 3250 kJ/kg) when the pyrolysis pressure was raised from 15 bar to 35 bar at 750 °C and for a constant value of fuel flow rate of 300 mL/min. Wu et al. (2018) have examined the effect of pressure on n-heptane cracking using a tubular reactor. At a temperature of 747 °C and for a fuel flow of 1 mL/min, as the reactor pressure was raised from 1 bar to 5 bar, the cracking percentage of heptane increased from 88% to 93%. Zhou et al. (2014) studied the effect of pressure on n-decane cracking using a flow reactor. The conversion and endothermicity of the fuel increased from 27% to 64% and 516 kJ/kg to 778 kJ/kg, respectively, as the reactor pressure was increased from 30 bar to 50 bar at a temperature of 640 °C and for a fuel flow rate of 80 mL/min. Jiao et al. (2019) examined the effect of pressure on RP-3 cracking conversion using a flow reactor. The fuel conversion increased from 38% to 47% as the reactor pressure was increased from 25 bar to 55 bar at a temperature of 647 °C.

Therefore, from the literature survey, it is noted that fuel conversion improved moderately with reactor pressure when the operating pressure was less than the critical pressure of fuel. However, when the operating pressure was above a critical pressure, the influence of pressure on fuel conversion and endothermicity was relatively low.

2.8. Numerical Simulations on Supercritical Hydrocarbon Cracking

Goel et al. (2000) performed simulation studies to examine the supercritical cracking of Jet fuel. A single-step global kinetic model was developed to understand the pyrolysis mechanism. The simulation results were validated by performing experiments with n-dodecane at 600 °C and 48 bar for a flow range of 8 mL/min to 20 mL/min. The deviation between the model-predicted and experimental wall temperatures is less than 20%. Daniau et al. (2005) developed a global kinetic model to predict the product composition of long-chain saturated hydrocarbons (C_nH_{2n+2}). The kinetic model was formulated using Norpar-12 fuel (a combination of C_9 to C_{12} hydrocarbons), and the model results were validated experimentally using n-dodecane ($C_{12}H_{26}$) for a temperature range of 380 °C to 827 °C under 100 bar. The model-predicted data showed good agreement with the experimental results for most of the alkanes and alkenes except ethylene. However, the author does not reveal the model parameters in the article. Ward et al. (2005) used a flow reactor to investigate the thermal cracking of n-decane and n-dodecane at supercritical pressures. The Proportional Product Distribution (PPD) model was developed and validated based on a two-dimensional Computational Fluid Dynamics (CFD) simulation. The PPD model accurately characterizes the product species distribution for a fuel conversion of less than 20%. The study also revealed possibilities of bimolecular reactions for higher pressures. However, the coke deposition aspect was ignored in the study. Feng et al. (2018) also performed a similar kind of simulation study considering a lesser number of cracking reactions and species.

Gascoin et al. (2010) studied the cracking of n-heptane, n-decane, n-dodecane, and kerosene range fuels in a flow reactor. The experiments were performed for a wide range of temperature (477 - 827 °C) and pressure (10 - 60 bar) values. The experimental results were linked with the simulated combustion chamber (SCC). Dodecane was used as a coolant for the SSC. It is reported that the coolant (i.e., dodecane) temperature raised from 27 °C to 1027 °C at the exit of the regenerative cooling channel, and the heat sink by the coolant is 2270 kJ/kg. Zhu et al. (2014) performed a simulation of n-decane cracking for a temperature range of 600 to 630 °C and a pressure range of 42 bar to 53 bar. The simulation results were verified with experiments. However, the author did not mention the heat sinks and coke deposition aspects. Xu et al. (2015) proposed a mathematical model to investigate the fluid flow and heat transfer behavior of RP-3 fuel at supercritical conditions. An exhaustive reaction mechanism considering 18 species and 24 elementary reactions, along with transport equations, was incorporated into

the simulator to study the effect of pyrolysis on flow and heat transfer characteristics. However, the phenomena of coke deposition are not highlighted in the work.

Li et al. (2018) simulated the impact of cooling channel geometry on the cracking characteristics of HF-1 fuel. The study revealed that under a reaction condition of 700 °C and 40 bar pressure, a square-shaped (1.75 mm× 1.75 mm) channel showed a 17% greater conversion of HF-1 compared to a 2 mm diameter circular channel. However, the square channel offered 67% more coke compared to the circular channel. The heat sink aspects are not elucidated in the work. Bao et al. (2014) studied the supercritical cracking of n-decane fuel using a square-shaped (2 mm× 2 mm) flow channel at a constant heat flux of 1.5 kW/m² and with a feed flow rate of 82 mL/min. To understand the variation in fluid temperature and flow velocity within the reactor system, the team performed a simulation study considering a one-step global kinetic model. The simulation showed a sharp variation in temperature, velocity, and heat transfer profiles at the corners of the rectangular channel. However, the author did not emphasize the coking phenomena.

Xu et al. (2016) performed simulation studies to examine the influence of constant heat flux on the cracking characteristics of RP-3 fuel under 50 bar pressure and for a fuel flow rate of 150 mL/min. The fuel conversion increased by 70% (from 10% to 80%) with the increase in heat flux from 1.5 MW/m² to 2.5 MW/m². The wall temperature increased by 190 °C (from 637 °C to 827 °C), and the chemical heat sink improved by 2.6 times (from 535 kJ/kg to 1413 kJ/kg) for the corresponding increase in heat flux. Jiang et al. (2019) have performed numerical simulations of n-decane cracking under 30 bar pressure. The conversion of n-decane increased by 67% (from 17% to 84%) with the increase in heat flux from 1.7 MW/m² to 3.3 MW/m².

A summary of numerical simulations for different hydrocarbons are given in Table 2.6. From the literature, it is evident that simulation studies were performed for various fuels, like n-decane, HF-1, and RP-3, to examine the pyrolysis and heat transfer characteristics of fuels under a supercritical environment. However, simulation studies on coke formation under supercritical conditions are not found in any of the above articles.

Table 2.6: Summary of numerical simulations of hydrocarbon fuel cracking studies.

Fuel	Model used	Solution technique used	Software/code	Remarks	References
n-dodecane	ODE 15	Method of lines (MOL)	Matlab programming	Temperature profile validated with experiments	Goel et al. (2000)
n-decane	Proportional product distribution (PPD)	nonlinear equations are discretized with 2 nd order central difference scheme.	Inhouse code	Temperature profile validated with experiments	Ward et al. (2004)
n-dodecane	RESPIRE	governing equations are discretized in space with centered explicit scheme	Inhouse code	Temperature profile validated with experiments	Gascoin et al. (2010)
n-decane	PPD	governing equations are discretized in space with centered explicit scheme, using pressure-based solver and k-omega SST wall functions. Global kinetic (GKM) models were used to predict species distribution.	Ansys Fluent	Temperature profile validated with experiments	Zhu et al. (2014)
n-decane	PPD	governing equations are discretized in space with centered explicit scheme, using pressure-based solver and k-omega SST wall functions. Differential global reactions (DGR) models were used to define species distribution	Ansys Fluent	Temperature profile validated with experiments	Tiang et al. (2019)

2.9. Summary of Review

Numerous research groups have examined the cracking characteristics of various hydrocarbon fuels, such as JP-7, JP-8, RP-3, HF-1, JP-10, n-octane, n-decane, and n-dodecane, across a temperature range of 400-700 °C and at a pressure range of 10-50 bar. The studies showed that fuel conversion and fuel heat sink capacity depend on several factors like fuel composition, operating temperature, pressure, feed flow rate, reactor geometry, etc. Fuels comprised of C₈ to C₁₄ hydrocarbons have a heat sink capacity in the range of 2000-3200 kJ/kg at 550-750 °C and 20-50 bar pressure. Most fuels have an endothermic (chemical) heat sink capacity in the range of 500–1100 kJ/kg. Most of the researchers adopted reactor heating through direct current. In some studies, the fuel was heated by a preheater before entering the reactor zone. The heat sink capacity of hydrocarbon fuels is mentioned using different terminologies, such as total heat sink, total heat absorption, and physical heat sink. However, they look to be similar in some ways, if not identical.

Despite the operating temperature and pressure being nearly equal, various research groups have reported significantly different values of heat sink for the same fuel. We believe that the deviation is mainly due to the different quantities of heat loss assumed by different authors. Almost all studies claimed that the chemical heat sink capability of a fuel increased with an increase in temperature. In most articles, the computation of endothermicity is not clearly spelled out. In many articles, the NIST SUPERTRAPP database was used to estimate fluid properties. It is also noted that the fuel residence time in many studies exceeds 30 s. However, for hypersonic engines, the fuel residence time is expected to be significantly shorter, possibly less than 10 s. A few studies explicitly discussed the relationship between endothermicity, coke deposition, and fuel conversion.

Coking is unavoidable in the thermal cracking of hydrocarbons. The amount and type of coke formation depends on fuel type and composition, cracking severity, presence of contaminants in a fuel, reactor metallurgy, etc. Several articles mentioned the two important routes of coke deposition (namely, metal-catalyzed coking and pyrolytic coking). Coke vulnerability can be reduced in a variety of ways, including continuous purging of nitrogen into the fuel tank, coating of reactor tube, and lowering the sulfur and oxygen content in the fuel. Scientists have investigated the efficacy of heterogenous catalysts such as Pt-Al₂O₃, HZSM-5, SAPO-34, and zeolites to improve the heat sink capacity of n-heptane, JP-7, JP-8, JP-10, and n-octane. Though the catalysts have shown some favorable benefits on heat sink capacities,

=====
housing/coating catalysts inside a narrow (usually 1-2 mm ID) tube may pose a substantial problem in actual circumstances. The release of catalyst particles/fines from the coating's outer layer and the clogging of the fuel nozzle could be another concern.

Some studies have been conducted by researchers to examine the effectiveness of different initiators, such as nitropropane, tributylamine, and triethylamine, in enhancing endothermicity. Furthermore, it has been found that a significant portion of initiator investigations were conducted using single-component hydrocarbon fuels. The impact of pressure on endothermicity is negligible when the operating pressure exceeds 1.5 times the critical pressure of a fluid. While certain groups of scientists directed their attention toward the heat sink and coking characteristics, others concentrated on the conversion and kinetic aspects of hydrocarbon pyrolysis. Except for a limited number of modelling studies, the existing literature on endothermic fuel lacks a comprehensive mass-balance analysis required for a flow system. Simulation studies of the thermal cracking of hydrocarbon fuels such as decane, HF-1, and RP-3 were performed by a few researchers.

Chapter 2 provides a comprehensive overview of research updates pertaining to the field of hydrocarbon fuels for hypersonic engines. An effort was undertaken to integrate the aforementioned elements in a coherent fashion, with the intention of presenting the content in a concise and easily understandable manner, hence anticipated to be of significant worth to researchers.

2.10. Gaps/Limitation noted on Endothermic Fuel Development

From the literature survey on endothermic fuel development, it has been found that the primary focus of investigations was on fuel conversion and heat sink studies (Yue et al. (2014), Jin et al. (2017), Li et al. (2018), Sun et al. (2019)). Investigations on coke deposition aspects under supercritical cracking of hydrocarbon fuels are limited in numbers and also not in depth. As the heat sink capability of a fuel depends on many factors, such as the type of hydrocarbon fuel, operating conditions, combustor metallurgy, etc., the study needs careful consideration of these parameters. Based on the literature review, the major gaps noted in the available literature include:

- The majority of fuel cracking investigations have been carried out at a temperature range of 500-600 °C and below 45 bar pressure. The heat sink capacity reported for the temperature

range may be sufficient for the cooling requirements of up to Mach-5 speed engines. Generally, the cooling requirement increases with the engine speed. Hence, the heat sink capability offered by a fuel at 600 °C may not be enough to cool a scramjet engine above Mach-5 speeds.

- As the critical pressure of lighter hydrocarbons (e.g., C₁, C₂, and C₃) is greater than 45 bar. Hence, it would be preferable to study the fuel cracking experiments above 45 bar to maintain a single-phase system within the reactor.
- Only a limited number of articles are available on the heat sink capacity of hydrocarbon fuels above 600 °C and 50 bar pressure. Among the limited members, the majority are on single-component fuels, and only a few studies are related to multi-component fuels.
- While numerous studies reported the cracking and heat sink characteristics of different hydrocarbons, comprehensive details on fuel conversion, product composition, and coke deposition rates are not provided in a single document. As a result, establishing a general correlation between different operating parameters and fuel cracking characteristics becomes a challenge.
- In calculating the heat sink using a direct heating system and Eq 2.1-2.4, heat loss estimation is very crucial. In most of the literature, the heat loss information is either not considered or not reported.
- For a single-component fuel, the enthalpy calculation (Eq 2.3-2.4) at the inlet and exit conditions is much simpler. But for multi-component fuels, obtaining the enthalpy change value challenge. In many articles, researchers have considered an equivalent single-component fuel in computing the enthalpy change for multicomponent fuels.
- In more than 90% of the literature, scientists have reported only the reactor-containing coke and have not provided insights about carry-away or bulk-flow coke in mentioning the coke deposition data. The total coke should be a combination of both reactor-containing coke and carry-away coke.
- Although some studies mentioned about the use of initiators in enhancing cracking reactions, explicit details regarding feed and product characterization and the impact of initiators on coke deposition aspects are often ignored.
- Some researchers have studied the heat transfer characteristics of hydrocarbon fuels under supercritical conditions. However, simulation studies on coke depositions within the cooling channel are not explicitly studied.

Chapter-3

Materials, Experimental, and Characterization

Details

Materials, Experimental, and Characterization Details

3.1. Materials

The raw materials and analytical chemicals considered for the present work were procured from various sources. Hydrocarbon fuels, designated as HCF-1 and HCF-2, were procured from Ogene Systems India Pvt. Ltd., India. The fuels were used for pyrolysis studies without further treatment. n-Heptane (CAS: 142-82-5, 99%), methylcyclohexane (CAS: 108-87-2, 99%), toluene (CAS: 108-88-3, 99%) were procured from SRL Pvt. Ltd., India. Triethylamine (TEA) (CAS: 121-44-8, 99%) and di-tert-butyl-peroxide (DTBP) (CAS: 110-05-4, 99%) were procured from S D Fine Chemicals Ltd., India. Experimentally determined properties of the HCF-1, HCF-2, and other hydrocarbon fuels considered in this research are given in Table 3.1, and more details are available in subsequent chapters. A flow diagram of the hydrocarbons considered for the experimental work is shown in Fig 3.1.

Table 3.1: Properties of hydrocarbon fuels

Properties	n-heptane	MCH	Toluene	HCF-1	HCF-2
Specific gravity at 28 °C	0.67	0.76	0.86	0.790	0.795
Boiling range (°C)	95.8-96.1	98.2-98.8	107.8-108.7	168-220	172-219
Average boiling point* (°C)	96	98.5	108.4	187	191
Aniline point (°C)	68 ± 1	39 ± 1	< 20	66 ± 1	68 ± 1
Aromatic content (vol. %)	0	0	100	9.6 ± 0.2	8.3 ± 0.2

*Data are obtained from ASTM D86 distillation

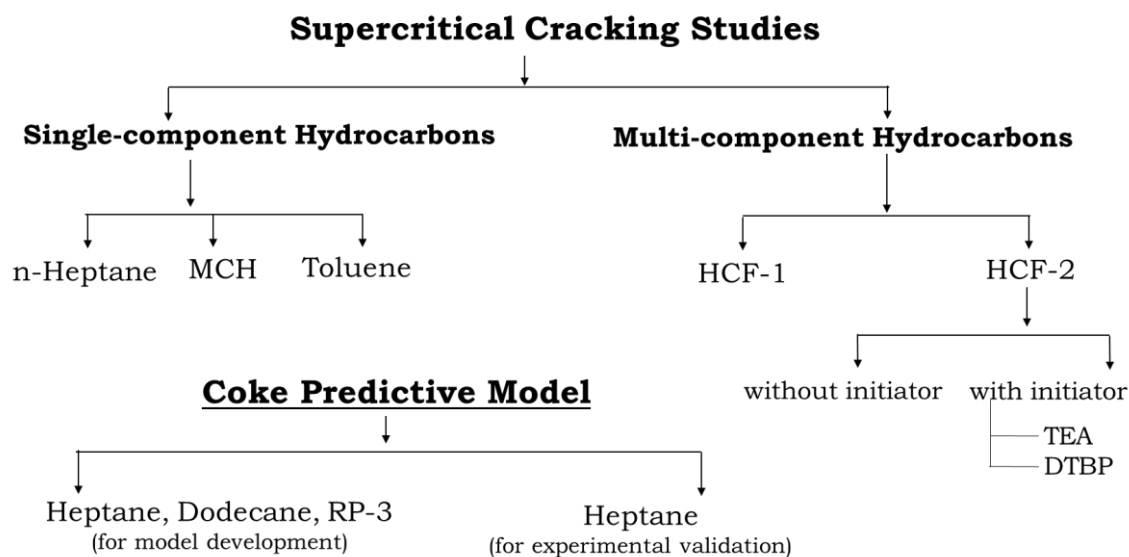


Fig. 3.1: Flow diagram of hydrocarbons considered for experimental studies.

Other laboratory-grade analytical reagents, such as n-pentane (CAS: 109-66-0, 99%) 1-hexene (CAS: 592-41-6, 99%), n-hexane (CAS: 110-54-3, 99%), benzene (71-43-2, 99%), cyclohexane (CAS: 110-82-7, 99%), 1-heptene (CAS: 592-76-7, 97%), 1-octene (CAS: 110-82-7, 99%), 1-octene (CAS: 111-66-0, 98%), n-octane (CAS: 111-65-9, 99%), m-xylene (CAS: 1330-20-7, 99%), o-xylene (CAS: 95-47-6, 98%), n-nonane (CAS: 111-84-2, 99%), n-decane (CAS: 124-18-5, 99%), n-undecane (CAS: 1120-21-4, 99%), n-dodecane (CAS: 112-40-3, 99%) were procured from Hychem Laboratories, India. Nitrogen (N₂) gas (99.9%) and oxygen (O₂) gas (99.9%) were procured from G.M. Tech, India. A calibration gas mixture comprising methane (15.4%), ethane (4.8%), ethylene (9.3%), propane (9.9%), propylene (5.1%), isobutane (4.2%), n-butane (3%), 1,3-butadiene (1.8%), 1-butene (4.8%), N₂ (25%), CO₂ (6.2%), H₂ (9.9%) was procured from Chemix Specialty Gases and Equipment, India. Another gas mixture composed of 20% CO₂ and 80% N₂ (by volume) was procured from Chemix Specialty Gases and Equipment, India, for calibration of CO₂ analyzer. For gas chromatography analysis, Helium (He) (99.9%) and argon (Ar) (99.9%) gases were procured from Chemix Specialty Gases and Equipment, India.

3.2. Experimental Setup and Procedure Details

Designing a suitable test rig for conducting pyrolysis experiments of hydrocarbon fuels under supercritical conditions is crucial in this work. The heat sink characteristics of hydrocarbon fuels cannot be accurately determined using a simple furnace-heating reactor setup. An autoclave or a batch reactor is not suitable for performing a constant pressure cracking experiment. Fabricating a setup that closely simulates the conditions of an actual supersonic vehicle is a challenging task. In the present work, a high-pressure tubular flow reactor was fabricated to perform the pyrolysis experiments under supercritical conditions.

A schematic of the experimental setup used to investigate the cracking behavior of hydrocarbon fuels under supercritical conditions is shown in Fig. 3.2 and the image of the setup is shown in Fig. 3.3. The setup consists of a 5 L capacity fuel tank, high-pressure fuel pump, direct power supply system, stainless steel reactor, filters, step-down transformer, temperature sensors, gas-flow meter, pressure sensor, back-pressure regulator, double pipe heat exchanger, and gas-liquid separator with necessary connections and fittings. The reactor section consists of a 750 mm long SS-316 tube with an internal diameter (ID) of 2 mm, spot-welded thermocouples, and a step-down transformer with a power regulator. The reactor section was covered with a 30 mm thick asbestos block from all sides to minimize heat losses to the surrounding environment. Five K-type thermocouples were spot-welded at equidistant along the reactor length to measure the reactor surface temperatures. A gap of 50 mm was left between the two ends to allow the clamps of the direct heating terminals. The temperature of the last thermocouple (placed at a distance of 80 ± 1 mm before the exit end) was considered as the reactor temperature in this study. The temperatures of the fuel at the reactor inlet and exit were measured using thermocouples that are directly in contact with the fuel. For safety purposes, a high-pressure alarm facility coupled with the fuel pump was always activated during the experiments. For additional safety, the reactor section was covered with a transparent enclosure during the experiment.

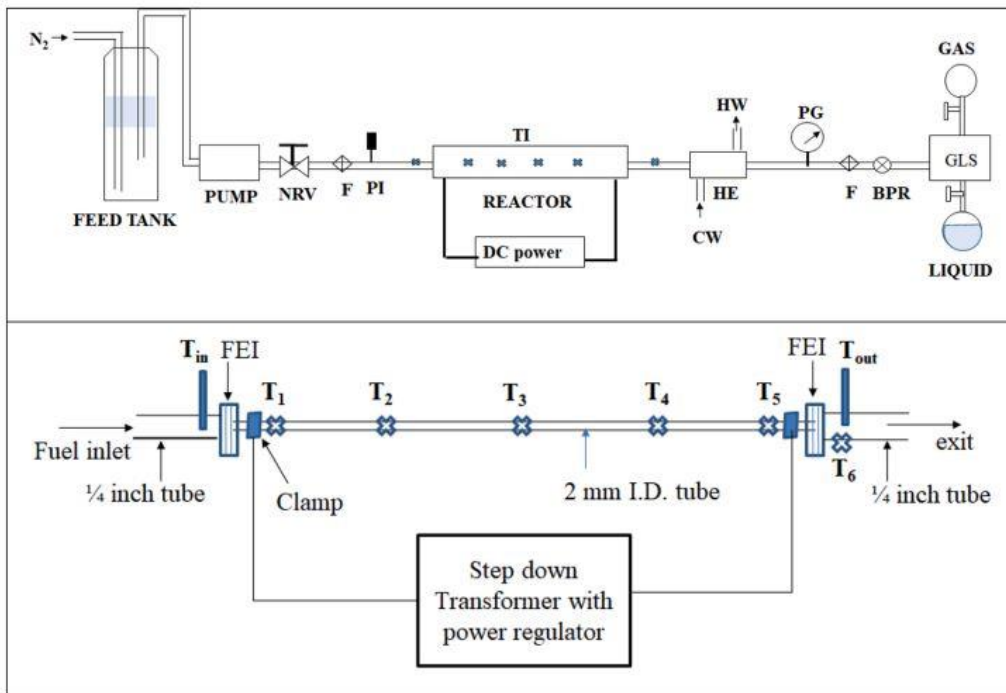


Fig. 3.2: A schematic (top) of test setup and a zoomed view of reactor section (bottom).
(NRV: non-return valve, filter, PI: pressure indicator, HE: heat exchanger, PG: pressure gauge, BPR: back-pressure regulator, GLS: gas-liquid separator, TI: temperature indicator, CW: cold water, HW: hot water, FEI: flanges with electrical isolation, T_1 – T_5 : spot-welded thermocouples, T_{in} and T_{out} : thermocouples inserted in fuel line).



Fig. 3.3: Photograph of experimental setup.

The fuel tank was filled with about 4 L of test fuel. During the experiment, the liquid fuel was constantly purged with N₂ gas to reduce the concentration of dissolved oxygen in the fuel. The fuel was pumped through the reactor line at a desired flow rate. The back-pressure regulator was used to increase the pressure in the reactor line to a desired value. After ensuring no leakage in the reactor line, the data logger software (Thermohumid, model PK2070-51) was enabled, and the electrical power supply was gradually increased to attain the experimental temperature using the step-down transformer and dimmer stat. Once the reactor temperature reached the desired value of experimental temperature, no further increments in power supply were performed. In all experiments, the temperature reading of the T₅ thermocouple (shown in Fig. 3.2) was considered as the reactor exit temperature or reactor temperature in the present thesis. After reaching a stable value of the desired temperature, the experiment was carried out for about 20 minutes to collect sufficient gas and liquid products. The reactor exit stream was depressurized to atmospheric pressure after passing through a water-cooled heat exchanger. After depressurization, the product stream was directed to the gas-liquid separator. The Gaseous stream was passed through a gas flow meter and collected in a gas bladder for its composition analysis. The gas flow rate reading was logged at 20-second intervals, and the average value was used in the subsequent mass balance analysis. The liquid product flow rate was measured three times at an interval of 6 ± 1 minute, and the average of the three readings was used for computational purposes. The liquid products were collected in a glass vessel for further investigation. After collecting the gas and liquid samples, the reactor power source was turned off, and the reactor was allowed to cool down. When the reactor temperature dropped below 60°C, the fuel flow was stopped, and N₂ gas flow was directed through the reactor to flush out the hydrocarbon fuel from the reactor line. Upon completion of the pyrolysis experiment, the downstream section was disconnected from the reactor portion for the coke analysis, and the procedure details are elaborated in section 3.4.

3.3. Numerical Simulation on Thermal Cracking of Hydrocarbons

Apart from the experimental work, simulation studies on hydrocarbon cracking were also performed in this research. The main purpose of the simulation work is to develop a predictive coke model based on cracking kinetics and fuel properties. FLUENT 21 software with the finite

volume method was used in numerical simulation. The SIMPLEC algorithm coupled with pressure and velocity parameters into the FLUENT. The least squares cell method with a second-order implicit scheme was chosen for spatial discretization. A second-order upwind scheme is used for turbulent kinetic energy and turbulent dissipation rate to improve accuracy and robustness in computation. A global kinetic model was used to estimate the product species distribution.

To investigate the fuel cracking, as shown in Fig. 3.4, and coking phenomena along the length of the reactor, a two-dimensional (2D) axisymmetric geometry, as shown in Fig. 3.5, was constructed for computation. S1 is the domain that represents the bulk fluid phase, and S2 indicates fluid and metal wall interfaces, L and r are the length and radius of the reactor tube. An inflated mesh with a thickness of 5×10^{-4} mm for fifty layers was assigned in the simulation to capture the variation in fluid properties and its influence on flow analysis. The aim of this study is to find the concentration of coke precursors at various points along the reactor length. The concentration of coke precursors, operating parameters, and feed properties were coupled to develop a coke model. More details about the Coke model are mentioned in Chapter 7.

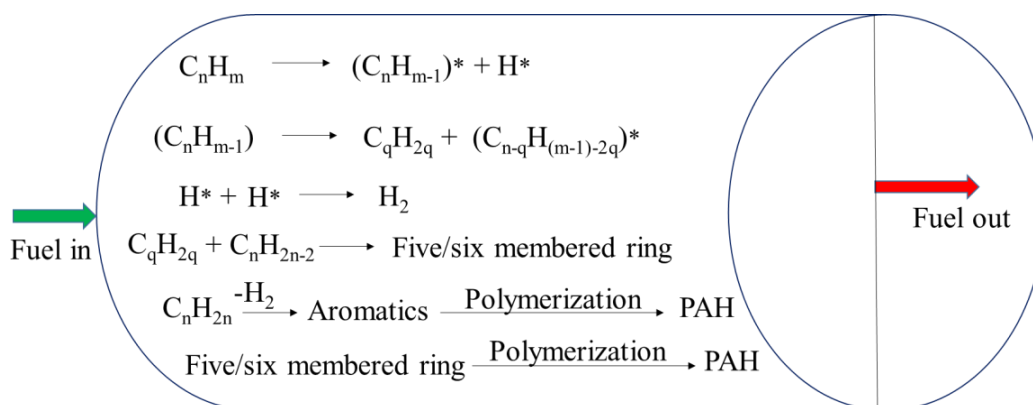


Fig. 3.4: A schematic of thermal cracking of hydrocarbon in a flow reactor.

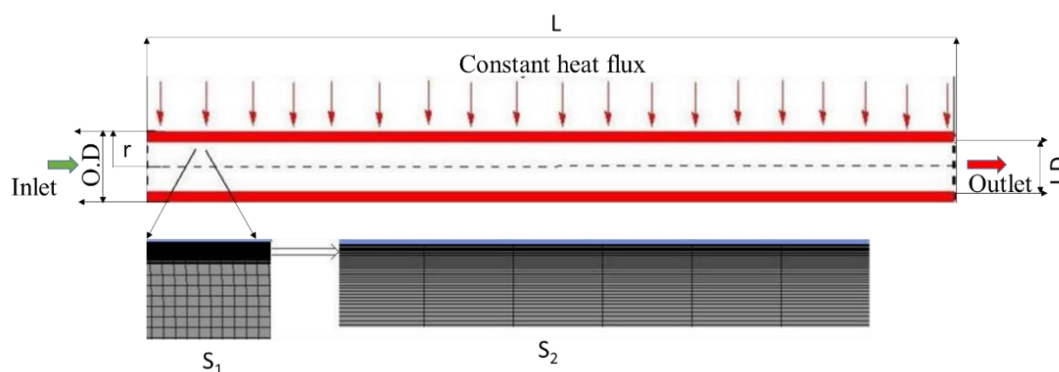


Fig. 3.5: Scheme of computational domain considered in numerical.

3.4. Characterization Techniques Used in Present Research

Several characterization techniques and methodologies were employed in the study to evaluate the physico-chemical properties of the fuels and cracked products. A brief description of the key analysis procedures is given below.

3.4.1. GC and GC-MS analysis

The gas chromatography (GC) technique was used to identify the composition of the gas and liquid mixture. To identify the components in the fuel samples, a GC instrument (Agilent 7820A) equipped with a BP-1 PONA column and a flame ionization detector (FID) was used in the study. N_2 gas was used as the carrier gas, and a mixture of H_2 and air was used for ignition. In the analysis, the temperature program used for the column includes a gradual increase in temperature from $70\text{ }^\circ\text{C}$ to $120\text{ }^\circ\text{C}$ at a rate of $5\text{ }^\circ\text{C}/\text{min}$, held for a minute at $120\text{ }^\circ\text{C}$, and then raised again to $280\text{ }^\circ\text{C}$ at a rate of $2\text{ }^\circ\text{C}/\text{min}$. A liquid mixture comprising of n-heptane, 1-hexane, benzene, cyclohexane, 1-heptene, iso-octane, methylcyclohexane, 1-octene, n-octane, toluene, o-xylene, n-nonane, n-decane, n-undecane, n-tetradecane, and n-hexadecane was used to calibrate the GC. Further, to quantify the various compounds in the liquid feed and products, a GC-MS (model Agilent 5977) analyzer coupled with an HP-5 column and an FID detector was used in the work. Helium gas was used as the carrier gas. The temperature program adopted for the column includes a ramp from $50\text{ }^\circ\text{C}$ to $180\text{ }^\circ\text{C}$ at a rate of $5\text{ }^\circ\text{C}/\text{min}$, hold at $180\text{ }^\circ\text{C}$ for 5 minutes, and then elevate to $300\text{ }^\circ\text{C}$ at a rate of $10\text{ }^\circ\text{C}/\text{min}$. The temperature of the detector was fixed at $300\text{ }^\circ\text{C}$, while the temperature of the quadrupole MSD was kept at $150\text{ }^\circ\text{C}$.

3.4.2. Micro-GC analysis

A multichannel micro-GC instrument (Agilent 490) was employed for analyzing the composition of cracked gas products. The GC system is equipped with three independent columns and thermal conductivity detectors (TCD). Channel-1, consisting of a molecular sieve 5A column (2.25 mm ID, 10 m long), was used to identify H₂, N₂, O₂, methane (C₁), and CO gases. Channel-2 consists of a PoraPLOT U column (0.25 mm ID, 10 m long) used to identify C₂ (i.e., ethane, ethylene, and acetylene) hydrocarbons. Channel-3 coupled with SP-1 column (0.15 mm ID, 10 m long) was used to identify mainly C₃ (propane and propylene) and C₄ (butane, butene, isobutane, 1,3-butadiene, etc.) hydrocarbons. In the analysis, Ar gas was used for Channel-1 and He was used for the other channels as carrier gases. The temperature and pressure program used for the three channels is listed in Table 3.2.

Table 3.2: Temperature and pressure program used for Micro-GC

	Channel-1	Channel-2	Channel-3
Injection temperature (°C)	110	110	110
Carrier gas pressure (kPa)	150	110	80
Temperature (°C)	80	120	120

3.4.3. Scanning electron microscope (SEM) analysis

An SEM apparatus (Apreo FESEM) paired with an Evehart-Thomley detector was used in the study to examine the surface morphology of solid deposits or coke samples. Back-scattered electrons (BSE) signals were employed in the analysis to generate surface pictures of the samples. To improve the electrical conductivity of the test samples, the samples were spread over a silicon wafer and sputtered with an Au material. The analysis was made in a vacuum mode with a voltage of 20 kV at various magnifications.

3.4.4. ASTM D86 distillation characteristics

ASTM D86 is the standard test technique used to measure the boiling range characteristics of petroleum-derived fuels under atmospheric pressure. The distillation curve produced by the ASTM D86 method is often called the D86 distillation curve. The test quantifies

the percentage of sample vaporized with temperature. An automated ASTM D86 distillation equipment (Haage DA 40.10, Estant GmbH) was used to find the boiling properties of feed fuel and product samples. The distillation flask was filled with 100 mL of the test sample and placed inside the heating chamber. The generated vapors passed through the condenser, maintained below 25 °C. The condensed vapors were collected in a measuring cylinder. The system automatically measured the volume of distillate and the corresponding vapor temperature. The analysis provides the Initial boiling point (IBP), Final boiling point (FBP), and average boiling point (T_{avg}) temperature of test samples. The following formula (Eq. 3.1) was used to calculate the T_{avg} value of the fuel samples.

$$T_{avg} (\text{°C}) = \frac{T_{10\%} + T_{20\%} + T_{30\%} + T_{40\%} + T_{50\%} + T_{60\%} + T_{70\%} + T_{80\%} + T_{90\%}}{9} \quad \text{Eq. (3.1)}$$

where, $T_{10\%}$ and $T_{20\%}$ indicate the temperature corresponds to 10% and 20% (by volume) of distillate collection, respectively.

3.4.5. Moisture content analysis

The moisture content of the fuel samples was determined using a Karl Fischer (KF) Titrator (Spectralab MA-101C). Initially, 50 mL methanol was added to the KF sample holder, and the moisture content of the methanol sample was neutralized with KF reagent. Then, about 10 mg fuel sample was added to the same vessel, mixed for 5 minutes, and titrated with KF reagent until neutralization. The moisture content percentage of the sample was calculated using the following expression (Eq. 3.2).

$$\text{Moisture content (wt.\%)} = \frac{\text{volume (ml) of KF reagent} \times F}{\text{weight (mg) of fuel sample}} \times 100 \quad \text{Eq. (3.2)}$$

where, 'F' is the KF reagent factor, mg/mL. The value of 'F' was estimated by titrating 10 mg of pure water in the neutralized methanol and the obtained value of the factor is 2.2 mg/mL.

3.4.6. Aniline point analysis

The aniline point test is used to get a qualitative idea about the relative value of aromatics present in fuel samples. In the work, the aniline point temperature of the fuel and liquid products

was measured using an aniline point apparatus (Popular Science Apparatus Workshop Pvt. Ltd. India). In the analysis, an equal volume (10 mL) of anhydrous aniline and the hydrocarbon sample was taken into a test jar. The mixture is heated gradually until the two phases blend into a single-phase solution. The minimum temperature at which the two-phase mixture converts to a single-phase solution during heating is referred to as the aniline point temperature of the test sample. A higher value of aniline temperature signifies a lower amount of aromatic content in the test sample.

3.4.7. Calorific value analysis

The calorific value of a fuel sample measures the amount of energy content in the fuel. The quantity of energy released during the complete combustion of a unit mass of a test sample is the calorific value of the sample. Fuel efficiency is directly related to the calorific value of a fuel. In the work, a bomb-calorimeter apparatus (Hamco Automatic Bomb calorimeter) was used to determine the gross calorific value of the hydrocarbon fuels. The calorimeter water bucket is filled with 2 L of distilled water. About 1 g of fuel sample was taken into the sample holder. The bomb is filled with oxygen gas to a pressure of 30 bar. The bomb was placed into the calorimeter, and the electrodes were safely attached to both the bomb and the ignition unit. After ignition, the temperature rise was recorded at regular intervals. The following expression was used to estimate the gross calorific value of test samples. The measured calorific value of the studied fuels is in the range of 40 to 50 MJ/kg.

3.4.8. Coke analysis

For a continuously-flow reactor, the total coke is the sum of ‘carry-away’ or ‘flow away’ coke and ‘reactor-containing’ coke. In the present research, different techniques (namely gravimetric and spectroscopic) were used to quantify the two types of coke. The gravimetric method was used to quantify the ‘carry-away’ or ‘flow-away’ coke, whereas the spectroscopic technique was used to estimate the amount of ‘reactor-containing’ coke. Most of the carry-away coke was deposited near the 7-micron filter, placed before the back-pressure regulator. The downstream segment of the reactor line was cleaned with acetone to collect the carry-away coke. The coke sediment was filtered and dried at $100 \pm 3^\circ\text{C}$ before measuring its weight. In the spectroscopic method, the reactor-containing coke was indirectly measured by converting the

=====

coke into CO₂. The reactor-containing coke was burned in the presence of air at about 700 °C. A non-dispersive infrared-based CO₂ analyzer was used to measure the concentration of CO₂ in the flue gas. The CO₂ concentration and gas flow results were used to estimate the amount of reactor-containing coke according to Eq. 3.3. The sum of the carry-away coke (obtained from the reactor downstream section) and reactor-containing coke (obtained from the reactor section) is the total amount of coke formed during the pyrolysis experiment. The following expression (Eq. 3.4) was used to determine the coke deposition rate in this thesis.

$$\text{Reactor - containing coke (g)} = \frac{\text{CO}_2 \text{ concentration (ppm)} \times \Delta t \text{ (min)} \times \text{gas flow rate (cc / min at STP)} \times M_w \text{ (g / mol)}}{V_m \text{ (cc / mol)}} \quad \text{Eq. (3.3)}$$

$$\text{Coke deposition rate (mg / (min))} = \left(\frac{\text{total coke (mg)}}{\text{experimental duration (min)}} \right) \quad \text{Eq. (3.4)}$$

where, M_w = molecular weight of carbon, and V_m = volume of gas at STP condition.

3.4.9. Mass balance analysis

For a flow process, mass or material balance analysis plays a vital role in considering a valid experiment. In the current study, to check the overall mass balance, 'mass in' into the reactor and 'mass out' from the reactor were calculated in each experiment. A brief of the steps followed in the analysis is:

$$\text{Mass inflow (g / min)} = \text{feed flowrate (mL / min)} \times \text{feed density (g / mL)} \quad \text{Eq. (3.5)}$$

$$\text{Mass outflow (g / min)} = \text{liquid overflow (g / min)} + \text{gas outflow (g / min)} + \text{coke formation rate (g / min)} \quad \text{Eq. (3.6)}$$

$$\text{Liquid outflow (g / min)} = \text{liquid flowrate (mL / min)} \times \text{density of liquid (g / mL)} \quad \text{Eq. (3.7)}$$

$$\text{Gas outflow (g / min)} = \text{gas flowrate (mL / min at STP)} \times \text{average density of gas (g / mL at STP)} \quad \text{Eq. (3.8)}$$

The flow rate of gas and liquid products was measured during the experiment. The average density of gas was estimated from the composition analysis of gaseous products. Eq. 3.4

was used to find the coke formation rate. For all the reported results in this thesis, the mass balance analysis satisfied between 95% and 99%.

3.4.10. Repeatability and Uncertainty

In most circumstances, experimental investigations are not fully free from some degree of error and uncertainty. Generally, the error percentage is relatively higher for small-scale (< 1 g) studies compared to bench-scale experimental studies. A significantly larger amount (\approx 15 - 40 g/min) of fuel material was considered for the present studies. To find the difference in results between two identical runs, about 70% of the cracking experiments were repeated, and the observed variation was less than 5% in all the experimental results. However, in the case of gas analysis results, the difference between the two identical analyses was slightly higher side (nearly 5- 8%). To accommodate the percentage deviation in the experimental results, an error bar symbol has been used in most of the results presented in this thesis. Uncertainty in experimental data may be due to fluctuations in operating variables. The typical value of fluctuation noted in the instrumental readings are: reactor temperature: ± 3 °C; reactor pressure ± 1 bar; fuel flow rate ± 0.1 g/min, and power input from stepdown transformer: ± 15 watts.

Chapter-4

Investigation of Cracking Characteristics of Single-Component Hydrocarbons Under Supercritical Conditions

Investigation of Cracking Characteristics of Single-Component Hydrocarbons Under Supercritical Conditions

4.1. Introduction

The efficacy of hypersonic vehicles depends on the management of thermal loads that arise due to fuel combustion, especially at speeds exceeding Mach-5 (Curran et al. (2001)). Passive cooling techniques, like insulating and coating materials, can enhance safety and speed limits, but the extra weight can reduce the overall performance of an engine. Cryogenic fuels, such as liquid methane and hydrogen, can offer efficient cooling but require a larger volume for storage. Cooling of hypersonic engines by the utilization of onboard fuel can be an efficient technique, as reported by many authors. However, the sensible heat sink of a fuel alone cannot provide enough cooling capacity. Hence, the extraction of additional heat by fuel cracking reactions is a viable approach to enhance the overall heat sink capacity of a fuel and engine efficiency (Zhang et al. (2021), Mahapatra et al. (2008)). The suitability of catalytic cracking of hydrocarbons under supercritical conditions to improve fuel conversion and heat sink value has also been investigated by several authors (Yeh et al. (2015), Xian et al. (2010)). However, coating of catalytic material within a narrow tube is a significant challenge in practice. The formation of coke at high temperatures is a critical issue for achieving high conversions (Hou et al. (2014)). Studies have been conducted to evaluate the efficacy of additives/initiators in reducing coke deposition during pyrolysis reactions (Liu et al. (2008), Wang et al. (2020)). The pyrolysis of hydrocarbons with differing molecular structures was investigated by Liu et al. (2020). The study concluded that the heat sink capacity of iso-alkanes is greater than that of straight-chain alkanes and cyclic alkanes under similar environments.

In most thermal cracking studies, experiments were conducted at a temperature range of 450-650 °C and a pressure below 40 bar. Although for most hydrocarbon fuels with a carbon number of more than six, the critical pressure is less than 30 bar, the cracked products, such as methane, ethane, and ethylene, can exit under a subcritical state below 40 bar pressure. The critical pressure for methane, ethane, and ethylene are approximately 46, 48, and 51 bar, respectively. In most of the literature, heat sink values for different fuels are furnished without the details of heat loss percentage and the basis of endothermicity calculation. It is also noted

that the information related to fuel conversion, product composition, and coke deposition is not furnished in a single document. Hence, the limitations in the current literature prompted us to design an appropriate test setup to perform fuel-cracking experiments at high temperatures (up to 750 °C) and under 60 bar pressure. The objective is to examine the cracking characteristics and heat sink capacity of different hydrocarbons under supercritical conditions. In the present chapter, hydrocarbons with an equal number of carbon atoms but with different configurations were chosen to investigate their cracking characteristics under supercritical environments. Three hydrocarbons, namely n-heptane (straight-chain alkane), methylcyclohexane (cyclo-alkane), and toluene (aromatic compound), were considered in the investigation. The other aspect of the present investigation is establishing a standard methodology for analyzing and estimating various parameters like fuel conversion, coke deposition, and heat sinks. The experimental results are compared to understand the influence of hydrocarbon types on cracking conversion, coke deposition rate, and heat sink capacities for a temperature range of 500 °C to 700 °C. Additionally, a kinetic study was performed to determine the kinetic parameters of the cracking reactions.

4.2. Materials, Experimental Procedure, and Characterization Techniques

For the present work, n-heptane, methylcyclohexane, and toluene were procured from SRL Pvt. Ltd., India. Other analytical reagents were procured from Hychem Laboratories, India. N₂ gas (99.9%) and O₂ (99.9 %) were procured from G.M. Tech., India. A calibration gas mixture comprising methane (15.4%), ethane (4.8%), ethylene (9.3%), propane (9.9%), propylene (5.1%), isobutane (4.2%), n-butane (3%), 1,3-butadiene (1.8%), 1-butene (4.8 %), N₂ (25%), CO₂ (6.2%), H₂ (9.9%) was procured from Chemix Specialty Gases and Equipment, India.

A high-pressure flow reactor was used to conduct the pyrolysis experiments under supercritical conditions. The schematic of the experimental setup is presented in Fig. 3.1 in Chapter-3. In each case, after attaining a stable temperature, the experiment was performed for about 20 min to collect the gas, liquid, and coke data. Gas and liquid samples were collected separately for further analysis. Further details about the experimental procedure are reported in Chapter-3.

About 40 % of the cracking experiments were repeated to find the deviation between two repeated runs, and the observed variation lies within 5% in all the experimental results. However, in gas analysis using micro GC, a slightly higher percentage (5% to 8%) difference between two identical analyses was noted specifically for the gases with less than 5 % contribution in the gas mixture. An error bar is kept in most of the experimental results to indicate the deviation in the experimental results. Uncertainty in experimental results can arise due to fluctuations in operating variables. The typical value of fluctuation noted in the instrumental readings is reactor temperature: ± 3 °C; reactor pressure ± 1 bar; fuel flow rate ± 0.1 g/min, and power input from the stepdown transformer: ± 12 watts (which is about 1% of total power input).

4.3. Results and Discussion

In the present investigation, the pyrolysis studies of three hydrocarbons, namely n-heptane, methylcyclohexane (MCH), and toluene, were conducted under supercritical conditions between a temperature range of 500 °C to 700 °C. In each run, the reactor pressure was maintained at 55 ± 1 bar to eliminate phase separation within the reactor line. In each run, the feed flow rate was maintained at 24 ± 0.1 g/min. A comprehensive analysis was performed to examine the impact of temperature on cracking conversion, gas and liquid product compositions, coke deposition rate, and heat sink capacity.

4.3.1. Physico-chemical properties of n-heptane, MCH, and toluene

The physico-chemical characteristics of n-heptane, methylcyclohexane (MCH), and toluene hydrocarbons are given in Table 4.1. The methods used to find and estimate the various properties are reported in section 3.4 of Chapter-3. Among the three hydrocarbons, the specific gravity of the straight-chain alkane (i.e., n-heptane) is minimal, and the aromatic compound (i.e., toluene) is maximum. The order of calorific value is n-heptane > MCH > toluene.

Table 4.1: Properties of n-heptane, MCH, and toluene

Properties	n-heptane	MCH	toluene	Method/Instrument
Chemical formula	C ₇ H ₁₆	C ₇ H ₁₄	C ₇ H ₈	-
Type of hydrocarbon	alkane	cycloalkane	aromatic	-
Specific gravity at 30 °C	0.674	0.761	0.864	Hydrometer
Normal boiling point (°C)	98.4	101	110.6	NIST database
Aniline point (°C)	68 ± 1	39 ± 1	8 ± 1	Aniline point apparatus
Critical temperature (°C)	267 ± 1	299 ± 1	318 ± 1	NIST database
Critical pressure (bar)	27.3 ± 1	34.7 ± 1	41 ± 1	NIST database
Calorific value (MJ/kg)	46.9 ± 0.5	45.5 ± 0.3	41.8 ± 0.2	Bomb calorimeter

4.3.2. Effect of Temperature on Cracking Percentage of n-heptane, MCH, and toluene

Temperature plays a significant impact on a thermal cracking process. Thermal cracking of hydrocarbons generally occurs at temperatures above 400 °C, and the cracking temperature depends on hydrocarbon carbon chain length and structural orientation. To examine the effect of temperature on fuel conversion of n-heptane, MCH, and toluene, the pyrolysis experiments were conducted at five temperatures, ranging between 500 °C and 700 °C under 55 bar pressure. The cracking percentage of hydrocarbons was determined using the following expression (Eq. 4.1). The mass flow rate of the liquid products above the initial boiling point (IBP) of the feed was estimated using the ASTM D86 distillation. The distillation characteristics of the feed and products obtained at different temperatures are shown in Fig. 4.1. The plots depict that the extent of cracking increased with the increase in reactor temperature. For toluene, the variation in distillation plots with temperature is insignificant. The temperature corresponds to 0.5 vol.% (i.e., $T_{0.5\%}$) and 95 vol.% (i.e., $T_{95\%}$) of distillates are presented in Table 4.2, along with the average boiling temperature ($T_{avg.}$) of the feed and liquid products. Due to inconsistency in IBP readings, the temperature corresponding to 0.5 vol.% (i.e., $T_{0.5\%}$) was considered as a reference temperature. For n-heptane and MCH, the decreasing trend in the $T_{0.5\%}$ and $T_{avg.}$ values with the reactor temperature indicates the presence of low-boiling components in the liquid products.

$$\text{Cracking percentage (wt.\%)} = \left(1 - \frac{\text{mass flow rate of liquid } (\geq \text{feed boiling point}) \text{ product}}{\text{mass flow rate of feed}} \right) \times 100 \quad \text{Eq. (4.1)}$$

Table 4.2: T_{0.5%}, T_{95%}, and T_{avg.} values of feed and products

Feed/product	n-heptane			MCH			Toluene		
	T _{0.5%} (°C)	T _{95%} (°C)	T _{avg.} (°C)	T _{0.5%} (°C)	T _{95%} (°C)	T _{avg.} (°C)	T _{0.5%} (°C)	T _{95%} (°C)	T _{avg.} (°C)
Feed	95.8	96.1	96.0	98.2	98.8	98.5	107.8	108.7	108.4
Product @ 500 °C	92.7	96.2	95.6	98.1	98.9	98.4	107.8	108.7	108.4
Product @ 550 °C	90.4	96.2	95.3	97.2	99.0	98.3	107.7	108.8	108.4
Product @ 600 °C	87.8	96.3	94.4	96.1	99.1	98.2	106.6	108.9	108.4
Product @ 650 °C	79.8	96.7	93.6	94.7	99.7	97.9	107.0	108.6	108.1
Product @ 700 °C	71.8	97.9	92.2	89.8	99.9	97.0	106.2	108.7	108.3

where, $T_{\text{avg.}} = (T_{0.5\%} + T_{5\%} + T_{10\%} + T_{20\%} + T_{30\%} + T_{40\%} + T_{50\%} + T_{60\%} + T_{70\%} + T_{80\%} + T_{90\%} + T_{95\%})/12$

The variation in cracking percentage of n-heptane, MCH, and toluene at different temperatures is shown in Fig. 4.2. The result shows a positive correlation between reactor temperature and cracking percentage. For a fixed temperature, the cracking percentage is in the order of n-heptane > MCH > toluene. At 600, 650, and 700 °C, the cracking percentage of n-heptane is approximately 17, 23, and 31 wt.%, respectively. The cracking percentage of MCH is approximately 8, 14, and 20 wt.% at 600, 650, and 700 °C, respectively. The estimated value of the cracking percentage of toluene at 700 °C is nearly 2.5 wt.%. Based on the experimental results, it can be said that the toluene is thermally stable up to 650 °C. The analysis further revealed that among the three hydrocarbons, toluene (an aromatic compound) exhibits higher thermal stability in comparison to MCH (cycloalkane) and n-heptane (alkane). The stability of aromatic compounds mainly arises due to dense structures and strong Van der Waals interactions.

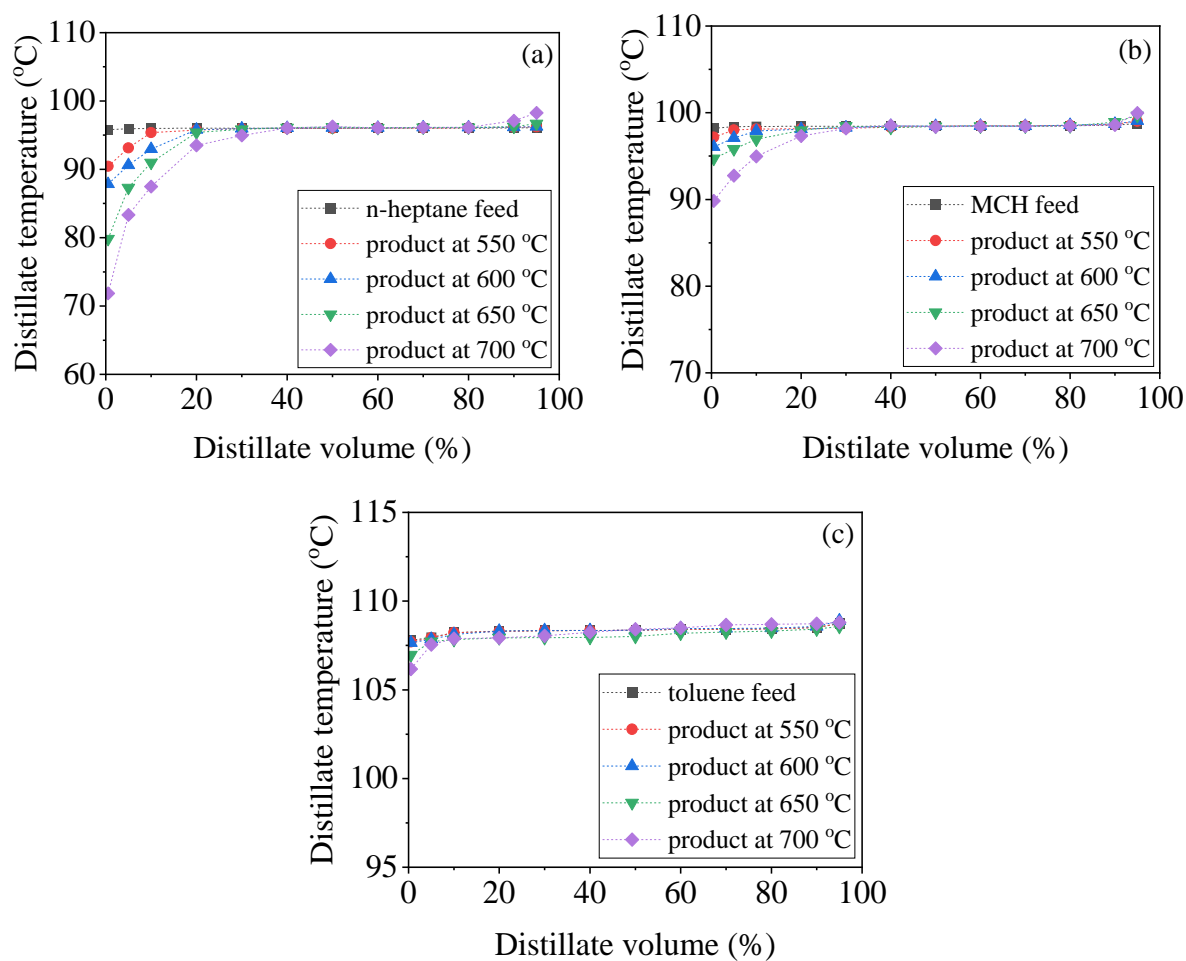


Fig. 4.1: ASTM D86 results of feed and liquid products obtained at different temperatures for a) n-Heptane, b) MCH, and c) Toluene.

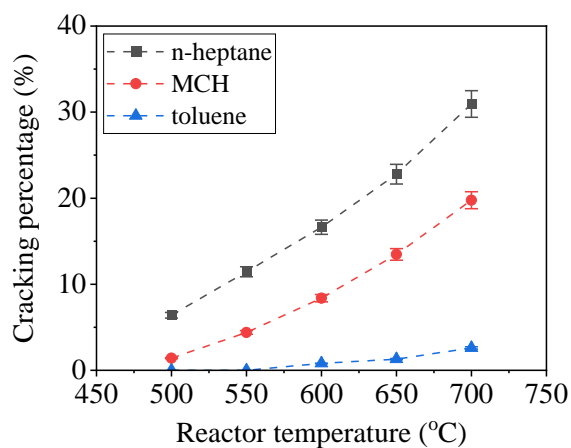


Fig. 4.2: Effect of temperature on cracking percentage of n-heptane, MCH, and toluene.

4.3.3. Effect of temperature on coke deposition of n-heptane, MCH, and toluene

Coking is an unavoidable phenomenon during pyrolysis of hydrocarbons. In the context of present research, coke deposition within a fuel flow line has the potential to cause engine failure by blocking the fuel flow. Unsaturated and cyclic hydrocarbons have a greater tendency to form agglomeration at elevated temperatures. The agglomerated material can act as a precursor for coke formation. Coke deposition can be influenced by various factors, such as cracking temperature, reactor pressure, residence time, hydrocarbon structure, and feed composition. The cracking experiments were conducted at different temperatures to examine the impact of temperature on the coke deposition rate. For a continuously-flow reactor, the total quantity of coke is the sum of 'carry-away' coke and 'reactor-containing' coke. Different techniques were adopted to measure the two types of coke.

A gravimetric technique was used for quantifying the carry-away coke. To collect the carry-away coke, the downstream section was disconnected from the reactor section after each experiment and washed thoroughly with acetone. The sedimentation of solid mass was filtered using the Whatman-42 filter paper. The filtered coke was dried at a temperature of 100 ± 3 °C. Following the drying process, the mass was cooled inside a desiccator and measured its weight. A spectroscopic technique was used to determine the reactor-containing coke. In this method, the coke was converted into carbon dioxide (CO₂) in the presence of oxygen at temperatures greater than 650 °C. The concentration of CO₂ in the flue gas was monitored using a non-dispersive infrared CO₂ analyzer. The flow rate of the exit gas was measured using a flow meter. Eq. 3.3 was used to estimate the reactor-containing coke. The total amount of coke was calculated by adding the carry-away coke to the reactor-containing coke. The coke deposition rate was estimated using Eq. 3.4. The contribution of reactor-containing coke with respect to the overall coke varied between 30% to 60%. At lower temperatures, the contribution of the reactor-containing coke is relatively less.

Fig. 4.3 shows the variation in the coke deposition rate of the three hydrocarbons at different temperatures. The plot illustrates a direct relationship between the reactor temperature and the rate of coke deposition. For a fixed temperature, the coke deposition rate is in the order of n-heptane > MCH > toluene. The analysis also revealed that the rate of coke deposition exhibits an exponential relationship with reactor temperature for n-heptane and MCH. However,

in the case of toluene, the rate of increment is almost linear. Above 550 °C, the exponential increase in the coke deposition rate could be due to secondary cracking and dehydrogenation reactions at higher temperatures. The coke deposition rate of n-heptane, MCH, and toluene at 700 °C is about 19.1 mg/min, 12.9 mg/min, and 4.5 mg/min, respectively. The study shows that the coke deposition rate for n-heptane, MCH, and toluene increased by 1.6, 1.7, and 1.8 times, respectively, as the reactor temperature increased from 650 °C to 700 °C. Further, the analysis showed that, at a fixed cracking percentage, the order of the coke deposition rate is toluene > MCH > n-heptane. Although the cracking conversion of toluene at 700 °C is low (< 3%), the rate of coke deposition is considerably higher (~ 4.5 mg/min). This indicates a higher susceptibility to polymerization reactions for aromatics compared to paraffins at higher temperatures. Li et al. (2021) also noted a similar order of magnitude of coke deposition for the supercritical cracking of EHF-851 fuel.

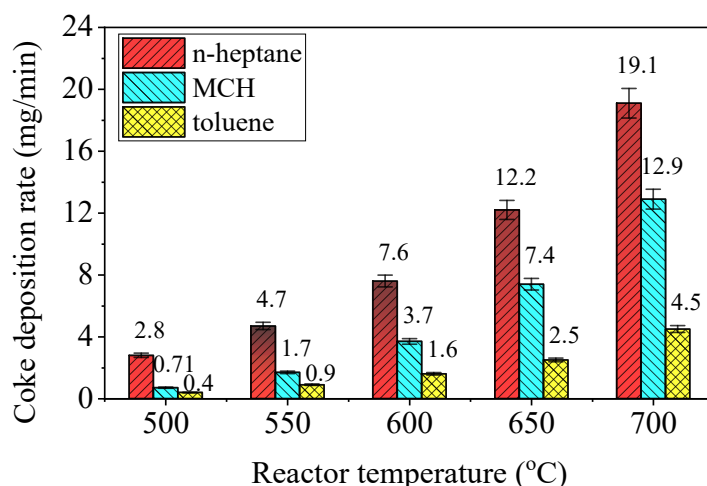
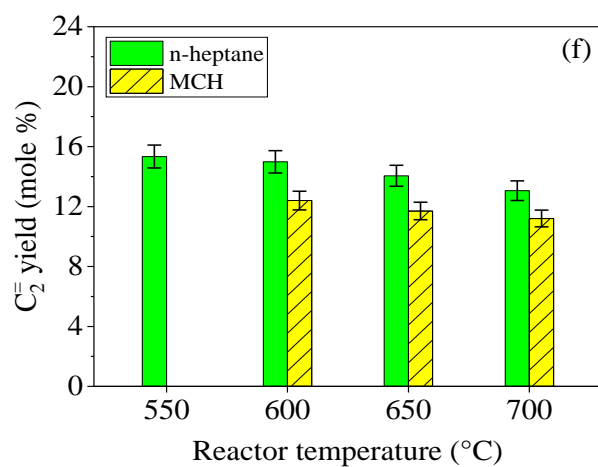
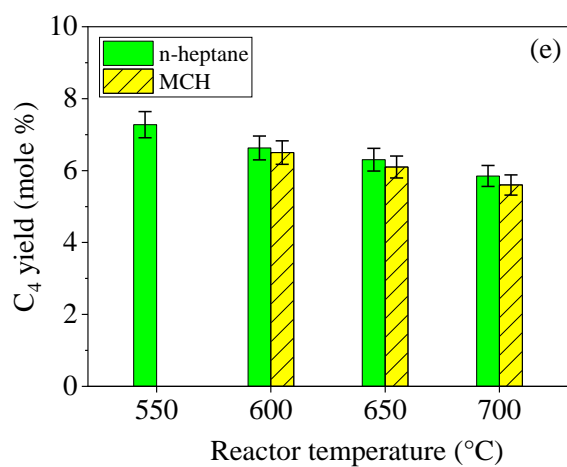
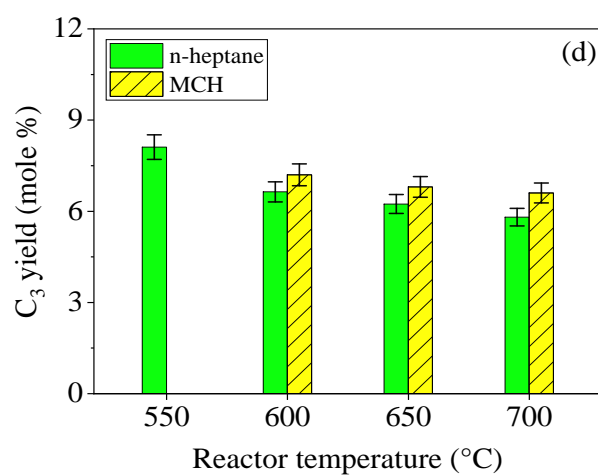
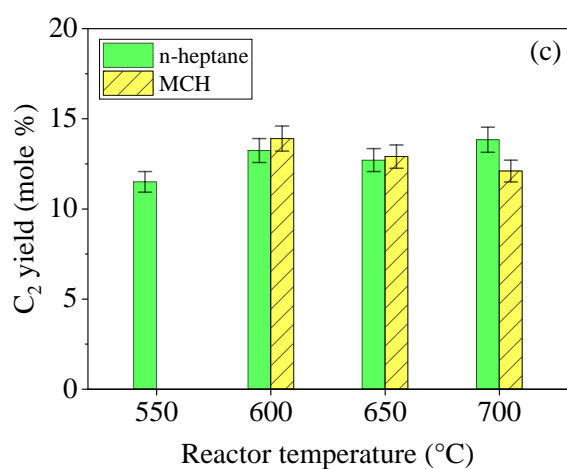
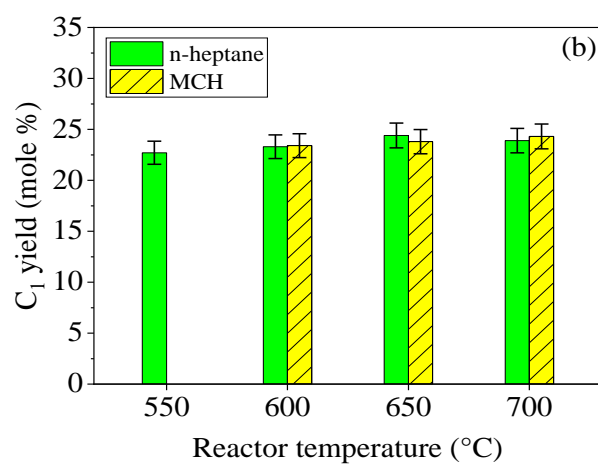
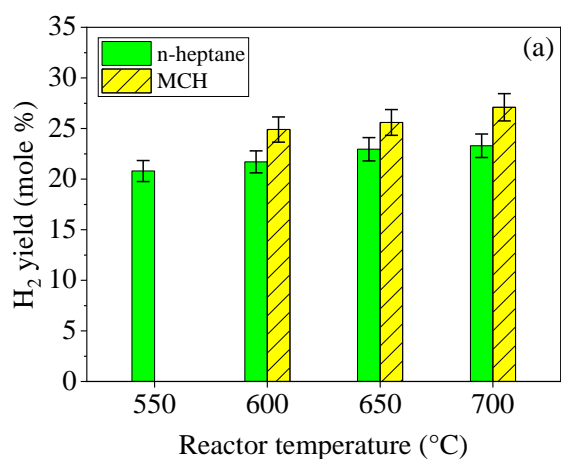


Fig. 4.3: Effect of temperature on coke deposition of n-heptane, MCH, and toluene.

4.3.4. Effect of temperature on gas composition

To ascertain the composition of the gaseous products, the product gas was collected and analyzed using a multi-channel gas chromatography system. The product gas was collected into gas bladders for GC analysis. Before the analysis of the cracked gas product, the GC was calibrated using a calibration gas mixture comprised of hydrogen (H₂), nitrogen (N₂), carbon dioxide (CO₂), and C₁ to C₅ hydrocarbons. Fig. 4.4 shows the composition of the product gases obtained at three different temperatures during the cracking of n-heptane and MCH. The gas

formation rate was significantly low for the 500 °C and 550 °C and was inadequate for the GC analysis. Also, the gas analysis for the toluene samples was not performed due to an inadequate amount of gas collection. The major components found in the gaseous products are hydrogen (H₂), methane (CH₄), ethane (C₂H₆), ethylene (C₂H₄), propane (C₃H₈), propylene (C₃H₆), butane (C₄H₁₀), and butene (C₄H₈). The result shows that the yield of H₂, ethane (C₂), propane (C₃), ethylene (C₂[≡]), propylene (C₃[≡]), and butene (C₄[≡]) increased with the increase in reactor temperature for the n-heptane fuel. A drop in the yield of observed as the temperature decreased. The increase in H₂ concentration and decrease in C₃ concentration with increasing temperature is possibly due to the enhanced rate of dehydrogenation reaction under the current experimental conditions. In the case of MCH cracking, the yield of H₂, C₁, C₃, and C₄ increased as the temperature of the reactor increased. Fig. 4.4a shows that the yield of H₂ for MCH is notably higher (~ 4%) compared to n-heptane at a fixed temperature. A higher value of H₂ yield indicates that the dehydrogenation reaction is favorable for MCH cracking. The dehydrogenation of MCH can lead to the formation of toluene. The yield of methane, as shown in Fig. 4.4b, is higher for MCH compared to n-heptane. Above 600 °C, the pyrolysis of MCH can occur through demethylation and ring-opening reactions. The cracking of MCH can lead to the formation of the methyl cyclohexyl radical. The radical subsequently undergoes a dehydrogenation reaction, resulting in the formation of a toluene. Li et al. (2022) reported a similar phenomenon. Fig. 4.4i illustrates the variation in the molar ratio of olefin- (C₂[≡] + C₃[≡]) to-alkane (C₂ + C₃) as a function of temperature. The plot demonstrates that the olefin-to-alkane ratio is almost constant for n-heptane, while a slight increase is noted for the MCH. The observed upward trend could potentially be attributed to the growing rate of the dehydrogenation reaction. Fig. 4.4j shows an increasing trend in the H₂-to-CH₄ ratio with temperatures for both the hydrocarbons.



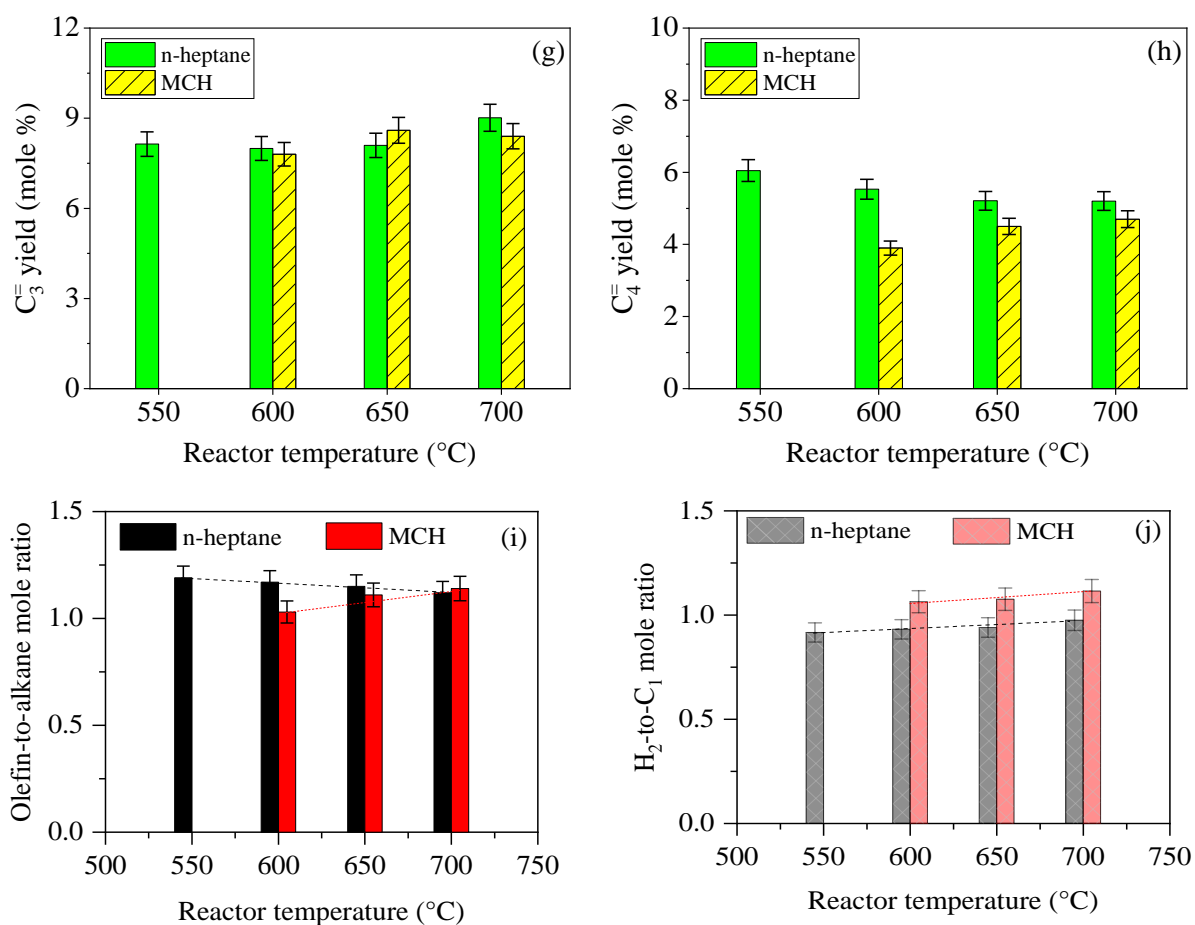


Fig. 4.4: Variation of a) H_2 , b) C_1 , c) C_2 , d) C_3 , e) C_4 , f) C_2^- , g) C_3^- , h) C_4^- compositions, i) olefin-to-alkane ratio, and j) H_2 -to- C_1 ratio in the product gas at different temperatures.

4.3.5. Effect of temperature on liquid product composition

The liquid products were analyzed for hydrocarbon composition using gas chromatography equipped with a PONA column and FID detector. To identify the probable compounds in the liquid products, the GC was calibrated with pure compounds with a carbon number range between C_5 and C_{12} hydrocarbons. The retention time data of the selected pure components is shown in Fig. 4.5. It is noted that the retention time value of the compounds increased with the increase of molecular weight and boiling point of the compounds.

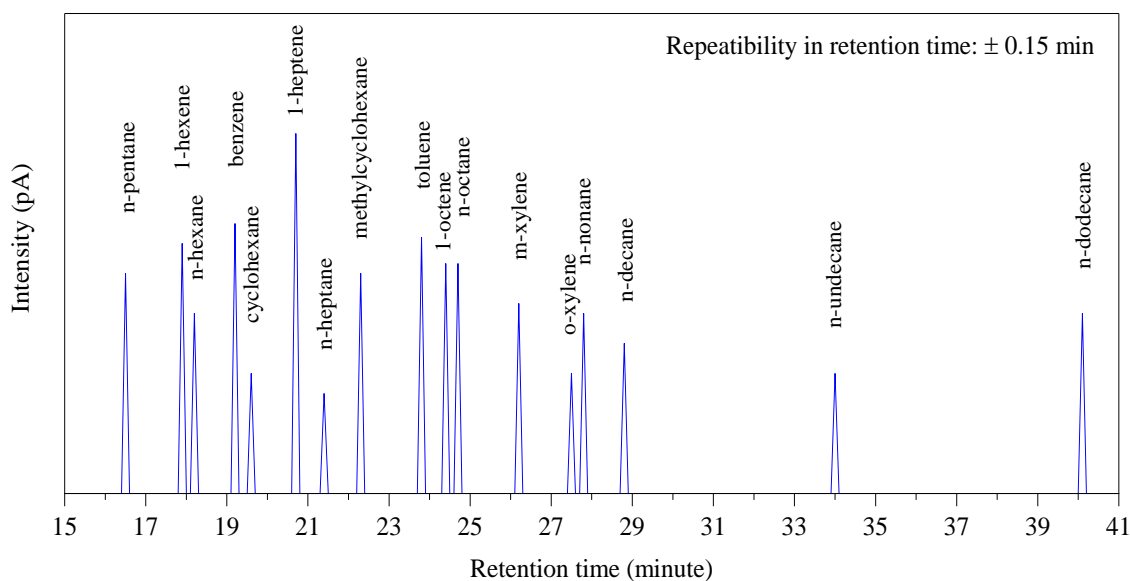


Fig. 4.5: Retention time of selected hydrocarbons.

Following the determination of the retention time of the pure hydrocarbons, the cracked liquid samples were analyzed under similar conditions. The chromatograms of the n-heptane, MCH, and toluene-derived product samples obtained under the conditions of 650 and 700 °C reactor temperatures are shown in Fig. 4.6(a-c). The minor peaks with individual contributions of less than 0.1% are not shown in the figures, and the area percentage mentioned in the figures is truncated to the nearest decimal point. The result shows that the concentration of lighter hydrocarbons (i.e., C₅, C₆) in the liquid products increased with reactor temperature. A few higher boiling components with longer retention times are also noted in the analysis results. The presence of cyclohexane and toluene compounds in the product samples obtained from the cracking of n-heptane (Fig. 4.6a) suggests the possibility of dehydrocyclization reaction during the cracking process at temperatures of 650 and 700 °C. The peaks of high boiling components in the product samples indicate the possibility of polymerization reactions. The ASTM D86 result also supports the possibility of polymerization and/or dehydrocyclization reactions. In the case of MCH (Fig. 4.6b), the GC analysis shows the concentration of dehydrogenated product (i.e., toluene) is significantly higher at 700 °C. This may be because of the formation of more stable aromatic compounds. The higher concentrations (> 99.5%) of toluene in the toluene-derived liquid products (Fig. 4.6c) indicate the thermal stability characteristic of toluene. Even at 700 °C, the cracking percentage of toluene is less than 2%, as found from the GC analysis.

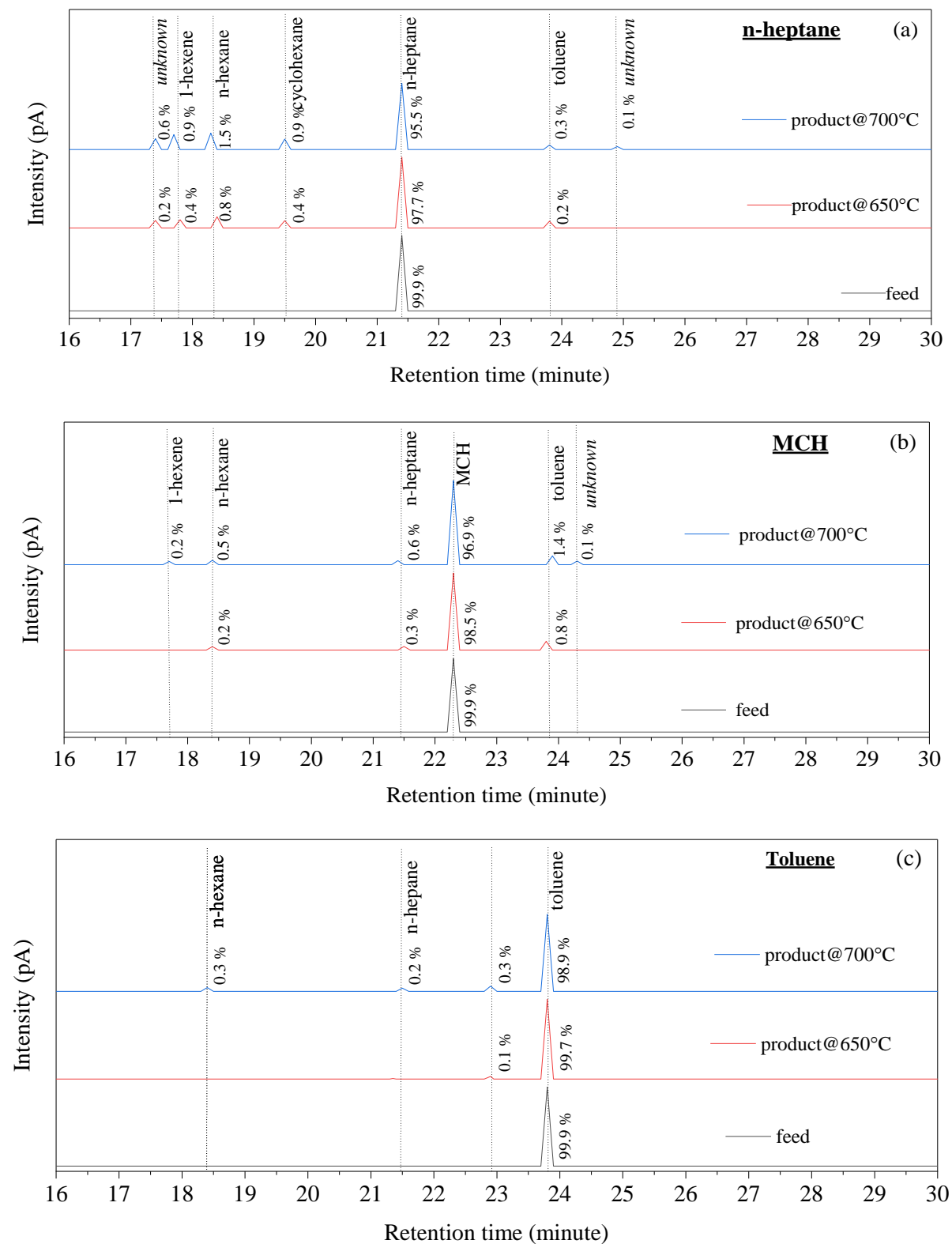
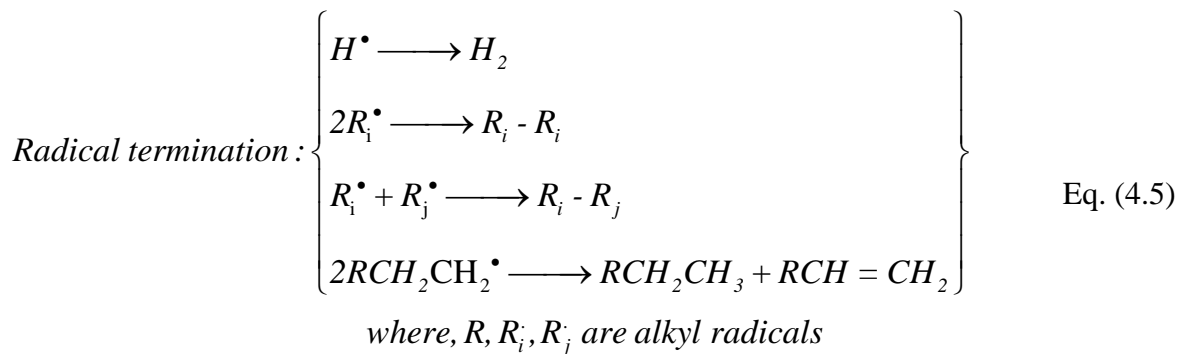
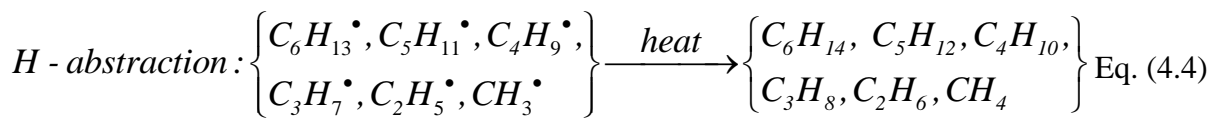
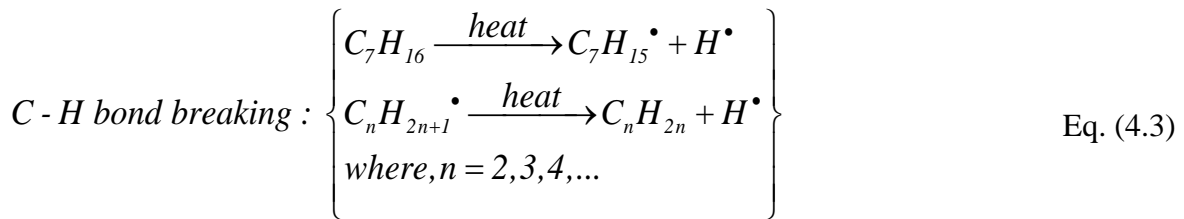
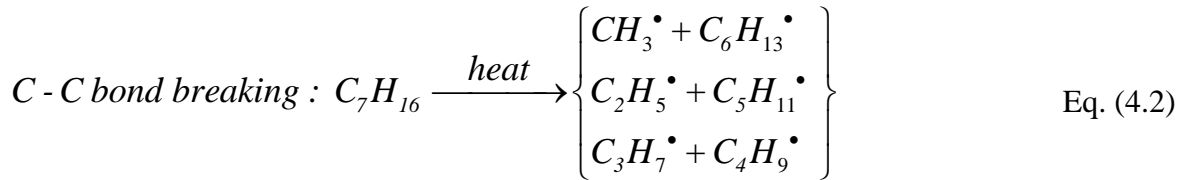
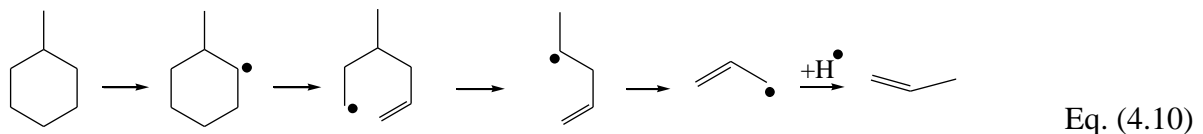
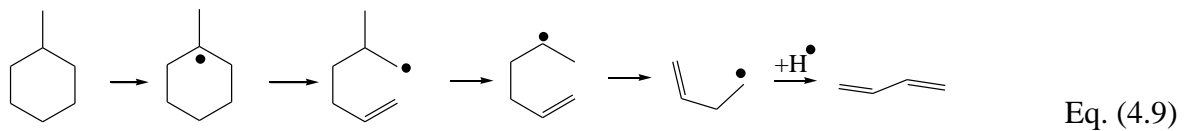
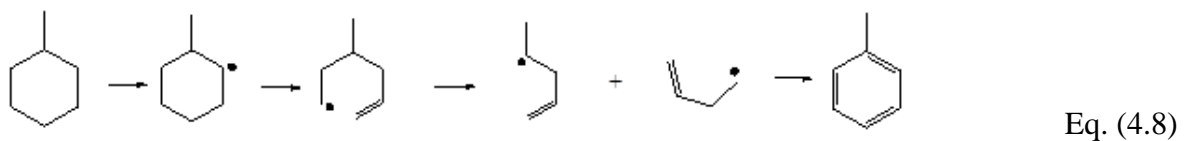
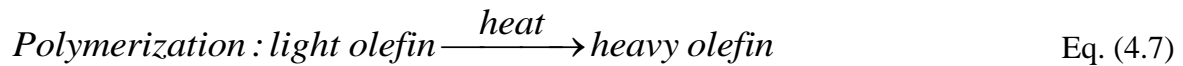
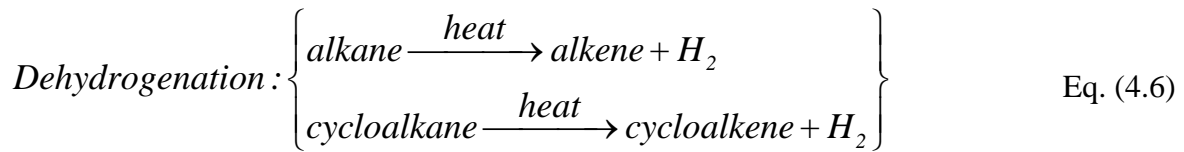


Fig. 4.6: Chromatograms of a) n-heptane, b) MCH, and c) toluene-derived samples.

4.3.6. Probable mechanism of n-heptane and MCH cracking

During the thermal cracking process, various reactions are likely to occur. The free radical chain reaction pathway is one of the most common mechanisms for the thermal cracking of hydrocarbons, as reported by many authors (Jian et al. (1997), Zhang et al. (2018)). The reactions include the formation of alkyl radicals from the cleavage of C-C and C-H bonds, H-abstraction, chain propagation, radical termination, disproportionation, and lighter olefins recombination reactions. The following expressions illustrate the potential steps involved in the cracking of n-heptane (Eq. 4.2 - 4.7) and MCH (Eq. 4.8 - 4.10).





4.3.7. Effect of temperature on heat sink capacities of n-heptane, MCH, and toluene

During the cracking process, the heat sink capacity of a fuel is a combination of the sensible heat sink and the chemical heat sink. In the present work, the total heat sink capacity was estimated by subtracting the energy loss from the energy input to the reactor. The following expressions (Eq. 4.11 and 4.12) were used to estimate the total heat sink capacity of the fuels. The energy loss quantity can be influenced by various factors, such as the type of reactor system, operating temperature and pressure, fuel flow rate, and ambient conditions. Hence, it is essential to determine the energy loss quantity for a particular system and operating conditions.

$$\text{Total heat sink (kJ/kg)} = \left(\frac{\text{power input (kJ/s)} - \text{power loss (kJ/s)}}{\text{mass flow rate of feed (kg/s)}} \right) \quad \text{Eq. (4.11)}$$

$$\text{Power input (W)} = \text{voltage (V)} \times \text{current (I)} \quad \text{Eq. (4.12)}$$

In this study, thermally stable toluene was used to investigate the energy loss percentage at various temperatures. The following energy conservation equation (Eq. 4.13) was used in calculating the energy loss quantity. The NIST SUPERTRAPP library was used to determine the enthalpy value at the inlet and outlet conditions. The analysis revealed that the contribution of the kinetic energy term (i.e., $V^2/2$) to the total energy loss is almost insignificant (< 0.1%). The analysis details of energy loss percentage for various temperatures is presented in Table 4.3. The data shows that for every 50 °C increase in reactor temperature, the energy input increased by about 10% to 12%. The energy loss quantity increased two-fold as the temperature increased from 500 °C to 700 °C. The energy loss percentage at 550, 600, 650, and 700 °C is 8.1, 9.1, 9.9, and 11.1%, respectively, of the total energy input. The loss percentage at 700 °C may be slightly lower than 11.1% due to minor cracking of toluene, as mentioned in section 4.3.2. The heat loss percentage obtained from the toluene experiments was used to estimate the total heat sink capacities of the n-heptane and MCH fuel for the studied range of operating conditions.

$$\text{Energy loss } (q_{loss}) = q_{input,exp} - \left(h_{exit} + \frac{V_{exit}^2}{2} - h_{inlet} - \frac{V_{inlet}^2}{2} \right) \quad \text{Eq. (4.13)}$$

where, h = specific enthalpy, q = specific energy, and V = velocity of the fluid.

Table 4.3: Heat loss values at different temperatures under 55 bar pressure

Feed rate (g/min)	T _{inlet} (°C)	T _{exit} (°C)	h _{inlet} (kJ/kg)	h _{exit} (kJ/kg)	(h _{exit} - h _{in}) (kJ/kg)	q _{input} (kJ/kg)	q _{loss} (kJ/kg)
24	30	450	138.1	1258.1	1120.7	1205.3	84.4
24	30	500	138.1	1392.1	1254.0	1360.1	106.1
24	30	550	138.1	1526.2	1388.1	1509.8	122.3
24	30	600	138.1	1662.5	1524.4	1674.5	150.7
24	30	650	138.1	1801.3	1663.2	1846.6	182.8
24	30	700	138.1	1942.7	1804.6	2031.3	225.5

The experimentally obtained heat input values for n-heptane, MCH, and toluene at different temperatures are shown in Fig. 4.7a. In each case, the experiment was conducted under 55 bar reactor pressure and with a mass flow rate of 24 ± 0.1 g/min. The heat input values

increased monotonically with the increase in reactor temperatures. Fig. 4.7b shows the variation in heat sink capacity of the three hydrocarbon fuels at different temperatures. For a fixed temperature, the heat sink capacity of n-heptane is considerably greater than that of toluene, and the difference in heat sinks becomes more noticeable as the temperature increases. The heat sink capacity of n-heptane, MCH, and toluene at 700 °C is 2118 kJ/kg, 1902 kJ/kg, and 1806 kJ/kg, respectively. Liu et al. (2015) reported a heat sink value of approximately 1850 kJ/kg for toluene at 700 °C and 50 bar. In the case of toluene, the slope of the heat sink curve is almost constant. The constant slope signifies a limited possibility of toluene cracking within the temperature range. On the contrary, beyond 600 °C, the slope of the heat sink curve of n-heptane increased gradually with temperature, which signifies the greater extent of cracking.

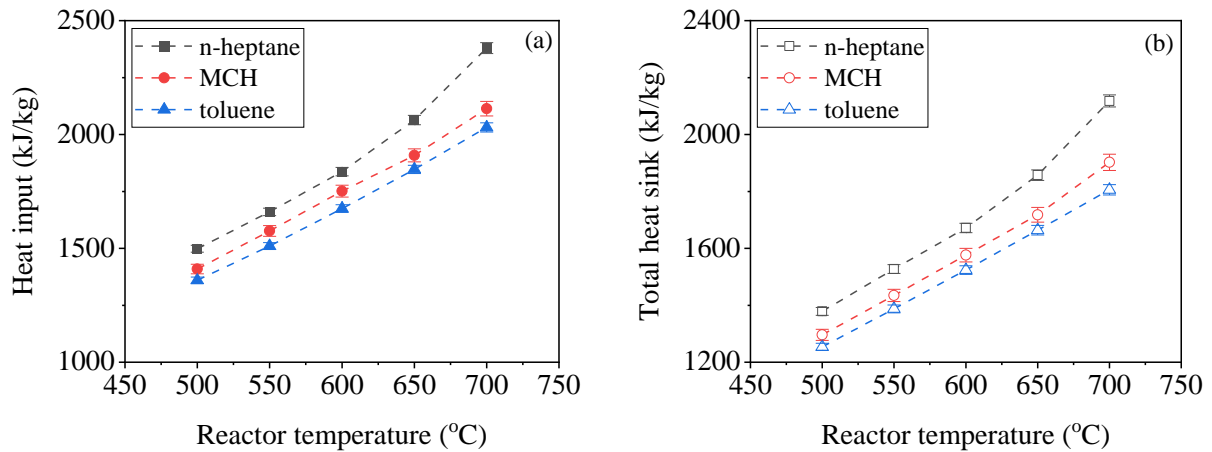


Fig. 4.7: Effect of temperature on a) heat input, and b) total heat sink values of n-heptane, MCH, and toluene.

The estimated value of the total heat sink capacity is the sum of the sensible heat sink and the cracking (or chemical) heat sink capacity of the fuel. The chemical heat sink capacity of the fuels was obtained by subtracting the sensible or physical heat sink from the total heat sink capacity according to Eq. 4.14. The sensible heat sink value was calculated based on the fuel temperature at the reactor inlet and exit conditions. The NIST database was used to compute the specific enthalpy under different operating conditions.

$$\text{Chemical heat sink (kJ/kg)} = \text{Total heat sink (kJ/kg)} - (h_{\text{exit, avg.}} - h_{\text{inlet}}) \quad \text{Eq. (4.14)}$$

where, $h_{\text{exit,avg.}}$ = average value of the specific enthalpy of product at the reactor exit, and h_{inlet} = specific enthalpy of feed at the reactor inlet conditions.

Table 4.4 presents the estimated values of the chemical heat sink capacities for n-heptane and MCH at different temperatures. Additionally, the table includes the cracking percentage for each hydrocarbon at the corresponding temperatures. As the chemical heat sink capacity of the thermally stable toluene is insignificant up to a temperature of 700 °C, it is not included in the table. The result shows a direct correlation between the chemical heat sink and the cracking percentage of the fuels. For a fixed temperature, the chemical heat sink capacity of n-heptane is more than the heat sink offered by MCH. The differences in heat sink capacities between n-heptane and MCH increase with the increase in operating temperature. For 600, 650, and 700 °C, the difference in heat sink capacities between n-heptane and MCH is 68, 101, and 175 kJ/kg, respectively. The chemical heat sink capacity for MCH is approximately 15-20 kJ/kg greater than that of n-heptane for a similar range of cracking conversion. The analysis revealed that the cracking temperature for MCH is nearly 7-8% higher than n-heptane for similar levels of chemical heat sink value due to the cyclic structure of MCH. The chemical heat sink capacity of n-heptane at 550 °C (fuel temperature) and 38 bar is 1176 kJ/kg, as reported by Wickham et al. (2001). The total heat sink capacity of MCH at 650 °C and 40 bar pressure is about 2240 kJ/kg (Liu et al. 2016).

Table 4.4: Heat sinks and cracking percentage values of n-heptane and MCH

Reactor temp (°C)	n-heptane			MCH		
	Total heat sink (kJ/kg)	chemical heat sink (kJ/kg)	Cracking percentage (wt.%)	Total heat sink (kJ/kg)	Chemical heat sink (kJ/kg)	Cracking percentage (wt.%)
500	1379	615	6.4	1296	569	1.4
550	1527	673	11.5	1435	620	4.5
600	1672	739	16.6	1576	671	8.4
650	1857	822	22.8	1718	721	13.5
700	2118	987	30.9	1902	812	19.8

Note: heat sink values are truncated to the nearest whole number

4.3.8. Analysis of kinetic parameters

The kinetics of n-heptane and MCH cracking under supercritical conditions were investigated based on the experimental results. The analysis assumes that the fluid exists in a single phase, and the tubular reactor functions as a plug-flow reactor. To determine the ‘order’ of the cracking reactions, the experimental data were fitted into a first-order (Eq. 4.15) and a second-order (Eq. 4.16) kinetic model, as shown below.

$$k_1 = \frac{1}{t} [-\ln(1-x)] \quad \text{Eq. (4.15)}$$

$$k_2 = \frac{1}{C_o t} [x/(1-x)] \quad \text{Eq. (4.16)}$$

where, k_1 = first-order kinetic rate constant, k_2 = second-order kinetic rate constant, x = fractional conversion of feed, C_o = initial concentration of feed, and t = residence time.

The following expression (Eq. 4.17) was used to estimate the residence time (t) of the feed at different temperatures. The volume of the reactor considered in the calculation is $2.36 \times 10^{-6} \text{ m}^3$. The compressibility data were obtained from the NIST SUPERTRAPP database. The compressibility and residence time data for n-heptane and MCH at different temperatures are tabulated in Table 4.5.

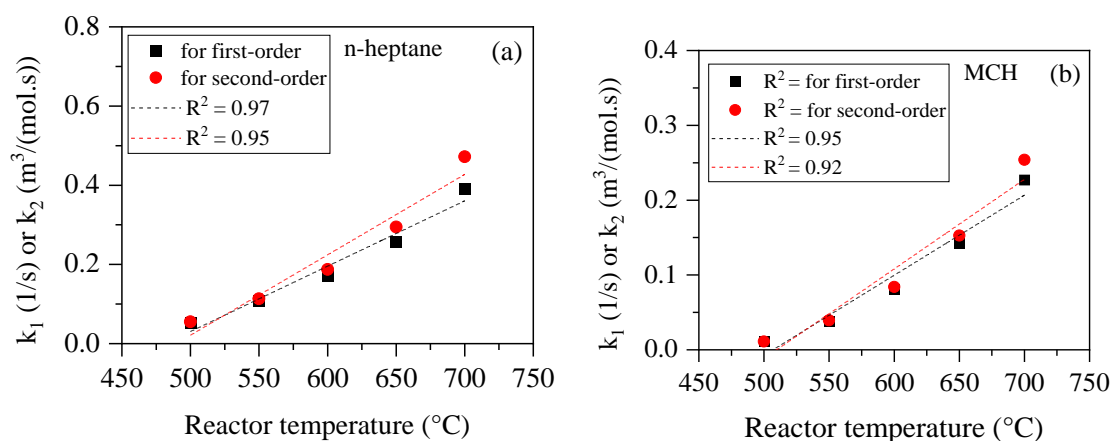
$$\text{Residence time } (t) = \frac{\text{Volume of reactor}}{\text{Average volumetric flowrate}} = \frac{V_R}{v_o \left(\frac{T_{avg.}}{T_o} \times \frac{P_o}{P_{avg.}} \times \frac{Z_{avg.}}{Z_o} \right)} \quad \text{Eq. (4.17)}$$

where, V_R = volume of the reactor, v_o = volumetric flow rate of feed at reactor inlet, $T_{avg.}$ = average temperature of reactor, T_o = inlet temperature, P_o = inlet pressure, $P_{avg.}$ = average pressure of reactor, Z_o = compressibility factor at reactor inlet, and $Z_{avg.}$ = average compressibility factor.

Table 4.5: Residence time values at different temperatures under 55 bar pressure

Hydrocarbons		Reactor temperature (°C)					
		30	500	550	600	650	700
n-heptane	compressibility	0.321	0.850	0.893	0.926	0.950	0.969
	residence time (s)	4.01	1.24	1.14	1.06	1.00	0.95
MCH	compressibility	0.279	0.821	0.866	0.900	0.925	0.945
	residence time (s)	4.47	1.28	1.17	1.09	1.02	0.97

Between the two models, the experimental data shows a better fit (with a higher value of R^2) for the first-order kinetics model, as shown in Fig. 4.8. Chakraborty et al. (2012) and Zhang et al. (2018) also noted the suitability of first-order kinetics for the cracking of n-heptane and n-dodecane under supercritical conditions. Though the R^2 value for the second-order model is relatively less than that of the first-order model, it is still greater than 0.9. This suggests the possibilities of second-order bimolecular reactions in addition to the first-order unimolecular reaction during the cracking process. However, based on the present analysis and literature information, the first-order kinetic model was considered in estimating the rate constant and apparent activation energy in the work.

Fig. 4.8: Variation in k_1 or k_2 with reactor temperature.

During the cracking of hydrocarbons, long-chain molecules decompose into shorter-chain compounds. The volumetric flow rate of the fluid will vary as a result of the formation of smaller hydrocarbons. Therefore, to accommodate the volume expansion, the volume expansion parameter (ϵ) was included in the first-order kinetic expression, as shown in Eq. 4.18, in estimating the kinetic parameters. However, due to experimental limitations in the measurement, some typical values of ϵ were considered to estimate k_1 and apparent activation energy, and the results are presented in Fig. 4.9. The plot shows an exponential growth in rate constant with both the temperature and ϵ values. For n-heptane, the value of k_1 increased by nearly 1.6 to 2 times for every 50 °C increase in reaction temperature from 500 °C to 700 °C. For MCH, the corresponding increase is approximately 1.6 to 3.4 folds. The first-order rate constant value for n-heptane is almost 1.7 times higher than the MCH value at 700 °C.

$$k_1 = \frac{1}{t} \left[-\ln(1-x) + \epsilon \{ -\ln(1-x) - x \} \right] \quad \text{Eq. (4.18)}$$

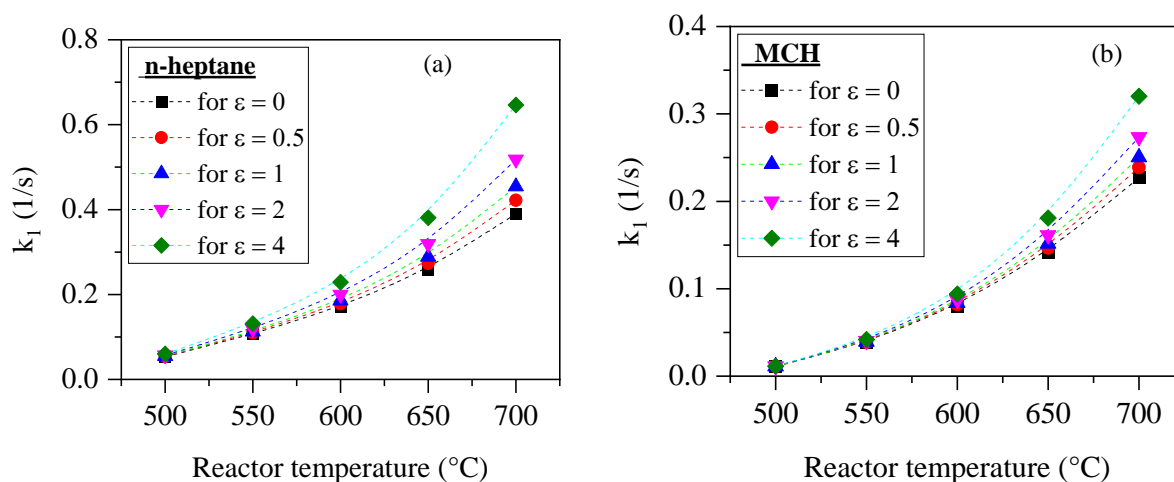


Fig. 4.9: Variation in k_1 with temperatures for different values of volume expansion parameter for a) n-heptane, and b) MCH.

The Arrhenius plot, as shown in Fig. 4.10, was used to estimate the apparent activation energy of the cracking reactions. The apparent activation energy for n-heptane and MCH is calculated to be 61.1 kJ/mol and 92.8 kJ/mol, respectively, for $\epsilon = 0$. A gradual increase in activation energy is observed as the value of ϵ increases. At an ϵ value of 4, the activation energy for n-heptane and MCH is 73 kJ/mol and 103 kJ/mol, respectively.

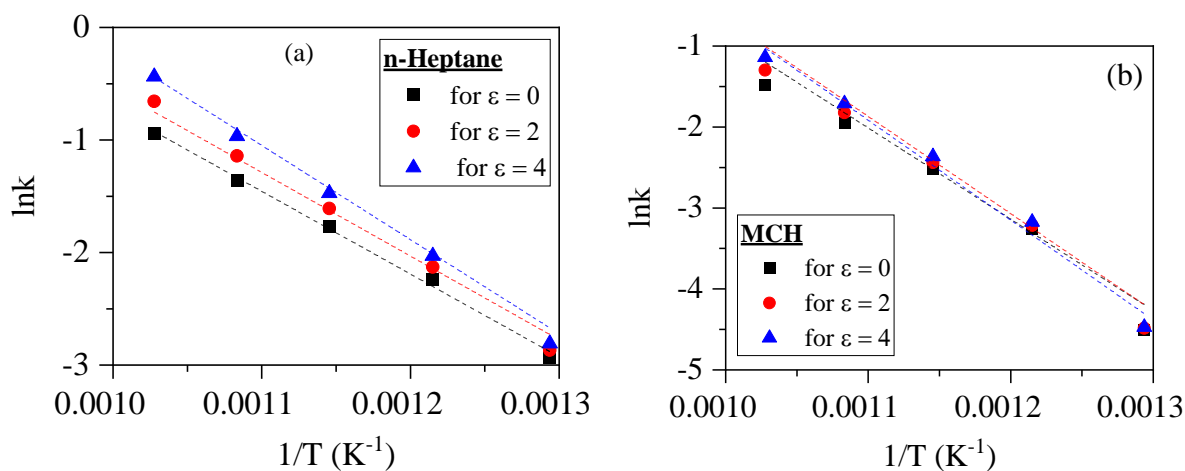


Fig. 4.10: Arrhenius plots for a) n-heptane, and b) MCH.

4.4. Conclusion

This study investigates the influence of chemical structure on the thermal cracking behavior of hydrocarbons under a supercritical environment. Three types of C_7 hydrocarbons, namely n-heptane, methylcyclohexane (MCH), and toluene, were considered for cracking experiments within a temperature range of 500 °C to 700 °C under 55 bar pressure. The increase in reactor temperature resulted in an increase in the cracking percentage, coke deposition rate, and heat sink capacity of the hydrocarbons. It is observed that the cracking percentage, coke deposition rate, and heat sink capacity of the hydrocarbons increased with the increase in reactor temperature. The investigation revealed that the chemical heat sink capacity of n-heptane, a straight-chain alkane, is more than the MCH, a cyclic alkane. However, for a fixed value of cracking percentage, the coke deposition rate of MCH is more than the n-heptane. Further, the experimental result showed a better fit with the first-order kinetics, and the estimated activation energy of the straight-chain n-heptane is significantly low compared to the cyclic MCH compound under similar operating conditions.

The outcome of Chapter 4 bridges the following four major objectives mentioned in Chapter 1.

- Establishment of new methodologies in estimating the fuel conversion and coke deposition rate.
- Understanding of hydrocarbon cracking behavior above 650 °C and 50 bar pressure.
- Influence of hydrocarbon structure on supercritical cracking characteristics.
- Establishment of a new methodology for the estimation of heat loss percentage.

Chapter-5

Thermal Cracking and Heat Sink Characteristics of Multi-component Fuels Under Supercritical Conditions

Thermal Cracking and Heat Sink Characteristics of Multi-component Fuels Under Supercritical Conditions

5.1. Introduction

For supersonic engines above Mach-5 speed, aerodynamic heating can induce severe thermal stresses to the engine (Li et al. (2021)). Regenerative cooling using onboard hydrocarbon fuel could be an effective cooling method to safeguard the engine structure (Liang et al. (2017), Liu et al. (2020), Zhong et al. (2009), Sobel et al. (1997)). Cracking of hydrocarbon fuel can offer sufficient heat sink to overcome the thermal load (Wen et al. (2011)), and the cracked products can improve the ignition delay and combustion characteristics (Puri et al. (2005), Bao et al. (2012)). The cracking of single-component alkanes such as n-heptane, n-octane, n-decane, and n-dodecane has been studied under supercritical conditions to find the heat sink capacity and coke propensity of the hydrocarbons (Zhang et al. (2020), Sun et al. (2017)). The cracking of n-octane and n-decane can offer a total heat sink capacity of about 2780 kJ/kg and 2700 kJ/kg of fuel, respectively, at 650 °C and 40 bar pressure (Huang et al. (2004)). A higher value of the olefin-to-alkane ratio in the cracked products can offer more endothermicity. Literature on multi-component fuel cracking under supercritical conditions is less in numbers. The chemical heat sink capacity of JP-7 and RP-3 fuels is in the range of 450 to 800 kJ/kg for a temperature range of 600 to 650 °C (Jin et al. (2017), Jiao et al. (2019)). In some studies, amine-based initiators were examined to enhance the heat sink capacity of hydrocarbon fuels. The addition of triethylamine (TEA) and tributylamine (TBA) improved the n-heptane conversion (Wang et al. (2008)). The addition of 4% nitropropane enhanced the endothermicity of n-decane by around 3 times at 614 °C (Xing et al. (2008)). The presence of 0.2 wt.% cetyl-hyperbranched polyethyleneimine, a micro-initiator, increased the JP-10 conversion from 16% to 34% at 675 °C (Ye et al. (2019)). Macro-initiators are also helpful in improving the heat sink capacity of hydrocarbon fuels (He et al. (2015), He et al. (2017), Mi et al. (2020)).

Though several articles are available on the thermal cracking of fuels under supercritical conditions, comprehensive information on fuel conversion, product composition, heat sink capacity, endothermicity, and the coke deposition rate is not found explicitly in a single document in most of the articles. The majority of the articles on endothermic fuels dealt with single-component or two-component fuels, and also, the operating pressure is less than 45 bar. Studies on endothermic cracking above 50 bar pressure are scanty in numbers. The limited and scattered information on fuel conversion, endothermicity, coke deposition rate, and product characterization intrigued us to develop an appropriate experimental setup and investigate the heat sink capacity of multi-component hydrocarbon fuel. The thermal cracking characteristics of a multi-component hydrocarbon fuel (namely HCF-1) at supercritical conditions are examined in the present work. The effects of operating parameters temperature, pressure, and space-time on fuel cracking percentage, coke deposition, heat sink capacities, and cracked-gas distribution are examined thoroughly. The second aspect of this research is the investigation of the surface morphology of coke deposits and the cracking kinetics of the HCF-1 fuel.

5.2. Materials and Experimental Details

5.2.1. Materials

In the present study, the hydrocarbon fuel (designated as HCF-1) was procured from Ogene Systems India Pvt. Ltd., India. The physicochemical properties of the fuel are mentioned in section 3 of this chapter. Other chemicals that are used for analysis purposes and calibration of gas chromatography (GC) are mentioned in Chapter-3 of the thesis.

5.2.2. Experimental setup and procedure

The schematic of the experimental setup used for the present work is given in Chapter-3 of this thesis. The feed section includes a 5-liter fuel tank, fuel purging line, and high-pressure feed pump. The reactor module consists of a 2 mm internal diameter and 750 mm long SS-316 tubular reactor fitted with temperature indicators, a step-down transformer, and a direct power supply system. The product cooling segment consists of a shell-and-tube heat exchanger, pressure gauge, thermocouple and temperature indicator, chiller unit, micron filter, and back-

pressure regulator. A detailed description of the experimental procedure is mentioned in Chapter-3 of this thesis.

5.2.3. Characterization of feed and product properties

Various techniques were adopted to characterize the hydrocarbon fuel. ASTM D86 distillation was conducted to find the boiling range characteristics of the fuel. The initial boiling point (IBP) and final boiling point (FBP) of the HCF-1 fuel are 131°C and 238 °C, respectively. The distillation characteristic curve of the HCF-1 fuel between the 5% and 95% distillate volume is shown in Fig. 5.1. The following expressions (Eq. 5.1 and Eq. 5.2) were used to estimate the critical temperature (T_c) and pressure (P_c) of the HCF-1 fuel (Yu et al. (1995)). The measured and estimated properties of the fuel are given in Table 5.1. The GC-MS chromatogram of the fuel is presented in Fig. 5.2. The analysis showed that the HCF-1 consists of primarily C₉, C₁₀, C₁₁, C₁₂, and C₁₃ hydrocarbons with a small quantity of C₈ and C₁₄ hydrocarbons.

$$T_c(^{\circ}F) = 186.16 + 1.6667 \times SG \times (T + 100) - 0.7127 \times 10^{-3} \times \{SG \times (T + 100)\}^2 \quad \text{Eq. (5.1)}$$

$$P_c(\text{psia}) = 3.4824 \times 10^9 \times (T + 460)^{-2.1377} \times SG^{2.4853} \quad \text{Eq. (5.2)}$$

where, T = average boiling temperature in °F, and SG = specific gravity of the fuel.

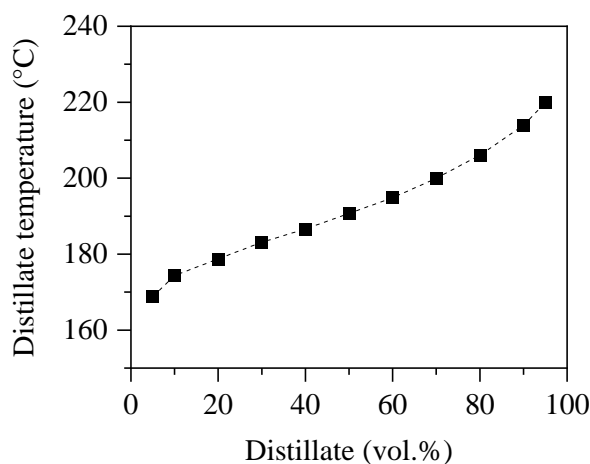
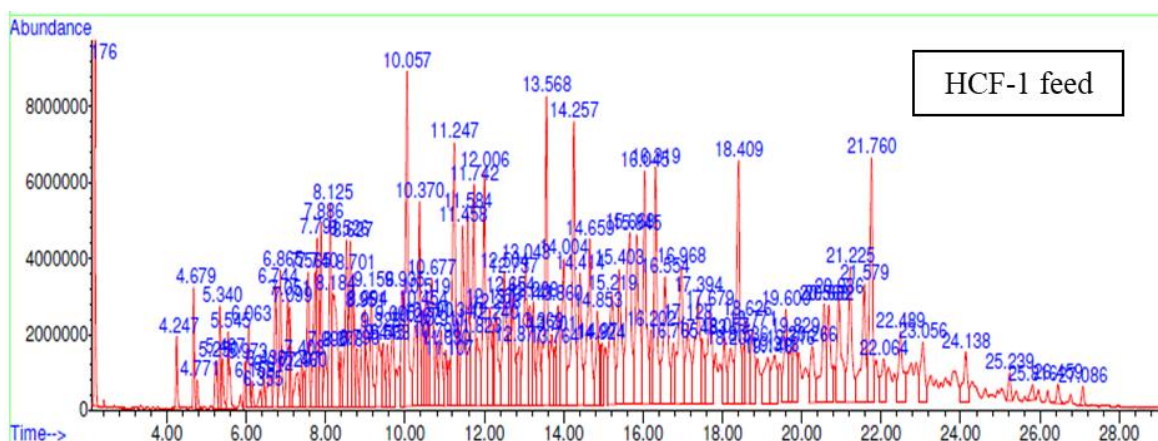


Fig. 5.1: ASTM D86 distillation characteristic curve of HCF-1 fuel.

Table 5.1: Physico-chemical properties of HCF-1 fuel

Properties	Value	Hydrocarbon composition	Vol.%
Specific gravity @ 28 °C	0.79 ± 0.01	≤ C ₇	1.2
Average boiling point (°C)	187 ± 0.5	C ₈	2.5
Flashpoint (°C)	58 ± 2	C ₉	6.26
Aniline point (°C)	68 ± 1	C ₁₀	25.7
Moisture content (wt.%)	0.1 ± 0.05	C ₁₁	31
Critical temperature (°C)	381.6	C ₁₂	16.47
Critical pressure (bar)	23.2	C ₁₃	7.2
Calorific value (MJ/kg)	45.7 ± 0.1	≥ C ₁₄	3.5



been studied in-depth. Almost 75% of the cracking experiments were repeated to find differences in experimental results obtained under identical conditions. The overall deviation between two identical runs lies in the range of 2- 6 %.

5.3.1. Influence of temperature on cracking characteristics of HCF-1

5.3.1.1. Effect of temperature on fuel cracking and coke deposition

To investigate the effect of temperature on the cracking characteristics of the HCF-1 fuel, the thermal cracking experiments were performed at four different temperatures under 55 bar pressure with a fuel flow rate of 50 ± 0.2 mL/min. The following expression (Eq. 5.3) was used to estimate the fuel cracking percentage in the work. The ASTM D86 distillation data, as shown in Table 5.2, was used in calculating the cracking conversion. The data shows that the initial boiling point (IBP) and average boiling point ($T_{avg.}$) temperature of the liquid products decreased gradually with the increase in reactor temperature. The decrease of IBP and T_{avg} value of the liquid products with temperature indicates the presence of low-boiling components in the liquid products. The calculated value of fuel cracking percentage at different temperatures is shown in Fig. 5.3a. The figure shows that the fuel cracking percentage increased with reactor temperature. The calculated value of cracking percentage at 550, 600, 650, and 680 °C is 1.2, 3.3, 7.6, and 10.3 %, respectively. The cracking percentage of HCF-1 increased by about 3-fold as the temperature increased from 600 °C to 680 °C. Due to the experimental limitation and the excessive coke deposition in the flow line, it was challenging to perform the experiments beyond 680 °C.

$$\text{Cracking percentage (wt.\%)} = \left(1 - \frac{\text{mass flow rate of liquid } (\geq \text{feed boiling point}) \text{ product}}{\text{mass flow rate of feed}} \right) \times 100 \quad \text{Eq. (5.3)}$$

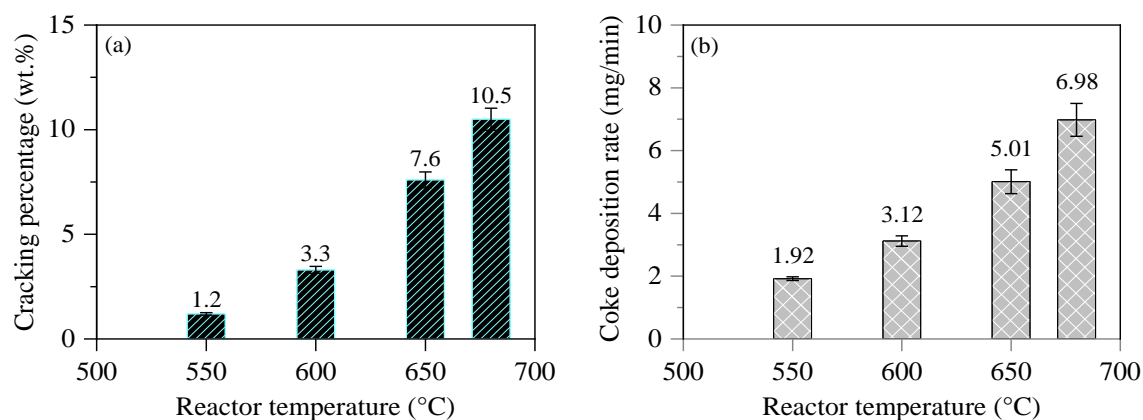


Fig. 5.3: Effect of temperature on a) cracking percentage, and b) coke deposition rate.

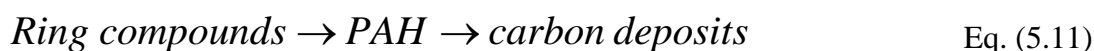
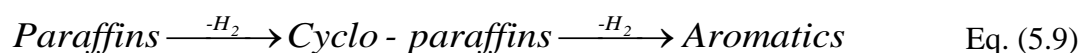
Table 5.2: ASTM D86 distillation results of HCF-1 feed and liquid products

	HCF-1 feed	product at 550 °C	product at 600 °C	product at 650 °C	product at 680 °C
Distillate (vol.%)	Temp. (°C)	Temp. (°C)	Temp. (°C)	Temp. (°C)	Temp. (°C)
IBP	130.7	121.8	104.0	78.94	40.3
5	167.8	166.1	157.0	143.1	112.2
10	174.4	174.1	171.4	167.1	154.9
20	178.8	177.5	176.6	175.8	173.1
30	183.1	183.1	181.0	180.7	179.0
40	186.6	186.1	184.5	183.1	183.1
50	190.7	190.2	189.0	188.8	187.4
60	194.8	194.4	193.3	193.5	192.0
70	200.0	199.7	198.9	199.1	197.8
80	206.1	205.9	205.0	205.3	205.8
90	213.9	212.9	213.4	213.4	214.6
95	219.9	219.7	219.1	220.4	222.6
T _{avg.} (°C)	187.2	186.0	182.8	179.1	171.9

The phenomenon of coking is one of the primary concerns during the thermal cracking of hydrocarbon fuels for its effective utilization in scramjet engines. Unsaturated and cyclic hydrocarbon compounds are prone to agglomerate and act as a precursor for coke formation. The amount of coke formation during a cracking process depends on several factors, such as operating temperature, pressure, and hydrocarbon composition. To know the effect of temperature on coke deposition rate, the amount of deposited coke was estimated for each of the studied temperatures, and the results are shown in Fig. 5.3b. The plot shows that the coke deposition rate increased with the increase in reactor temperature. The plot also shows that the increasing trend of coke deposition rate with temperature is quite similar to the cracking percentage trend up to 650 °C. Beyond 650 °C, the incremental percentage of coke deposition rate is more than the cracking percentage, which may be due to an enhanced rate of secondary cracking (i.e., cracking of smaller hydrocarbons that are formed as a result of primary cracking of heavier hydrocarbons) and dehydrogenation reactions at high temperatures. The coke deposition rate increased by more than 2-fold as the temperature increased from 600 °C to 680 °C. Apart from the cracking coke, the two major types of coke formation, namely oxidative coke and amorphous coke, can occur during the thermal cracking of hydrocarbon fuels.

In a thermal cracking process, when metallic species such as Fe, Mn, etc., come in contact with dissolved oxygen or oxygen-bearing components present in the fuel, an undesirable oxidative process can lead to oxidative coke deposition. The oxygen combines with hydrocarbon in the heated section to produce alkyl peroxides at a temperature range of 300 to 400 °C. During the thermal cracking of hydrocarbon (RH), radicals (R[•]) are formed due to the cleavage of the C-H bond (Eq. 5.4). These radicals can react with oxygen present in the fuel under the influence of metallic species to form a (RO₂[•]) radical (Eq. 5.5). The (RO₂[•]) radical abstracts hydrogen from the hydrocarbon (R₁H) and form new radical (R₁[•]) and hydroperoxide (RO₂H) (Eq. 5.6). The formed hydroperoxides are highly susceptible to decomposition to form peroxide (RO[•]) radicals (Eq. 5.7). In the presence of fuel impurities like sulfur/ phenols/ thioenes, the hydrocarbons can react with peroxide radicals to form gum materials (Eq. 5.8). Amorphous coke generally forms as a result of polymerization and polycondensation reactions. Generally, dehydrogenation

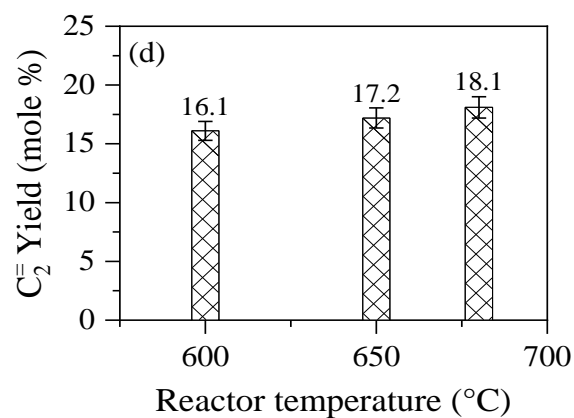
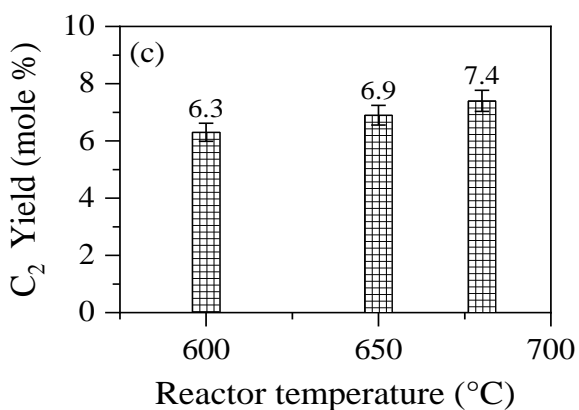
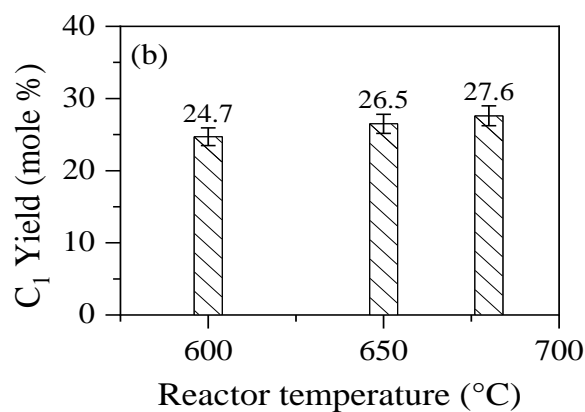
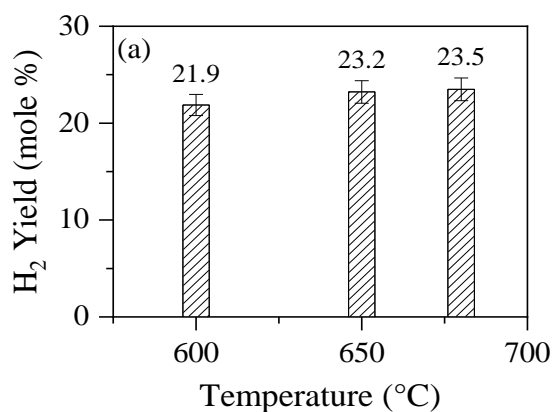
reactions are energy-intensive and occur above 480 °C, and the condensation process which can lead to pyrolytic coke deposition starts above 400 °C. The probable schemes of amorphous coke formation are shown below (Eq. 5.9 to 5.11). The Diels-Alder reaction is also a potential route for the formation of pyrolytic coke.



5.3.1.2. Effect of temperature on cracked-gas composition

To know the composition of the gaseous products, the cracked-gas samples were analyzed using a multi-channel Micro GC. Before analyzing the cracked-gas samples, the GC was calibrated using a known composition of calibration gas mixture consisting of 14 gases (H₂, N₂, CO₂, and C₁ to C₄ alkanes and alkenes). The distribution pattern of the major components for 600, 650, and 680 °C is shown in Fig. 5.4(a-h). Due to the negligible amount of cracking at 550 °C, the gas production was not sufficient to analyze its composition. The significant species obtained from the analysis include hydrogen (H₂), methane (C₁), ethane (C₂), ethylene (C₂⁼), propane (C₃), propylene (C₃⁼), butane (C₄), and butene (C₄⁼). The plot shows that the concentration of H₂, methane, ethylene, propane, propylene, butane, and butene increased with cracking temperature. However, the increment is marginal for species like propane and ethane. The decreasing trend of the olefin-to-alkane ratio (Fig. 5.4i) with cracking temperature may be due to the polymerization of lighter olefins. In the analysis, the olefin (C₂⁼ + C₃⁼)-to-alkane (C₂ + C₃) ratio shows a

marginal decrease from a value of 2.2 to 2.1 as the temperature increased from 600 to 680 °C. The higher value of ethylene and propylene yield in the cracked-gas mixture is an important aspect of the thermal cracking behavior of hydrocarbons under supercritical conditions. A similar kind of phenomenon is reported by Liu et al. (2009) for the cracking of dodecane fuel. The typical value of the H₂/ CH₄ mole ratio lies in the range of 0.8-0.9, and it decreased marginally with the increase in temperature.



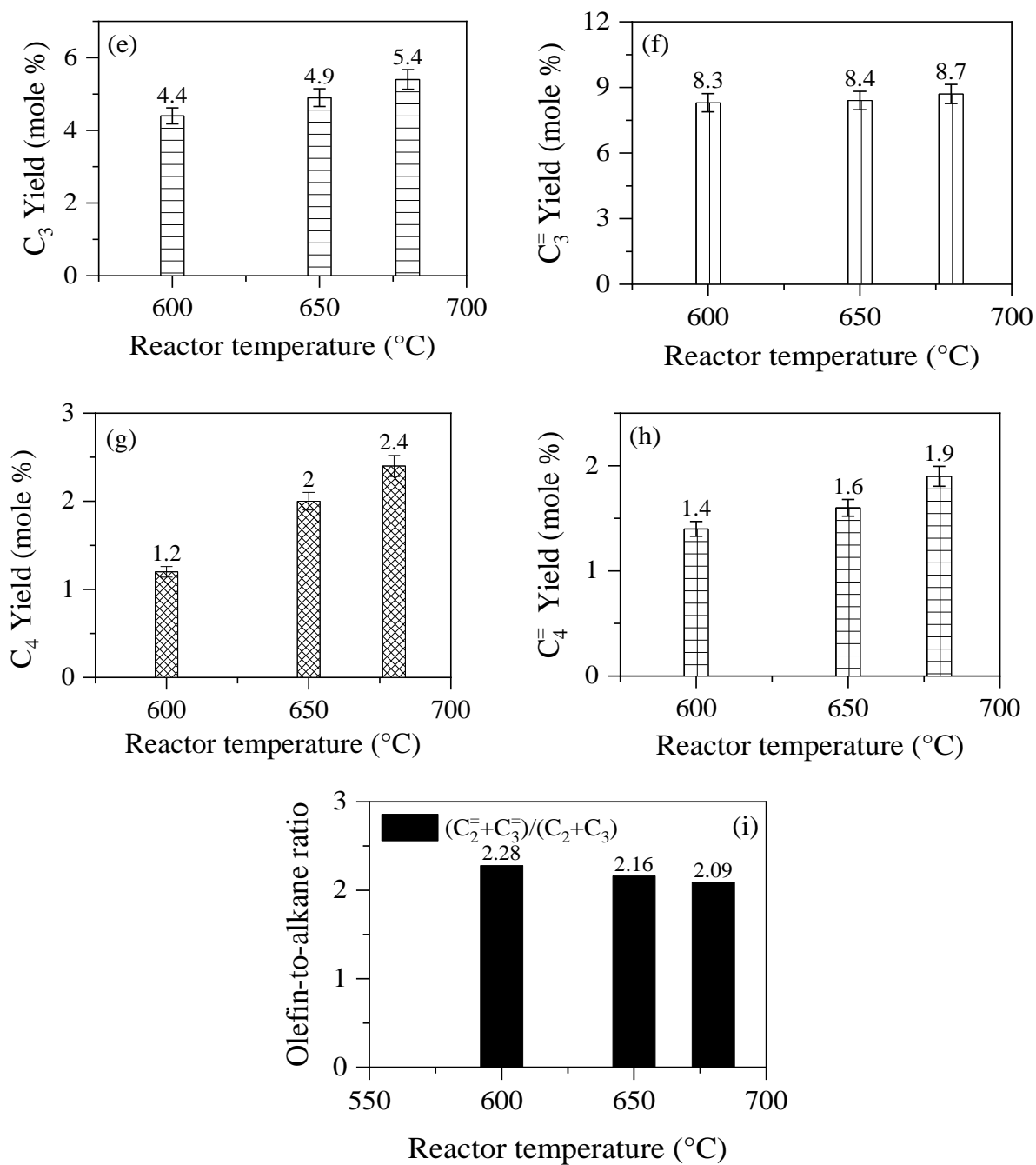
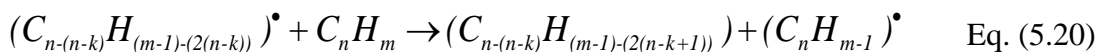
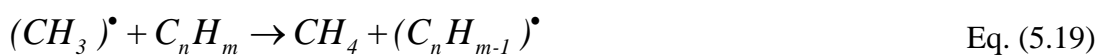
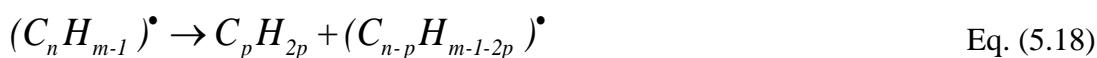
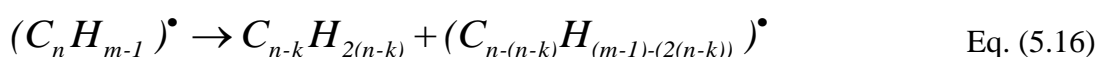
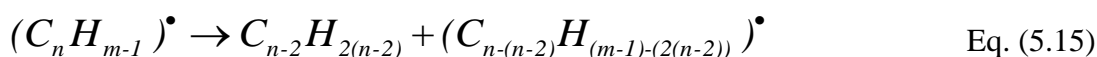
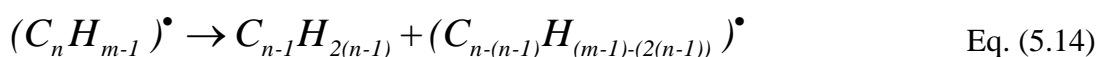
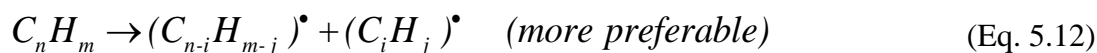


Fig. 5.4: Effect of temperature on the gas composition and olefin-to-alkane ratio.

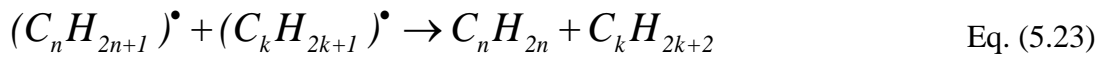
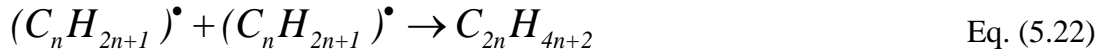
The free-radical mechanism is considered to be a dominating route for the thermal cracking of hydrocarbons under supercritical conditions (Jiang et al. (2013)). Thermal cracking of hydrocarbons initiates *via* C-H and C-C bond breakage to form alkyl radicals (Eq. 5.12-5.13)

from the parent hydrocarbons. The radicals with a carbon number of more than five may undergo an isomerization reaction. The alkyl radicals can undergo further decomposition to form lower alkyl radicals and olefins (Eq. 5.14-5.18). In addition to the unimolecular radical decomposition, bimolecular hydrogen abstraction (Eq. 5.19-5.21) reactions from the parent hydrocarbons can also occur simultaneously during the propagation reactions.



Recombination and disproportionation reactions are the common pathways for the termination of chain reactions. Two smaller radicals can combine to form a paraffinic hydrocarbon. In the recombination mechanism (Eq. 5.22). In the disproportionation reaction, one olefin and one paraffin are formed from two radicals (Eq. 5.23). Apart from the above reactions, reactions such as the dehydrogenation of paraffin/cyclo-paraffins (Eq. 5.9), the combination of olefins and di-olefins (Eq. 5.10), polymerization, etc. are also possible under the present experimental environments. The aromatic/ ring compounds can further polymerize to form

polycyclic aromatic hydrocarbons (PAHs) (Eq. 5.11). These PAHs can act as precursors for carbon deposition on the surface of the reactor tube at elevated temperatures.



5.3.1.3. Effect of temperature on heat sink capacity of HCF-1 fuel

Initially, the fuel absorbs heat to increase its sensible temperature before it undergoes a cracking reaction, and that energy intake is designated as the ‘physical or sensible heat sink’ of the fuel. Once the cracking starts, the heat intake by the fuel is a combination of both the physical and chemical heat sink capacity. In the present study, the chemical heat sink capacity of the fuel was obtained by subtracting the physical heat sink from the total heat sink capacity. The total heat sink value was estimated after subtracting the heat loss from the energy supplied to the reactor. The following expressions (Eq. 5.24 - 5.26) were used to estimate the sensible and endothermic sink capacities of the HCF-1 fuel.

$$\text{Total heat sink (kJ / kg)} = \left(\frac{\text{power input (kJ / s)} - \text{energy loss (kJ / s)}}{\text{mass flow rate of feed (kg / s)}} \right) \quad \text{Eq. (5.24)}$$

$$\text{Power input (W)} = \text{voltage (V)} \times \text{current (I)} \quad \text{Eq. (5.25)}$$

$$\text{Chemical heat sink (kJ / kg)} = \left(\text{Total heat sink (kJ / kg)} - (h_{\text{exit}} - h_{\text{inlet}}) \right) \quad \text{Eq. (5.26)}$$

where, h_{exit} = specific enthalpy of product at the reactor exit, and h_{inlet} = specific enthalpy of feed at the reactor inlet conditions.

In the work, the energy loss quantity from the reactor system at different temperatures was estimated experimentally using a thermally-stable toluene hydrocarbon. The conservation of energy equation (Eq 5.27) was used to find the energy loss, as shown in Table 5.3. NIST

=====

SUPERTRAPP database was used to obtain the enthalpy of toluene at the inlet and outlet conditions. The data shows that the energy loss increased almost two-fold when the exit temperature increased from 500 °C to 700 °C. In the majority of cracking experiments, the fuel (HCF-1) flow rate was varied between 25 and 50 mL/min, so the energy loss quantity was estimated for these two flow rates, and the results are shown in Fig. 5.5.

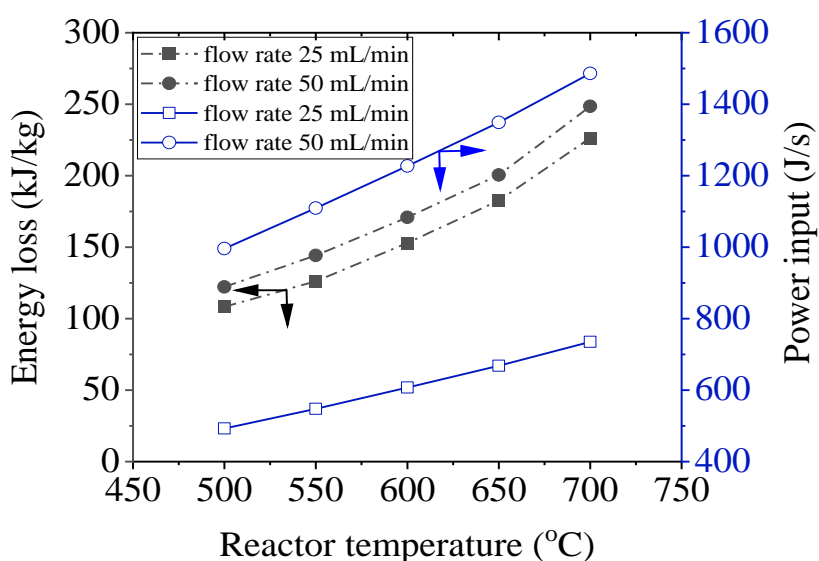
$$\text{Energy loss } (q_{loss}) = q_{input,exp} - \left(h_{exit} + \frac{V_{exit}^2}{2} - h_{inlet} - \frac{V_{inlet}^2}{2} \right) \quad \text{Eq. (5.27)}$$

where, h = specific enthalpy, q = specific energy, and V = velocity of the fluid.

Though the energy loss per unit mass, being an intensive property, is supposed to be the same, the actual result shows a minor (about 15 to 20 kJ/kg) difference in energy loss for the two flow rates. This small difference may be partially due to experimental inaccuracy, variation in surrounding environmental conditions, and partly due to scale-dependent effects such as heat loss through the heating wires between the transformer and the reactor terminals. The figure also shows an almost linear variation in power input with reactor temperatures for the two flow rates. The heat loss values obtained from the toluene experiments are used to estimate the heat sink capacity of the HCF-1 fuel using the same reactor setup and for a similar range of operating conditions. However, for simplicity, the average value (e.g., at 650 °C, energy loss with 25 mL and 50 mL feed flow is 182.6 and 200.6 kJ/kg, respectively, and hence the average value of 191.6 kJ/kg is used for 650 °C. Similarly, for 700 °C, the average value is 237.4 kJ/kg) of the energy loss quantities are used in subsequent calculations.

Table 5.3: Heat loss quantity at different temperatures under 55 bar pressure

Feed flow rate (mL/min)	T_{inlet} (°C)	T_{exit} (°C)	h_{inlet} (kJ/kg)	h_{exit} (kJ/kg)	$(h_{exit} - h_{in})$ (kJ/kg)	q_{input} (kJ/kg)	q_{loss} (kJ/kg)
50	30	500	138.0	1391.7	1253.7	1375.8	122.1
50	30	550	138.0	1525.8	1387.8	1531.9	144.1
50	30	600	138.0	1662.1	1524.1	1694.9	170.8
50	30	650	138.0	1800.9	1662.9	1863.5	200.6
50	30	700	138.0	1942.3	1804.3	2052.7	248.4

**Fig. 5.5:** Variation of energy loss and power input with temperature for toluene feed.

The ASTM D86 distillation, gas chromatography analysis, and specific gravity data were used to find a typical surrogate composition of the HCF-1 equivalent fuel (Chickos et al. (2005)). The NIST SUPERTRAPP database was used to find the thermo-physical properties of the surrogate compounds, as shown in Table 5.4. The composition mentioned in the table is used in SUPERTRAPP to estimate the enthalpy of the fuel at the experimental temperatures and pressure conditions.

Table 5.4: Properties of surrogate components obtained from NIST database

Components	Boiling point (°C)	Specific gravity	Molecular weight (g/mol)	Composition (mol %)
Ortho-xylene	140	0.879	106.2	3
n-decane	174	0.730	142.3	15
n-undecane	196	0.740	156.3	15
Butyl benzene	183	0.867	134.2	10
n-dodecane	216	0.750	170.3	22
1-decene	172	0.740	140.3	5
2-methylbutylbenzene	197	0.900	148.2	5
Naphthalene	218	1.162	128.2	3
Bi-cyclohexane	227	0.882	166.3	15
n-tridecane	234	0.756	184.4	3
Mesitylene	165	0.864	120.2	4

Fig. 5.6 shows the variation of the total and chemical heat sink capacity of the HCF-1 fuel at different temperatures. The plot shows that the heat sink capacities of the fuel increased with the increase of reactor temperature. However, the incremental rate of the endothermic heat sink is relatively lower than the corresponding value of total heat sink capacity. The estimated values of endothermic (chemical) heat sink capacity of the HCF-1 fuel at 550, 600, 650, and 680 °C are about 321, 463, 635, and 805 kJ/ kg of fuel, respectively. The increase of chemical heat sink with temperature is aligned with the increase of cracking percentage. About 73% enhancement in endothermicity is noted when the cracking temperature was increased from 600 °C to 680 °C. The enhanced endothermicity can be beneficial to manage the thermal load for a hypersonic engine system. A brief comparison of the endothermic heat sink capacity of various fuels is shown in Table 5.5 along with relevant operating conditions. The endothermic heat sink capacity of the studied HCF-1 is comparable with other hydrocarbon fuels.

For further investigation, GC-MS analysis was performed for the 650 °C sample to find the change in hydrocarbon composition between the feed and cracked liquid product. The carbon

number-wise area percentage, extracted from the chromatogram, is shown in Fig. 5.7 for the major hydrocarbon groups. The plot shows that the concentration of C₇, C₈, and C₉ hydrocarbons increased in the liquid product due to the cracking of C₁₀, C₁₁, and C₁₂ hydrocarbons. On the other side, the increase of C₁₃ and C₁₄ hydrocarbon concentration could be due to the contribution of polymerization reactions.

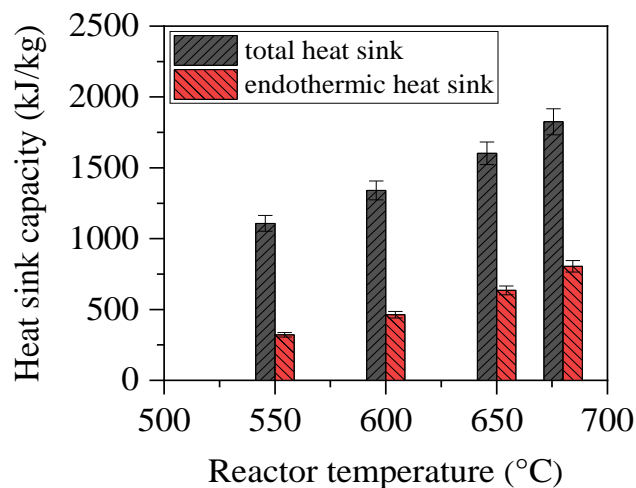


Fig. 5.6: Effect of temperature on heat sink capacities of HCF-1 fuel.

Table 5.5: Endothermic heat sink capacity of various fuels

Fuel	SG	Boiling range (°C)	Temp (°C)	Pressure (bar)	Feed flow rate (g/min)	EHS* (kJ/kg)	Reference
JP-7	0.79	206-239	700	23	10	988	Heinrich et al. (2001)
n-Octane	0.70	125±1	700	23	0.6	953	Huang et al. (2004)
JP-8	0.8	175-219	700	23	0.6	802	Huang et al. (2004)
n-Decane	0.73	174±1	667	40	40	550	Zhu et al. (2014)
RP-3	0.79	180-237	750	60	-	740	Jin et al. (2017)
HCF-1	0.79	167-214	680	55	40	805	present work

*EHS: endothermic heat sink

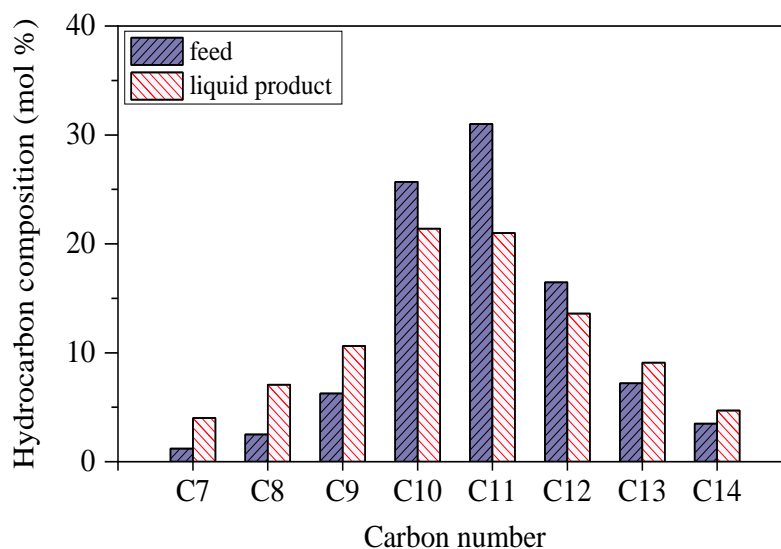


Fig. 5.7: Composition in feed and liquid product obtained at 650 °C and 55 bar.

5.3.2. Pressure effect on cracking characteristics of HCF-1 fuel

5.3.2.1. Effect of pressure on cracking percentage, coke deposition, and heat sink

To examine the effect of pressure on the cracking characteristics of the HCF fuel, a set of experiments was performed at four different pressures ranging between 25 bar and 55 bar. In all cases, the reactor temperature was maintained at 650 °C. The temperature was chosen due to the reasonable amount of endothermicity that can be obtained at 600 °C, as noted from previous experiments. The variation in cracking percentage and coke deposition rate at different pressures is shown in Fig. 5.8. The plot (Fig.5.8a) shows that the cracking percentage increased almost linearly with the increase in reactor pressure. The heat flux increased from 84 kW/m² to 194 kW/m² when the reactor pressure was raised from 25 to 55 bar for a fixed temperature of 650 °C. As a consequence, the cracking percentage increased from 2.6% to 7.6%, and the product gas flow rate increased from a value of 47 mL/min to 109 mL/min.

Coke deposition during the thermal cracking of high-boiling hydrocarbons is inevitable. Coke deposition on the reactor surface will alter the heat transfer effect, and excessive coke will block the fuel transfer line. Various factors, such as wall temperature, fluid pressure, fuel residence time, duration of the test, the effect of reactor metallurgy, fuel composition, and impurities present in the fuel, can influence the coke deposition rate Gascoin et al. (2008). The

coke deposition rate of the fuel increased with reactor pressure, as shown in Fig. 5.8b. As the reactor pressure increased from 25 bar to 55 bar, the coke deposition rate increased from 2 mg/min to 4.1 mg/min. The increase in reactor pressure can enhance the collision frequency of the coke-forming species and, consequently, the coking reaction rate. Higher pressure can also enhance the rate of polycyclic condensation reaction which may also lead to coke deposition. However, the coke formation pathway involving the condensation and agglomeration of polycyclic aromatic hydrocarbons requires higher residence times. Since in the present study, the effect of pressure studies is performed for a residence time of nearly 1 s, the increase in coke deposition may not progress linearly. Ervin et al. (2003) also noted a similar trend in the coke deposition with reactor pressure for a Jet-A fuel. The variation in heat input and heat sink capacities of the fuel at different pressures is shown in Fig. 5.9. The energy input and heat sink capacity of the fuel gradually increased with pressure. The total heat sink capacity of the fuel lies between 1446 kJ/kg to 1602 kJ/kg of fuel. The chemical heat sink capacity at 25, 35, 45, and 55 bar pressure is about 520, 557, 594, and 634 kJ/kg, respectively, at 650 °C.

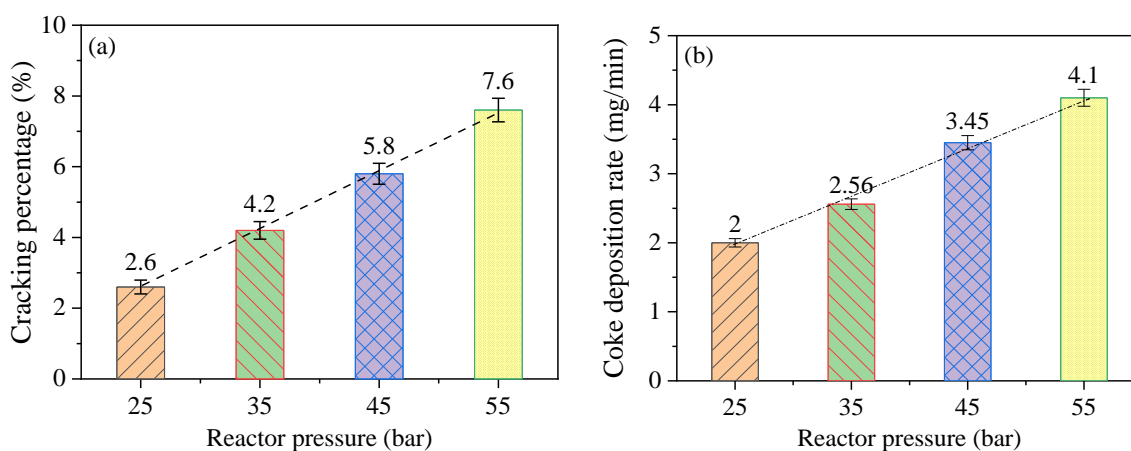


Fig. 5.8: Effect of pressure on a) cracking percentage, b) coke deposition rate at 650 °C.

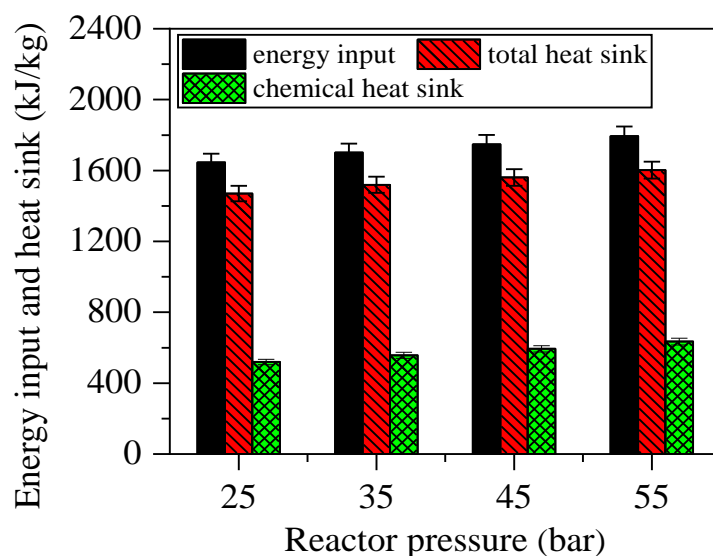


Fig. 5.9: Effect of pressure on energy input and heat sink capacities of HCF-1 at 650 °C

5.3.2.2. Effect of pressure on product gas composition

To find the effect of reactor pressure on product gas composition, the gaseous sample was analyzed in GC, and the results are shown in Fig. 5.10a. It is noted that the gaseous products are rich in methane (C_1), ethane (C_2), ethylene (C_2^-), propane (C_3), propylene (C_3^-), and hydrogen (H_2). The gases are formed mainly due to cleavage of the C-C or C-H bonds followed by unimolecular β -scission and hydrogen abstraction reactions. The decrease in methane concentration with pressure may be due to the enhanced rate of bimolecular radical recombination reaction of methyl radicals. The increase in ethane and propane yield with pressure may be because of the resultant effects of recombination of alkyl radicals, olefin hydrogenation reaction, and hydrogen abstraction by C_2 and C_3 radicals. The analysis further shows (Fig. 5.10b) a decreasing trend in the mole ratio of C_2^-/C_2 and C_3^-/C_3 with reactor pressure. However, the reduction is insignificant above 35 bar pressure. This decrease may be due to a bimolecular addition reaction which can promote alkanes formation.

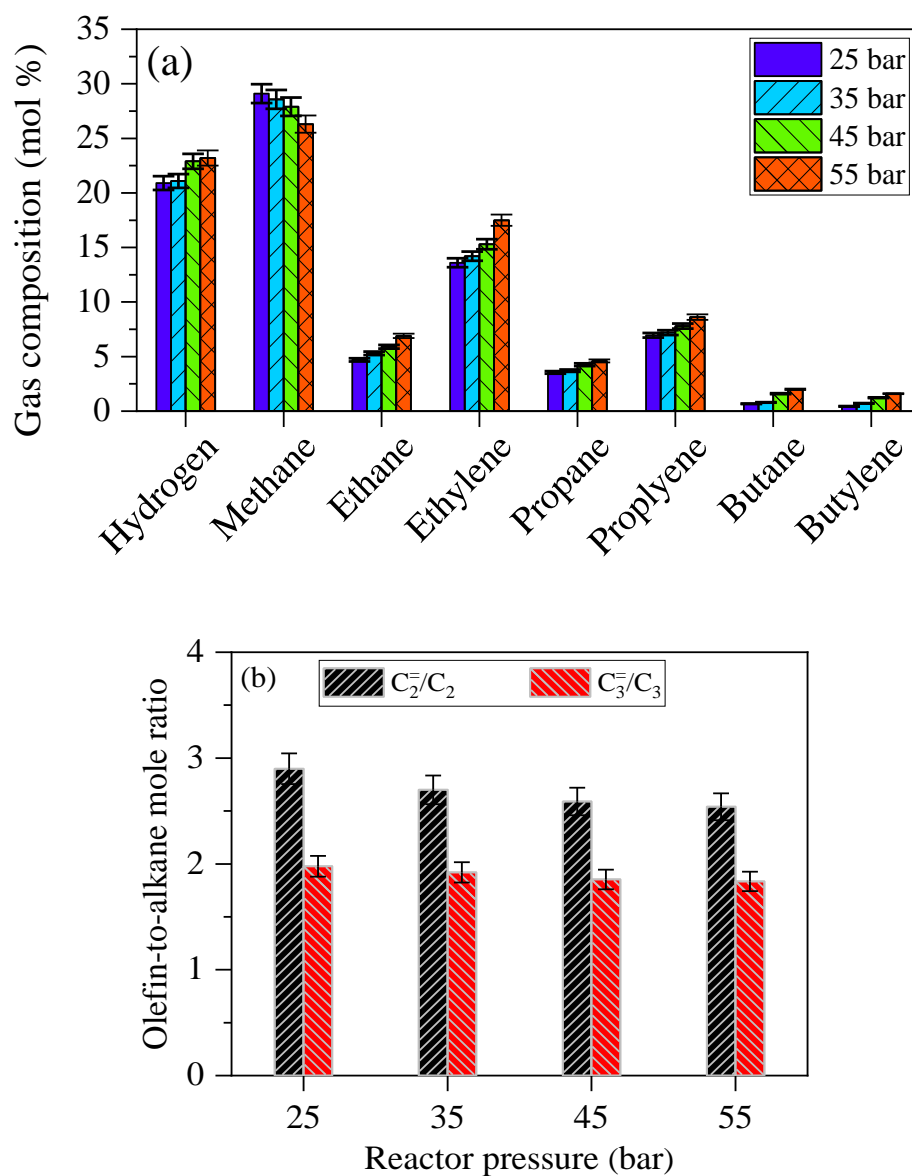


Fig. 5.10: Effect of pressure on a) gaseous product distribution, b) olefin-to-alkane ratio.

5.3.3. Effect of space-time on cracking percentage, coke deposition, and heat sink

To investigate the effect of space-time on cracking characteristics of HCF-1 fuel, a set of experiments was performed for different values of space-time for a fixed value of reactor temperature and pressure. In the work, the space-time was varied between 2.8 s to 8.5 s by changing the feed flow rate between 50 mL/min to 16.7 mL/min. The experiments were

performed at 650 °C under 55 bar pressure, and the results are shown in Table 5.6. The data shows that the cracking percentage, coke deposition rate, and endothermicity increased with space-time. However, the incremental rate of cracking percentage, coke deposition rate, and chemical heat sink decreased marginally with the increase of space-time. The cracking percentage and endothermicity of the fuel increased by about 59% and 33%, respectively, as the space-time increased from 2.8 s to 5.6 s. Further increase of space-time from 5.6 s to 8.5 s shows that the increment in cracking percentage and endothermicity is about 51% and 35%, respectively. The low value of incremental percentage of endothermicity compared to the cracking percentage maybe because of exothermic hydrogenation and polymerization reactions of the lighter olefins under the present experimental conditions.

To examine the possibility of a hydrogenation reaction of lighter olefins, the cracked-gas analysis was performed, and the results are shown in Table 5.6. The analysis shows a decreasing trend in H₂, ethylene (C₂⁼), and propylene (C₃⁼) compositions with the increase of space-time. It is also found that the olefin (C₂⁼ + C₃⁼)-to-alkane (C₂ + C₃), and H₂/CH₄ mole ratio decreased with the increase of space-time. The reduction in olefin yield with residence time is also reported by Jiang et al. (2011) for cracking dodecane under supercritical conditions. The analysis depicts the possibility of hydrogenation reaction with the increase of space-time. Hydrogenation being an exothermic reaction, can reduce the endothermicity of a fuel to some extent. Polymerization of olefins is another possible reason for the low values of olefin yield with higher residence time. The ASTM D86 distillation shows that the 95 vol.% (T_{95%}) and final boiling point (FBP) temperatures of the liquid products (shown in Table 5.6) increased with the increase of space-time. The increasing trend in FBP confirmed the possibility of a greater extent of polymerization reaction with space-time.

Table 5.6: Effect of space-time on cracking percentage, gas composition, coke deposition, and heat sink capacity of HCF-1 at 650 °C and 55 bar

Space-time (s)	2.8	5.6	8.5
Fuel conversion (wt.%)	7.6	12.1	18.3
Coke deposition rate (mg/min)	4.1	5.7	7.5
Total heat sink capacity (kJ/kg)	1602	1816	2111
Chemical heat sink capacity (kJ/kg)	634	849	1144
Cracked-gas composition (mol %)			
H ₂	23.2	22.5	21.7
C ₁	26.3	27.2	27.7
C ₂	1.79	7.13	7.91
C ₂ ⁼	22.6	16.8	16
C ₃	4.6	5.5	5.7
C ₃ ⁼	8.5	8.1	7.6
C ₄	2.0	2.1	2.4
C ₄ ⁼	1.6	1.8	2
Olefin-to-alkane mole ratio	2.17	1.97	1.73
H ₂ /CH ₄ mole ratio	0.88	0.83	0.78
T _{95%} of liquid products (°C)	220.3	221.6	224.2
FBP of liquid products (°C)	221.7	224.2	227.3

5.3.4. Analysis of coke morphology

In the present work, scanning electron microscopy (SEM) analysis was performed to examine the surface morphology of coke samples. Fig 5.11 shows the SEM images of coke samples that are obtained from the 650 °C operating temperature. At 200-micron magnification (Fig. 5.11a), the coke sample shows two distinct (particle agglomeration and ribbon/wire-like) surface morphology. On magnifying the selected portion, the agglomerated image shows a flower-like structure (Fig. 5.11c). Further magnification to 0.5-micron resolution, the image

shows that the flower-like structures are comprised of oval-shaped particles (Fig. 5.11d) with a diameter range of 30 nm to 70 nm. In contrast, the magnification of the ribbon-shaped structures shows fiber morphology with small branches/sheets/coils, as shown in (Fig. 5.11b). The diameter of the fibers lies in the range of 5 to 30 μm . The round-shaped particle indicates the characteristic of amorphous coke, and the ribbon-shaped morphology is a characteristic of filamentous coke. The two types of surface morphology indicate two different mechanisms/ pathways followed to form coke deposits during the thermal cracking of HCF-1. In general, amorphous coke developed due to the polymerization and deposition of high molecular weight hydrocarbons. In contrast, filamentous coke is formed due to the interaction of the poly-nuclear aromatic precursors with the metal surface and condensation reaction. A similar kind of coke morphology was also noted by Liu et al. (2015) for a kerosene range hydrocarbon.

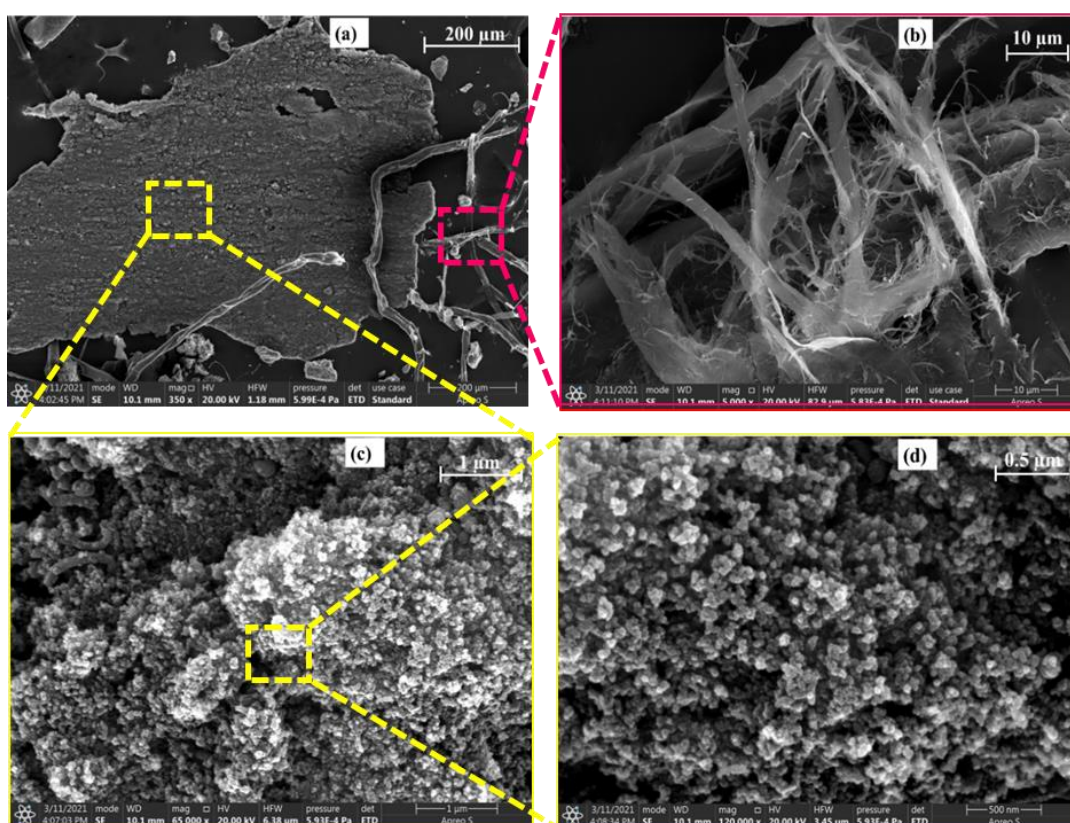


Fig. 5.11: SEM images of coke sample obtained at 650 $^{\circ}\text{C}$ for a) 200 μm , b) 10 μm , c) 1 μm , and d) 0.5 μm magnification.

5.3.5. Estimation of kinetic rate constant and activation energy

In estimating the kinetic parameters for the cracking of HCF-1 fuel, it was assumed that the reactant and product exist as a single phase under supercritical conditions, and the reactor behaves like an ideal plug flow reactor. Eq. 5.28 is used to estimate the residence time (t) of the fuel at different temperatures. Eq. 5.29 was used to estimate the first-order rate constant (k_1) at different temperatures, and the results are tabulated in Table 5.7. Fig. 5.12a shows that the first-order rate constant (k_1) increased exponentially with the increase of reactor temperature. The value of k_1 increased by nearly 4-time with the increase in reaction temperature from 600 °C to 680 °C. The Arrhenius plot, as shown in Fig 5.12(b), was used to find the apparent activation energy of the cracking reaction for two different scenarios. The estimated value of the apparent activation energy is about 125 kJ/mol for $\varepsilon = 0$, and the corresponding value for $\varepsilon = 5$ is 135.3 kJ/mol.

$$t = \frac{\text{Volume of reactor}}{\text{Average volumetric flowrate}} = \frac{V_R}{v_o \left(\frac{T_{avg.}}{T_o} \times \frac{P_o}{P_{avg.}} \times \frac{Z_{avg.}}{Z_o} \right)} \quad \text{Eq. (5.28)}$$

$$k_1 = \frac{1}{t} \left[-\ln(1-x) + \varepsilon \{ -\ln(1-x) - x \} \right] \quad \text{Eq. (5.29)}$$

Table 5.7: Values of first-order rate constant (k_1) at different temperatures

Temperature (°C)	550	600	650	680
Cracking percentage (wt.%)	1.2	3.3	7.6	10.3
Reactor volume (mL)	2.36	2.36	2.36	2.36
Residence time (s)	1.17	1.03	0.94	0.90
' k_1 ' for $\varepsilon = 0$ (1/s)	0.010	0.033	0.084	0.121

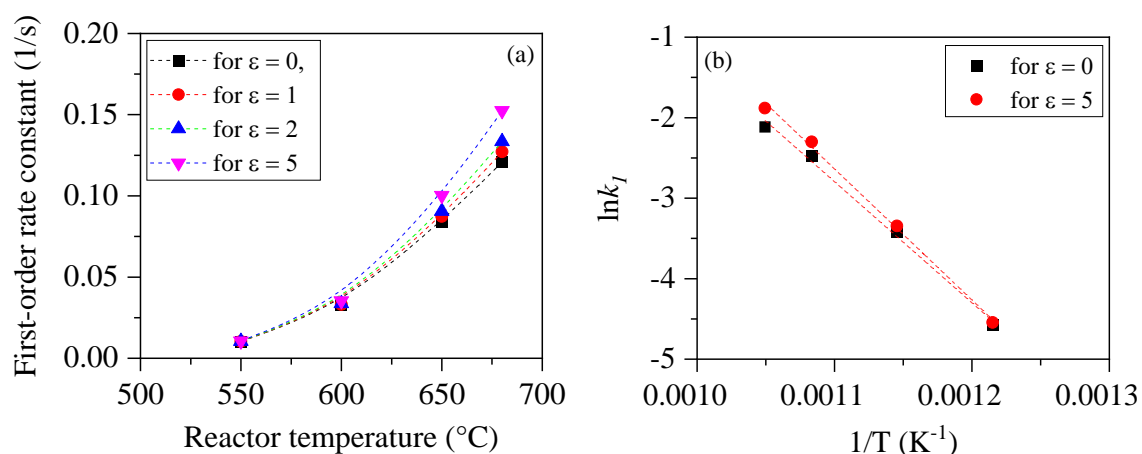


Fig. 5.12: a) Variation of first-order rate constant with temperature, b) Arrhenius plots.

5.4. Conclusion

In this chapter, the cracking characteristics of a multi-component hydrocarbon fuel (i.e., HCF-1 with a boiling range of 131-223 °C) are investigated. The effects of reactor temperature, space-time, and initiator loading on fuel conversion, endothermicity, coke deposition rate, and product-gas yield are examined in-depth. The cracking experiments were performed for a temperature range of 550 to 680 °C at 55 bar pressure. The space-time parameter was varied from 2.8 s to 8.5 s. It is observed that the cracking percentage, coking rate, and endothermicity of the fuel increased with the increase in temperature. The cracking percentage of HCF-1 at 600 °C is 3.3 wt.% and increased to 10.5 wt.% at 680 °C. The coke deposition rate and endothermic heat sink capacity increased from 3.1 to 7 mg/min and 463 to 805 kJ/kg, respectively, as the temperature increased from 600 °C to 680 °C. A decreasing trend in the olefin-to-alkane ratio is observed with the increase in cracking temperatures. With the increase in pressure from 25 to 55 bar, the fuel conversion increased by 2.5 times and endothermicity by about 20% (520 to 634 kJ/kg). With the increase in space-time from 2.8 s to 8.5 s, the cracking percentage improved by 2.4-fold, and endothermicity increased by 1.8 times (from 635 to 1144 kJ/kg) at 650 °C. A decreasing trend in olefin yield is noted with residence time. The SEM analysis confirmed that the surface morphology of the coke deposits consists of spherical-shaped (amorphous) and ribbon-like (filamentous) structures. Also, the kinetic investigation showed a good fit of the experimental data with the first-order kinetics, and the calculated values of the first-order rate

constant (k) lie between 0.01 to 0.15 (1/s) for the studied temperature range depending on the volume expansion factor. The estimated value of the apparent activation energy of the HCF-1 cracking reaction is about 125 kJ/mol.

The outcome of Chapter 5 bridges the following objectives mentioned in Chapter 1.

- Understanding of cracking characteristics of multi-component fuel above 650 °C and 50 bar pressure and for a fuel residence time of less than 3 s.
- Establishment of a modified methodology for the estimation of heat loss percentage.
- Establishment of new methodologies for estimating the enthalpy change for heat sink.

Chapter-6

Efficacy of Initiators on Cracking Characteristics of Hydrocarbon Fuel Under Supercritical Conditions

Efficacy of Initiators on Cracking Characteristics of Hydrocarbon Fuel Under Supercritical Conditions

6.1. Introduction

Hydrocarbon fuels are capable of performing the dual role of propellant and coolant (Stashkiv et al. (2019)). In an advanced engine, the fuel that flows through the exterior wall of the combustor can absorb combustion heat (Fortin et al. (2013), Xiao et al. (2021)). The absorption of heat by the fuel facilitates the phase transition and cracking of the fuel during its journey through the fuel transfer lines (Liu et al. (2021)). It can be an efficient approach in managing the thermal load of the engine structure. Jet A-1, JP-4, JP-5, JP-7, JP-8, JP-9, RP-1, hydrogenated carene, and RP-3 are examples of kerosene range fuels consisting of carbon numbers in the range of C₉ to C₁₆ (Wang et al. (2023)). The fuels are typically comprised of 40–60% of alkanes/isoalkanes, 20–30% naphthenes, and less than 10% in aromatics (Zhou et al. (2017), Sun et al. (2019)). The cracking performance of hydrocarbons depends on the H/C ratio of the fuel (Lei et al. (2016), Zhou et al. (2017)). JP-10 (tetrahydro-dicyclopentadiene) fuel, a high-energy-density single-component hydrocarbon with a carbon number of C₁₀, can offer high heat sink capacity (Huang et al. (2017)). The cracking of fuel molecules can lead to the formation of cyclic hydrocarbons which can further polymerize into polycyclic aromatics and act as a precursor for coke deposition (Liu et al. (2015), Qu et al. (2011)). A good fuel should offer a high heat sink capacity and low coke deposition under a supercritical environment. The suitability of several heterogeneous catalysts, such as ZrO₂-TiO₂, ZrO₂-TiO₂-Al₂O₃, zeolites, HZSM-5, and SAPO-34, has been examined by various authors for the supercritical cracking of hydrocarbon fuels (Kim et al. (2020), Jiao et al. (2018), Zhang et al. (2013)). However, catalyst coatings have certain limitations, such as quick deactivation and low heat transfer rate, and they require strong adhesion between the catalysts and the metal surface (Liu et al. (2022)). The housing of uniform coating of catalysts inside a narrow tube (nearly 2 mm internal diameter) is another challenge. These limitations can be mitigated by choosing homogenous initiators that are soluble in fuel.

From the literature survey, it is found that in most of the studies, single-component hydrocarbons were used to examine the influence of initiators. But in actual applications, multi-

component fuels such as RP-3, and JP-7, derived from a kerosene-range hydrocarbon, are more appealing than a single-component hydrocarbon due to cost factor. Also, a multi-component fuel can absorb heat from the wide region of the supersonic combustor due to differential values of heat capacity and crackability of different hydrocarbons at various temperatures. The aim of the present research is to examine the suitability of initiators on the cracking characteristics of a multi-component fuel under a supercritical environment is investigated. The study also includes the effect of initiator on liquid product composition, alkane-to-aromatic, and alkane-to-cycloalkane ratios in liquid products, and its impact on coke deposition.

6.2. Materials and Methods

6.2.1. Materials

A hydrocarbon fuel (named as HCF-2), used in the work, was purchased from Ogene Systems India Pvt. Ltd., India. The physicochemical characteristics of the fuel are presented in Table 1. Triethylamine (TEA), and di-tert-butyl peroxide (DTBP) were purchased from S.D. Fine Chemicals Ltd., India. Other chemicals used for calibration and analytic purposes are detailed in Chapter-3.

6.2.2. Experimental setup and procedure

The experiments were conducted using a high-pressure flow reactor, and the details are explained in Chapter 3. Nearly 75% of the pyrolysis experiments were repeated to examine the repeatability of the power input to the reactor, and the observed deviation in power input lies below 3%. To indicate the deviation in the experimental results, an error bar is kept in most of the results. Uncertainty in experimental results is inevitable in most cases, and it can arise due to fluctuations in operating variables. The fluctuations noted in the instrumental readings were reactor temperature: ± 3 °C; reactor pressure ± 1 bar; fuel flow rate ± 0.1 g/min, and power input from the transformer: ± 15 watts.

6.3. Results and Discussion

6.3.1. Characterization of HCF-2 fuel

Several techniques were used to find the physicochemical properties of the hydrocarbon fuel, as shown in Table 6.1. ASTM D86 distillation analysis revealed that the boiling range

temperature of the fuel lies between 149-224 °C, and the average boiling temperature (T_{avg}) is 190.7 °C. The critical temperature and critical pressure of the fuel are estimated using Eq. 6.1 and Eq. 6.2, respectively. The GC-MS chromatogram of the HCF-2 fuel is presented in Fig. 6.1a. GC-MS analysis showed that the fuel consists of primarily C₁₀, C₁₁, C₁₂, and C₁₃ hydrocarbons with a minor quantity of C₉ and C₁₄ hydrocarbons, as shown in Fig. 6.1b. The GC analysis also revealed (Fig. 6.1c) that the fuel is rich in paraffinic and naphthenic content.

$$T_c(^{\circ}F) = 186.16 + 1.6667 \times SG \times (T + 100) - 0.7127 \times 10^{-3} \times \{SG \times (T + 100)\}^2 \quad \text{Eq. (6.1)}$$

$$P_c(\text{psia}) = 3.4824 \times 10^9 \times (T + 460)^{-2.1377} \times SG^{2.4853} \quad \text{Eq. (6.2)}$$

where ‘T’ is the average boiling point in °F, and ‘SG’ is the specific gravity of fuel.

Table 6.1: Physico-chemical properties of HCF-2 fuel

Properties	Value	Properties	Value
Density @ 28 °C (kg/m ³)	795 ± 5	ASTM D86 boiling characteristics	
Aniline point (°C)	68 ± 1	5 vol.% temp. (T _{5%}), °C	171.8
Critical temperature (°C)	379 ± 0.5	10 vol.% temp. (T _{10%}), °C	176.2
Critical pressure (bar)	23 ± 0.1	20 vol.% temp. (T _{20%}), °C	179.1
Calorific value (MJ/kg)	45 ± 0.2	30 vol.% temp. (T _{30%}), °C	182.1
Average boiling point (°C)	190.7	40 vol.% temp. (T _{40%}), °C	185.2
Paraffin (P) (vol.%)	51.1 ± 1	50 vol.% temp. (T _{50%}), °C	188.6
Naphthene (N) (vol.%)	40.4 ± 1	60 vol.% temp. (T _{60%}), °C	192.6
Aromatic (A) (vol.%)	8.2 ± 0.5	70 vol.% temp. (T _{70%}), °C	197.3
		80 vol.% temp. (T _{80%}), °C	203.3
		90 vol.% temp. (T _{90%}), °C	211.8
		95 vol.% temp. (T _{95%}), °C	218.7

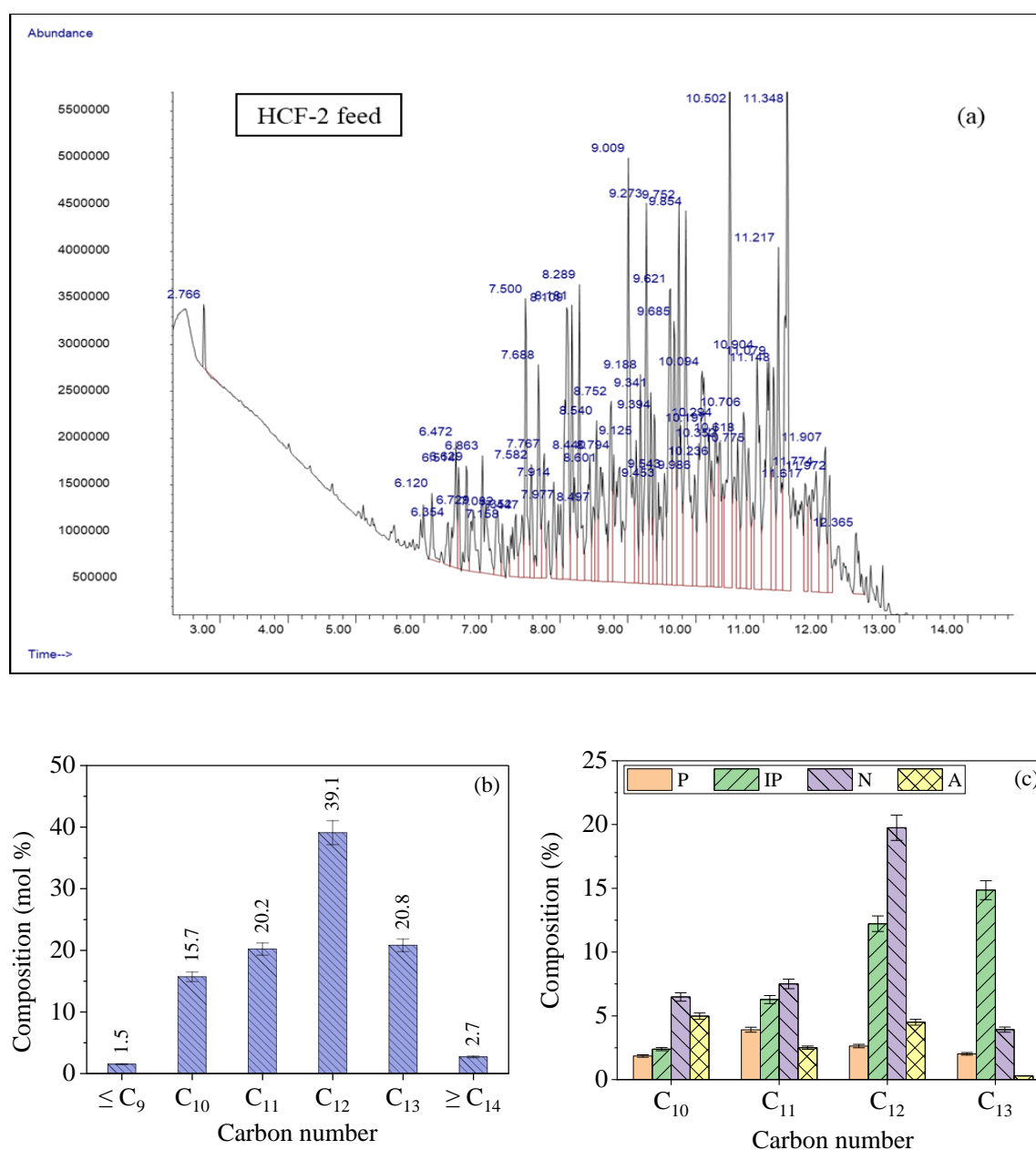


Fig. 6.1: a) GC-MS chromatogram, b) Carbon number-wise composition, c) P, N, and A composition among C_{10} to C_{13} hydrocarbons of feed HCF-2 fuel.

6.3.2. Influence of initiators on supercritical cracking characteristics of HCF-2

To investigate the effect of initiators on fuel cracking percentage, coke deposition rate, endothermicity, and product distributions of the HCF-2, cracking experiments were performed in the presence of two different initiators, namely triethylamine (TEA) and di-tert-butyl peroxide (DTBP) under similar operating conditions. The initiators were chosen due to the presence of

low-energy C-N and O-O bonds. The bond dissociation energy of a C–N-bond (nearly 305 kJ/mol) and O-O bond (nearly 160 kJ/mol) is lower than a C–C bond (nearly 346 kJ/mol) (Chakraborty et al. (2012)). The boiling point temperature of TEA and DTBP is 89.5 °C and 110 °C, respectively. The specific gravity value of the TEA and DTBP is 0.725, and 0.796, respectively. Under supercritical conditions, the C–N bond in TEA, and the O–O bond in DTBP can undergo homolytic fission, resulting in the formation of free radicals and the radicals can initiate the cracking process. To examine the impact of initiator concentration on fuel cracking performance, the concentration of the initiators in the fuels was varied between 0.1 wt.% and 1 wt.%. In each case, the cracking experiments were performed at 650 °C under 55 bar pressure and for a fuel flow rate of 50 mL/min. The details of analysis techniques, feed and product characterization, expressions, and equations used in estimating the cracking percentage, coke deposition rate, and heat sink calculation are mentioned in Chapter-4.

6.3.2.1. Effect of initiator on fuel cracking percentage and coke deposition

Fig. 6.2a shows the influence of TEA and DTBP on the cracking percentage of HCF-2. In each case, the concentration of initiators was kept at a level of 0.5 wt.% of HCF-2. The result shows that the cracking percentage of HCF-2 increased in the presence of initiators compared to the initiator-free case. Between the two initiators, the TEA shows better performance than the DTBP. The cracking percentage increased by 4.4% in the presence of TEA, and the corresponding increment is nearly 2.6 % for the DTBP case. The coke deposition rate during thermal cracking of HCF-2 without any initiator at 650 °C and 55 bar pressure is 4.1 mg/min. The investigation shows that the coke deposition rate increased in the presence of both initiators. The coke deposition rate in the presence of 0.5 wt.% loading of TEA and DTBP increased by a margin of 10% and 20%, respectively, as shown in Fig 6.2b.

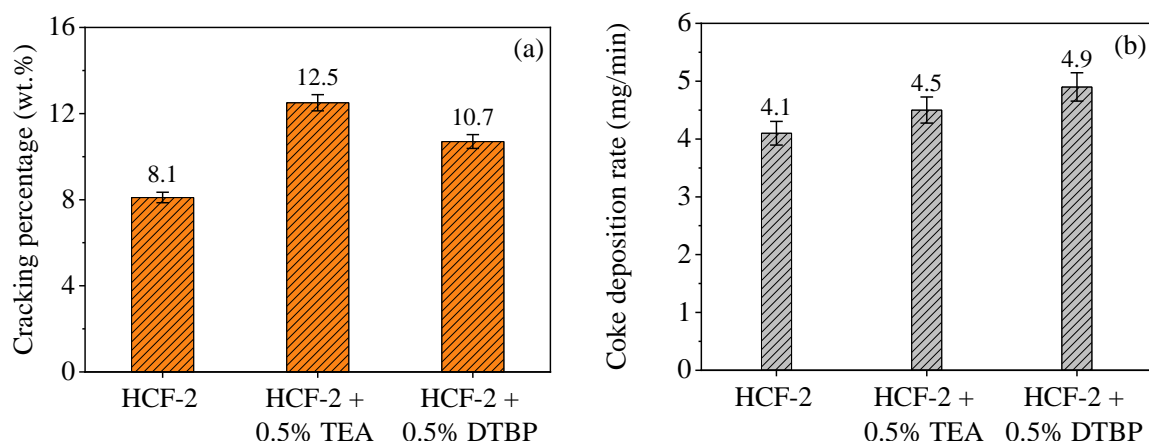
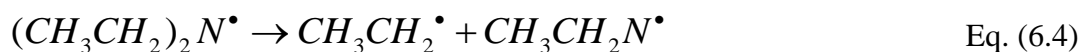
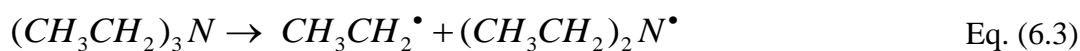


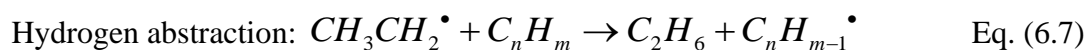
Fig. 6.2: Effect of TEA and DTBP on a) fuel cracking %, b) coke deposition rate.

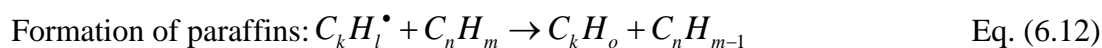
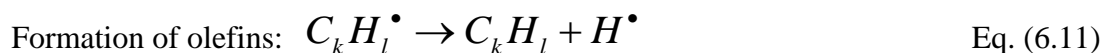
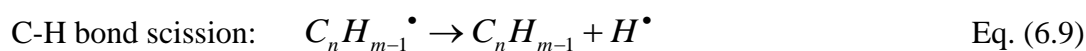
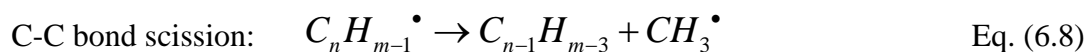
A probable mechanism for the formation of various radicals from TEA and parent hydrocarbon (C_nH_m) is shown in Eq. (6.3-6.15). Ethyl radicals are formed by the decomposition of TEA, as shown in Eq. 6.3 and Eq. 6.4. Ethyl radical might also undergo decomposition to form ethylene, as shown in Eq. 6.5. Ethane can form as per the hydrogen abstraction reaction described in Eq. 6.7. The cracking reaction propagates with the aid of the free radicals that are formed in the initiation steps, as shown in Eq. (6.7-6.12). Since the radical-radical combination involved less activation energy, radical termination reactions can happen involving Eq. (6.12-6.15). The fuel radicals formed in the initiation step can undergo a series of decomposition and bimolecular reactions to form lower allyl radicals, olefins, and paraffin.

Initiation steps:



Propagation steps:

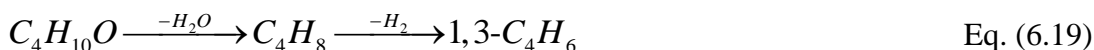
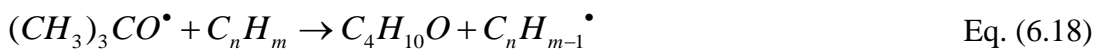
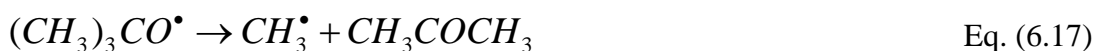




Termination steps:



A possible mechanism of DTBP dissociation can occur according to Eq. (6.16-6.20). DTBP decomposes by releasing two butoxy radicals. The butoxy radical can further decompose to form methyl radical and acetone. The formation of acetone was confirmed from the analysis of the liquid product. The tert-butanol (in Eq. 6.18) can further undergo dehydration and dehydrogenation reactions to form butylene and 1, 3 butadiene, as shown in Eq. 6.19. In the gaseous product, the methane yield was higher with DTBP than the corresponding value in the presence of TEA. The chain propagation and radical termination reaction can follow similar pathways as mentioned above.



Even though the bond dissociation energy of the O-O bond (nearly 160 kJ/mol) in DTBP is significantly lower than the C-N bond (nearly 305 kJ/mol) in TEA, the cracking percentage is relatively higher for TEA than with DTBP. This indicates that an initiator with lower bond dissociation energy may not be a sufficient condition in enhancing the cracking percentages. The nature and stability of free radicals formed from an initiator play a vital role in enhancing the fuel cracking percentage.

To examine the probable reasons for the increase in coke depositions with initiators, the GC-MS analysis was performed for the liquid products. The GC-MS chromatogram of the HCF-2 derived liquid products at 650 °C and 55 bar without and with initiators, is shown in Fig. 6.3. The analysis of GC-MS data revealed the presence of coke precursors like alkyl benzenes, naphthalene, and indene compounds in the liquid products.

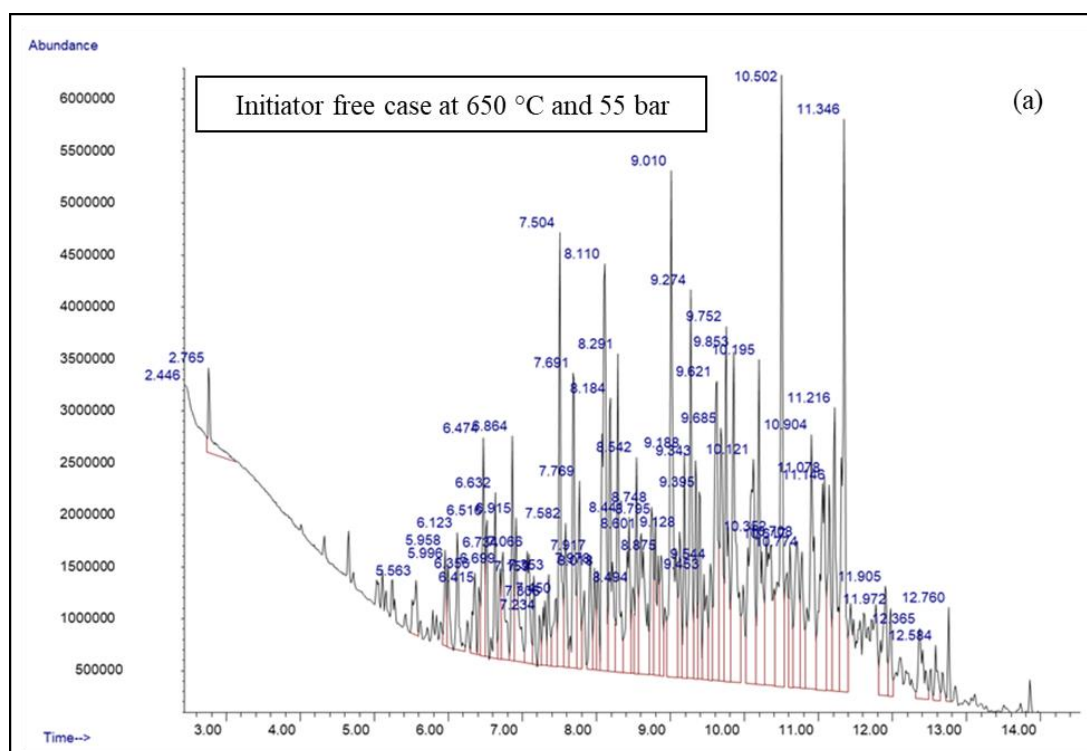


Fig. 6.4a shows the contribution of alkyl benzenes (C_2 to C_6 alkyl benzene) in the HCF-2 feed and cracked liquid products with and without initiator. The combined (i.e., C_2 to C_6) contribution of the alkyl benzenes in the HCF-2 feed and cracked product (without initiator) is about 1.6% and 6.9%, respectively. Whereas, in the presence of 0.5 wt.% of TEA and DTBP, the overall contribution of alkyl benzenes is nearly 4.3% and 2.5%, respectively. The decrease in concentration may be due to consumption of the alkyl benzenes in coke formation. The variation in alkyl benzene percentage in the cracked products is consistent with the coke results. The presence of stable aromatic compounds, such as benzene, toluene, and naphthalene, is beneficial as they can reduce the tendency of coke-forming radicals like benzyl, phenyl, and naphthyl. The formation of these radicals can enhance the probability of polycyclic aromatic hydrocarbons (PAHs), which can act as precursors in pyrolytic coking.

There might be another class of aromatics, like olefinic-bond containing aromatics, which might have contributed to the formation of pyrolytic coke. The overall concentration of olefinic-bond containing aromatics in the liquid products is nearly 0.5%, 0.4%, and 0.6% in the absence of an initiator, with TEA and DTBP, respectively, and the corresponding amount in the feed is nearly 0.7%, as shown in Fig. 6.4b. Generally, the reactivity of the olefinic bond containing aromatics increases with the increase of aromatic rings. Hence, a higher concentration of olefinic bonds, longer residence time, and higher cracking temperature can increase the addition and condensation reactions and finally lead to coke formation. A similar kind of observation is also noted by Wang et. al. (2023) for the supercritical cracking of heavy oil hydrocarbon.

Further, the alkane-to-aromatic and alkane-to-cycloalkane ratios in the feed and products were analyzed to examine their impact on coking phenomena. Fig. 6.4c and Fig. 6.4d show the alkane-to-aromatic and alkane-to-cycloalkane ratios of the C_{10} , C_{11} , C_{12} , to C_{13} hydrocarbons present in the feed and liquid products. Though the analysis shows some incremental change in the alkane-to-aromatic ratio in the presence of initiators, no specific correlation was noted between the coke deposition and the alkane-to-aromatic ratio. Due to cyclic structures, aromatics and cycloalkanes are less efficient for pyrolysis compared to alkanes under similar operating conditions (Jiang et al. (2011)). The coke-forming mechanisms of alkanes, cycloalkanes, and aromatics are different due to their structural variation and thermochemical stability. Coke deposition during the thermal cracking of alkanes progresses mainly by chain scission, ring formation by Diels-alder reactions, and polymerization reactions. Coke formation from

cycloalkanes can proceed through dehydrogenation, dealkylation, condensation, and polymerization reactions.

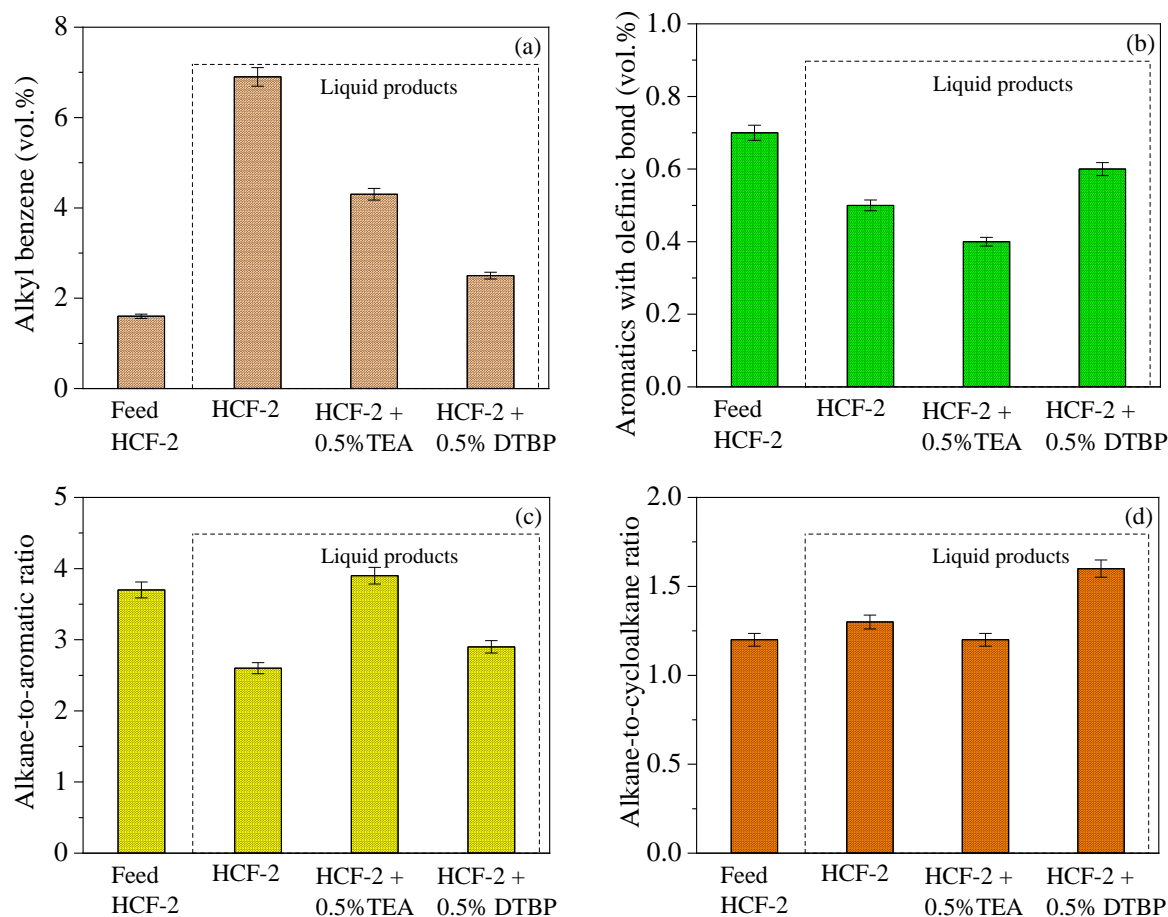


Fig. 6.4: Variation in a) alkyl-benzene concentration, b) olefinic-bond containing aromatics concentration, c) alkane-to-aromatic ratio, and d) alkane-to-cycloalkane ratio.

6.3.2.2. Effect of initiator on gas composition and heat sink

The formation of gaseous hydrocarbons and hydrogen in a thermal cracking process may help to improve the ignition and combustion quality in high-speed engines. The change in concentration of gaseous compounds due to the addition of initiators is an important factor in evaluating the efficacy of an initiator. Additionally, the formation of lighter olefins, such as ethylene and propylene, is beneficial in enhancing the heat sink capacity of a fuel. However, the light olefins can also enhance coking phenomena via the Diels-Alder reaction under a suitable reaction condition. The yield of the major components in the gaseous products obtained from the

=====

650 °C cracking temperature is shown in Fig. 6.5a. In the presence of 0.5 wt.% TEA, the yield of hydrogen increased by 7.6% due to the enhanced rate of hydrogen radical formation and its recombination to hydrogen gas in the termination step. The formation of ethyl radicals due to the C-N bond scission of the TEA initiator enhanced the ethylene (C_2^-) and ethane (C_2) yield in the gaseous product according to Eq. 6.9 and Eq. 6.11, respectively. Whereas, the reduction in propane (C_3) and propylene (C_3^-) yield may be due to the unimolecular decomposition of propyl radicals to lighter hydrocarbons. In the case of the 0.5 wt.% DTBP, the yield of methane increased remarkably compared to the initiator-free case. The increase in methane yield may be due to the decomposition of the butoxy radicals to methyl radicals (Eq. 6.21) and subsequently to methane formation (Eq. 6.24). An olefin-to-alkane ratio can be an important parameter to understand any significant change in the cracking behavior of hydrocarbons in the presence of an initiator. The ratio may be helpful in getting a qualitative idea about the variation in endothermicity. Generally, the higher the olefin-to-alkane ratio, the expected endothermicity will be higher. The calculated values of the $(C_2^-+C_3^-)/(C_2+C_3)$ mole percentage ratio in the gaseous products are 2.42, and 2.31 in the presence of 0.5% of TEA and DTBP. Whereas the corresponding value in the absence of an initiator is 2.21. The result signifies that the cracking mechanism is mostly unaltered with and without initiators. The marginal (nearly 8%) increment in the olefin-to-alkane ratio in the presence of initiators may be due increase in ethylene yield.

Fig. 6.5b shows the variation in heat sink capacity of HCF-2 with and without initiators under similar operating conditions. At 650 °C cracking temperature and under 55 bar pressure the overall heat sink capacity without initiator is 1632 kJ/kg. The overall heat sinks increased by 2.3% and 4.4% in the presence of 0.5% of TEA and DTBP loading, respectively. In the presence of TEA and DTBP, the $(C_2^-+C_3^-)/(C_2+C_3)$ mole ratio increased by 6.8% and 3.8%, respectively. The rise in the olefin-to-alkane ratio in the gaseous product may contributed in enhancing the overall heat sink of the fuel. It is also noted that the peroxide initiator (i.e., DTBP) offered higher heat sink capacity in spite of the lower value of fuel cracking percentage in comparison to the TEA initiator. With the DTBP initiator, the relatively higher value of the alkane-to-cycloalkane ratio (Fig. 6.4d) in the liquid product implies that more cycloalkanes have participated in the cracking reactions. The chemical heat sink values are increased by about 7% and 13% in the presence of TEA and DTBP, respectively, compared to the initiator-free case. In the case of

DTBP, the formation of butanol and its subsequent cracking percentage to butylene and 1,3-butadiene may be responsible for higher endothermicity in comparison to TEA.

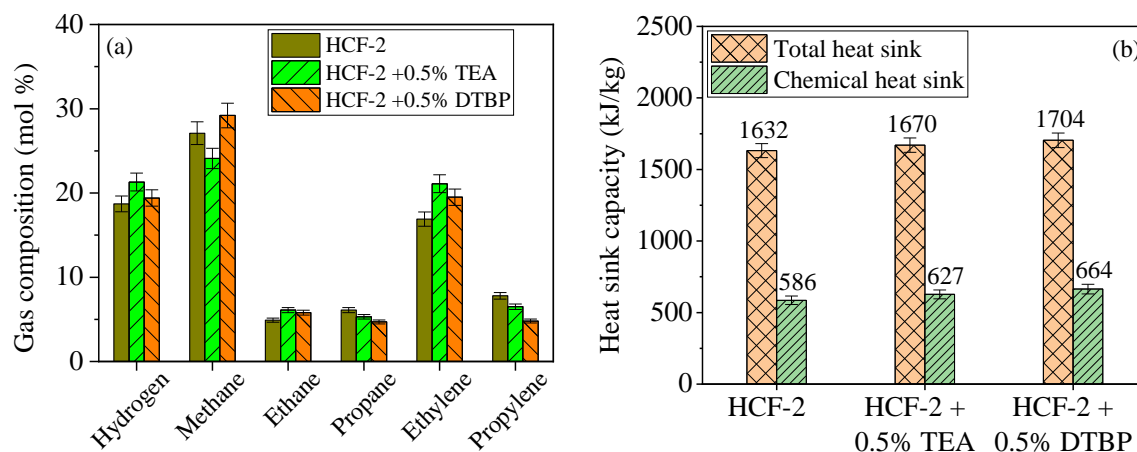


Fig. 6.5: Influence of initiators on a) gas composition, b) heat sink capacities.

6.3.2.3. Effect of initiator loading on cracking percentage, coke deposition, and heat sinks

To examine the impact of initiator loading on the thermal cracking characteristics of the HCF-2 fuel, the initiator loading was varied between 0.1% to 1% in the feed, and the cracking experiments were performed at 650 °C under 55 bar pressure with a feed flow rate of 50 mL/min. The variation in fuel cracking percentage, coke deposition rate, olefin-to-alkane ratio of the gaseous product, and heat sink capacities with initiator loading are presented in Table 6.2.

Table 6.2: Effect of initiator on cracking percentage, coke deposition, and heat sinks

	HCF-2	HCF-2+TEA			HCF-2+DTBP		
	-	0.1%	0.5%	1%	0.1%	0.5%	1%
Cracking percentage (wt.%)	8.1	8.9	12.5	16.7	8.3	10.7	14.2
Coke deposition (mg/min)	4.1	4.2	4.5	6.4	4.2	4.9	6.8
Olefin-to-alkane ratio	2.21	2.22	2.42	2.6	2.22	2.31	2.44
Total heat sink (kJ/kg)	1632	1640	1670	1706	1643	1705	1723
Chemical heat sink (kJ/kg)	586	593	627	667	596	664	689

The result shows an increasing trend in fuel cracking percentage, coke deposition rate, and heat sink capacity with the increase in initiator loading. The fuel cracking percentage increased by 8.6% and 6.1% in the presence of TEA and DTBP initiators of 1% loading. The coke deposition rate increased by 1.6 and 1.7 folds with TEA and DTBP of 1%, respectively. The chemical heat sink capacity increased by about 14% and 18% in the presence of TEA and DTBP of 1% loading, respectively. Though the result shows an increasing trend in the heat sink capacities with initiator loadings, the increasing trend in the coke deposition rates can be a critical issue.

6.4. Conclusion

In the present research, the impact of reactor pressure and the influence of initiators on cracking characteristics, such as fuel cracking percentage, coke deposition rate, gas and liquid product distribution pattern, and heat sink capacities, of hydrocarbon fuel under supercritical environments were examined in depth. A multi-component hydrocarbon fuel with a boiling range of 149-224 °C was considered in the work, and the pyrolysis studies were performed using a tubular flow reactor. The efficacy of two homogeneous initiators, triethylamine (TEA) and di-tert-butyl peroxide (DTBP), on heat sinks and coke deposition was also investigated. Though the initiators showed a positive impact on the heat sink capacity of the fuel, the coke deposition is also increased in the presence of initiators. The cracking percentage increased by 8.6% and 6.1% in the presence of TEA and DTBP initiators of 1% loading. The coke deposition rate increased by 1.6 and 1.7 folds with TEA and DTBP of 1%, respectively. The chemical heat sink capacity increased by about 14% and 18% in the presence of TEA and DTBP of 1% loading, respectively. Though the result shows an increasing trend in the heat sink capacities with initiator loadings, the increasing trend in the coke deposition rates can be a critical issue. Between the two initiators, the nitrogen-based TEA initiator showed somewhat better performance in terms of fuel cracking percentage and coke deposition rate, and the DTBP offered better heat sink capacity. From the investigation, it can be said that, although the homogeneous initiators are helpful in boosting the endothermicity of hydrocarbon fuels, coke formation can be a critical parameter in selecting an appropriate initiator.

The outcome of Chapter 6 bridges the following objectives mentioned in Chapter 1.

- Understanding of the influence of initiator on fuel conversion, heat sink, and coking behavior of multi-component fuel.

Chapter-7

***Development of Coke Model for Thermal
Cracking of Hydrocarbon Fuels under
Supercritical Conditions***

Development of Coke Model for Thermal Cracking of Hydrocarbon Fuels Under Supercritical Conditions

7.1. Introduction

An onboard fuel can be used to obtain energy for flying and as a regenerative cooling media to safeguard the internal structure of an engine (Qin et al. (2013), Li et al. (2021)). To achieve the objectives, fuel should have a high calorific value and higher heat sink capacity. Higher calorific content leads to better combustion quality for achieving greater than Mach-4 speed, whereas a higher heat sink capacity helps to absorb the heat loads emanating from the combustion chamber (Konda et al. (2022), Yang et al. (2012)). Before entering the combustion chamber, a hydrocarbon fuel may undergo thermal cracking reactions in the fuel transfer lines, which are fixed on the surface of the combustion chamber (Konda et al. (2022), Xu et al. (2015)). The smaller hydrocarbons can play an important role in improving combustion quality (Liu et al. (2014), Ning et al. (2012), Zuo et al. (2020), Yue et al. (2016)). Due to cost-effectiveness and easy availability, a hydrocarbon liquid can be a preferred choice for regenerative cooling. A long-chain hydrocarbon can crack at relatively lower temperatures than a short-chain hydrocarbon. However, the efficacy of thermal cracking hugely depends on coking phenomena that can occur inside the fuel transfer lines. Deposition of carbonaceous materials is inevitable in a thermal cracking process. Several studies are available on how coke precursors (e.g., light olefins and aromatics) are formed during the cracking process and which can lead to carbon deposition inside the fuel line (Edwards (2016), Dewitt et al. (2011), Jiang et al. (2013)). A quantification of coke precursors is important to estimate the coke deposition rate. It is difficult to isolate each intermediate species formed during the pyrolysis process for multi-component fuels, like kerosene range aviation fuel, JP-7, and RP-3. To overcome this difficulty, researchers have used a simplified approach of considering single-component hydrocarbons, such as n-decane and n-dodecane, whose molecular formulas are close to kerosene range jet fuels and can be represented as model hydrocarbons (Tianhao et al. (2020), Keke et al. (2015)). The kinetic representations of cracking reactions can be classified into descriptive (Keke et al. (2015)), lumped (Roohollahi et al. (2012)), and global (Ward et al. (2004)) kinetic models. The descriptive kinetic model for n-dodecane comprises 1175 reactions, and the lumped kinetic model for C₈ - C₁₆ alkanes

comprises about 7000 chemical reactions (Dahm et al. (2004)). Working with a large number of chemical reactions is too cumbersome for practical implementation in flow simulations, whereas a global kinetic model can offer more realistic predictions to describe cracking reactions inside a flow system (Tian et al. (2023)).

Zhu et al. proposed a single-step global kinetic model and validated it by performing pyrolysis experiments with n-dodecane under supercritical pressures (4.2 - 5.3 MPa) and temperatures (590 - 630 °C) using a flow reactor (Zhu et al. (2014)). Zhang et al. (2018) developed a global kinetic model for the pyrolysis of n-dodecane under supercritical conditions. Jiang et al. (2019) and Wang et al. (2020) have developed differential global kinetic models for the cracking of n-decane. Most of the kinetic models emphasized the possibilities of liquid and gaseous product formation, and the coke deposition aspect within the fuel line was ignored. Liu et al. (2013) developed a coke formation model for n-decane and RP-3 fuel. Mohamadalizadeh et al. (2013) developed coke-predicting models for naphtha cracking under subcritical pressure. Various properties such as fuel density, hydrocarbon composition, and impurities (e.g., sulfur, nitrogen, arsenic) can be crucial in forming coke precursors. Though the concentration of impurities is less than 1% by weight in most cases, their contribution can trigger the formation of filamentous coke and gum deposits exponentially. Additionally, the combined effects of operating parameters, like temperature, pressure, and residence time, can also propagate the formation of agglomeration and condensation of coke deposits due to the phase transition from subcritical to supercritical conditions (Wang et al. (2023), Hou et al. (2013)). Studies on the coke prediction models considering fuel property, operating condition, and the contribution of coke precursor on coking phenomena are scanty in literature.

The present research aims to explore the development of a coke model that can be used to predict the coke deposition rate of cracking reactions under supercritical conditions. To achieve the objective, numerical investigations are performed using FLUENT software to predict the concentrations of coke precursors like light olefins and aromatics that are likely to form during the progress of a cracking process under elevated temperature and pressure conditions. The simulated data of coke precursor concentration, operating temperature, pressure, fuel residence time, and fuel properties are fitted into a set of multi-coefficient linear equations to find the coke deposition rate. The set of linear equations is solved to compute the coefficient of

variables. The obtained coefficients are used to develop a predictive coke model to simulate the coke deposition rate. The developed coke model is validated with the literature-reported coke data and the in-house generated experimental data from the pyrolysis of n-heptane under supercritical conditions.

7.2. Methodology Adopted for Numerical Simulations and its Validation.

7.2.1. Computation setup used for numerical simulation

Thermal cracking involves the cracking of heavier hydrocarbons into lighter hydrocarbons. When heat is applied externally along the length of the reactor, the fuel undergoes a phase change from a subcritical liquid state to a supercritical state upon absorbing the heat. With further increase in heat flux, the fuel may undergo cracking reactions with C-C/C-H bonds scissions releasing free radicals. The free radicals initiate bimolecular reactions or undergo decomposition reactions. During the progress of cracking reactions, the formation of coke precursors, such as lighter olefins, aromatics, and dienes, can lead to coke depositions inside the reactor surface. Identifying the precursor concentration along the length of the reactor is vital in understanding the coke deposition phenomena. Fig. 7.1 presents the probable mechanism for precursor formation, which can lead to coking phenomena in a tubular reactor. Hydrocarbon fuel (C_nH_m) undergoes C-H scissions to form allyl radicals. The allyl radicals can form olefins and new radicals. Lighter olefins can undergo a Diels-Alder reaction at higher pressures and temperatures to form cyclic structures. The cyclic structure proceeds to polymerization reactions to form polycyclic aromatic hydrocarbons (PAHs), which coalesce into coke deposits. The coke deposition will offset the heat transfer from the exterior wall surface to the fuel flowing internally. Additionally, the properties of fuel strongly impact heat transfer phenomena and, consequently, the overall heat sink capability of a fuel. The objective is to find the concentration of coke precursors along the length of the fuel flow reactor.

To investigate the coking phenomena along the length of the reactor, a two-dimensional (2D) axisymmetric geometry, as shown in Fig. 7.2, was constructed for computation. S_1 is the domain that represents fluid and metal wall interfaces, and S_2 indicates the domain of bulk fluid phase, L is the length, r is the radius, I.D. is the inner diameter, and O.D. is the outer diameter of the reactor tube. An inflation-type mesh with a thickness of 5×10^{-4} mm for fifty layers was

assigned in the simulation to capture the variation in fluid properties and its influence on flow analysis.

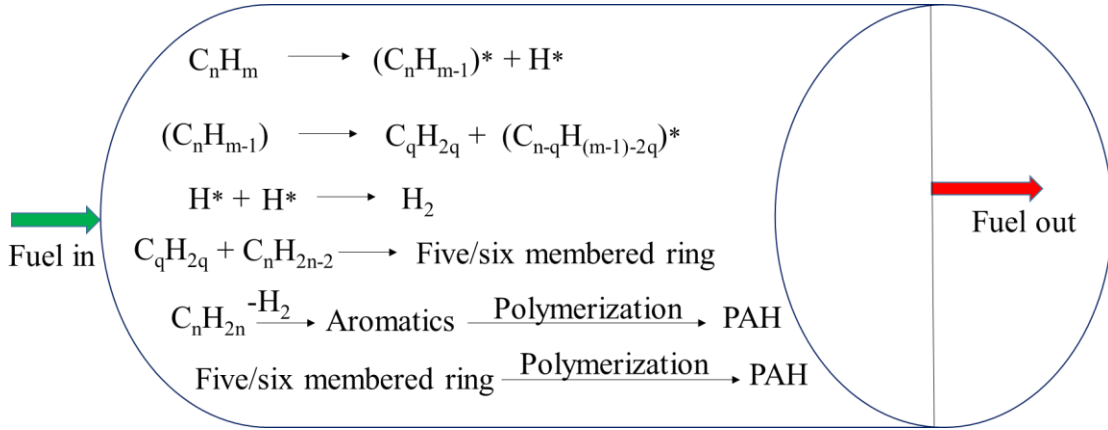


Fig. 7.1: A representation of thermal cracking of hydrocarbon in a flow reactor.

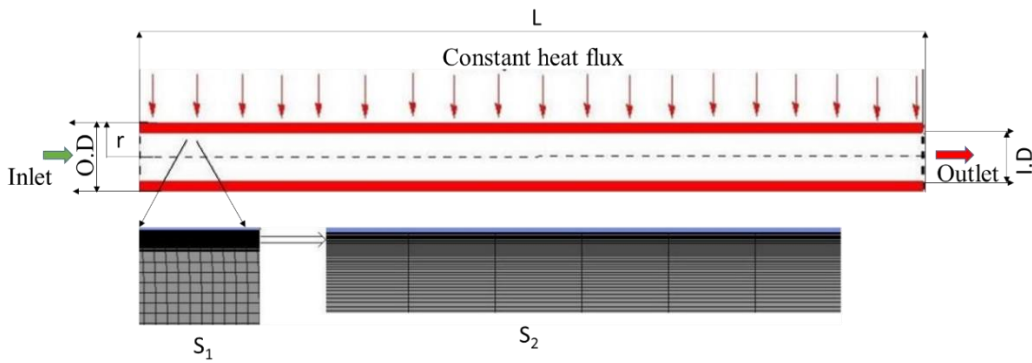


Fig. 7.2: Schematic of computational domain considered in numerical analysis.

7.2.2. Governing equations

For the fluid region, the conservation equations, namely the mass (Eq. 7.1), momentum (Eq. 7.2), and energy (Eq. 7.3) equations, were solved numerically to find the flow characteristics. The species distribution (Y_i) from the pyrolysis of hydrocarbons is described by the convective-diffusion species transport equations (Eq. 7.4 and 7.5).

$$\text{Mass conservation equation: } \frac{\partial \rho}{\partial t} + \nabla \cdot (\rho \mathbf{v}) = 0 \quad \text{Eq. (7.1)}$$

$$\text{Momentum conservation equation: } \frac{\partial}{\partial t} (\rho \mathbf{v}) + \nabla \cdot (\rho \mathbf{v} \mathbf{v}) = -\nabla p + \nabla \cdot \boldsymbol{\tau}_{eff} \quad \text{Eq. (7.2)}$$

$$\text{Energy conservation equation: } \frac{\partial}{\partial t}(\rho e_t) + \nabla \cdot (\rho v e_t) = \nabla \cdot (\lambda \nabla T) - \nabla \cdot (p v) \quad \text{Eq. (7.3)}$$

$$\frac{\partial}{\partial t}(\rho Y_i) + \nabla \cdot (\rho Y_i v) = -\nabla \cdot (\rho Y_i v_{d,i}) + S_i \quad \text{Eq. (7.4)}$$

$$S_i = \varpi M_{w,i} \quad \text{Eq. (7.5)}$$

where, ρ = density, v = velocity, p = pressure, τ_{eff} = viscous shear tensor, e_t = internal energy, λ = thermal conductivity, and T = temperature of the test fluid. ϖ = chemical reaction rate calculated by detailed pyrolytic reactions, and $M_{w,i}$ = molecular weight of individual species.

Various models, such as the k- ϵ model, renormalization-group (RNG) k- ϵ model, and shear-stress transport (SST) k- ω models, are commonly used to incorporate the extent of flow turbulence in solving the fuel flow characteristics. Zhu et al. (2014) have studied a comparison among the standard k- ϵ model, RNG k- ϵ model, and SST k- ω models for solving the fuel flow characteristics under supercritical pressure. Among the models, the SST k- ω model showed a good agreement between the model predicted and experimental value of wall temperatures. Hence, in the present work, the SST k- ω turbulence model equations (Eq. 7.6 and Eq. 7.7) were selected and included in the fluent solver to predict viscous flow behavior in the boundary layers for simulating the low-Reynolds number turbulent flows and to find heat transfer characteristics [Wilcox (2008), Wang et al. (2023)]. To predict the product species distribution, a simplified global kinetic model was defined in the fluent solver in the work.

$$\frac{\partial}{\partial t}(\rho k) + \nabla \cdot (\rho k v) = \nabla \cdot \left[\left(\mu + \frac{\mu_t}{\sigma_k} \right) \nabla k \right] + G_k - Y_k + S_k \quad \text{Eq. (7.6)}$$

$$\frac{\partial}{\partial t}(\rho \omega) + \nabla \cdot (\rho \omega v) = \nabla \cdot \left[\left(\mu + \frac{\mu_t}{\sigma_\omega} \right) \nabla \omega \right] + G_\omega - Y_\omega + D_\omega + S_\omega \quad \text{Eq. (7.7)}$$

where, k is turbulent kinetic energy, G_k is turbulent kinetic energy by the velocity gradient, G_ω is generation term in ω , Y_k and Y_ω are turbulence generation terms by diffusion, D_ω is orthogonal divergence term, S_k and S_ω are species source terms.

7.2.3. Simulation setup

FLUENT 21 software with the finite volume method is used in numerical simulation for hydrocarbon fuels under a supercritical state. The SIMPLEC algorithm coupled with pressure and velocity parameters into the FLUENT. The least squares cell method with a second-order implicit scheme was chosen for spatial discretization. A second-order upwind scheme is used for turbulent kinetic energy and turbulent dissipation rate to improve accuracy and robustness in computation. Global kinetic reaction models are defined with Finite-rate or eddy-dissipation concepts for the turbulence chemistry interactions to estimate the hydrocarbon product species distribution. To understand and calibrate the simulation model, ten cases (shown in Table 7.1) are considered for the numerical analysis. Some relevant properties of the fuels considered for the present work are given in Table 7.2. In the simulation, constant heat flux is applied as the thermal boundary condition at the reactor wall to maintain the experimental value of wall temperature. In each case (case-1 to 10), a separate 2D axisymmetric design with mesh cells ranging from 2.5×10^6 to 6×10^6 quadrilateral elements was constructed in fluent and global kinetic models representing the fuel were defined in the fluent solver. Since the reactor exit conditions are above the critical pressure and temperature of the individual fuel, the fluid state is strongly affected by temperature and pressure in the pseudo-critical region. Hence, transport and thermodynamic properties must be estimated to incorporate under real gas conditions. In the work, the Peng-Robinson equation of state is used to estimate fluid density, specific heat, thermal conductivity, and viscosity for each species. In the simulation, the dimensionless wall distance (y^+), the ratio of friction/shear velocity to kinematic viscosity, was kept at less than 1. The absolute convergence criterion for all the governing equations was set to less than 10^{-6} . To simulate the cracking behavior of hydrocarbon fuels and predict the product distribution, the global kinetic models, as shown in Table 7.3, were used in the simulation.

Table 7.1: Fuels and operating parameters used in numerical simulations

Cases	Fuel	T _{inlet} (°C)	T _{exit} (°C)	Pressure (bar)	Feed rate (g/min)	Length (mm)	I.D (mm)	Space- time (s)	Heat flux (kW/m ²)	Reference
Case-1	n-dodecane	30	675	37	7.5	700	3	29.7	88	Jiang et al. (2011)
Case-2	n-dodecane	250	670	40	2.25	900	2	56.5	68	Liu et al. (2009)
Case-3	n-dodecane	250	648	40	2.25	900	2	56.5	64	Liu et al. (2009)
Case-4	RP-3	250	651	40	2.25	900	2	56.5	63	Liu et al. (2009)
Case-5	RP-3	250	662	40	2.25	900	2	56.5	64	Liu et al. (2009)
Case-6	n-heptane	30	600	55	24.0	750	2	4.0	302	Konda et al. (2022)
Case-7	n-heptane	30	550	55	24.0	750	2	4.0	282	Konda et al. (2022)
Case-8	MCH	30	700	55	24.0	750	2	4.4	870	Konda et al. (2022)
Case-9	HCF-1	30	680	55	40.0	750	2	2.8	950	Vuchuru et al. (2022)
Case-10	EHF-1	30	710	35	60.0	900	2	2.2	600	Li et al. (2018)

Table 7.2: Physico-chemical properties of various fuels

Properties	n-heptane	MCH	n-dodecane	RP-3*	HCF-1**	EHF-1***
Density (kg/m ³)	674	761	750	796	800	791
Average boiling point (°C)	98.4	101	213	186	187	204
Paraffin (vol.%)	> 99.8	-	> 99.8	76.2	48.4	46.5
Naphthene (vol.%),	-	> 99.5	-	15.2	42.9	52.9
Aromatic (vol.%),	-	-	-	8.5	8.7	0.6
Critical temperature (°C)	267 ± 1	299 ± 1	385 ± 1	373 ± 1	378 ± 1	389 ± 1
Critical pressure (bar)	27 ± 0.5	34 ± 0.5	18 ± 0.5	24 ± 0.5	23 ± 0.5	21 ± 0.5

*Liu et al (2009), **Vuchuru et al. (2022), *** Li et al. (2018)

Table 7.3: Kinetic parameters used in simulation studies

Fuel	Proposed reaction scheme	Pre-exponential factor, 1/s	E _a , kJ/mol	Reference
	$C_{12}H_{26} \rightarrow 0.034 H_2 + 0.237 CH_4 + 0.394 C_2H_4 + 0.360 C_2H_6 + 0.286 C_3H_6 + 0.229 C_3H_8 + 0.082 C_4H_8 + 0.043 C_4H_{10} + 0.156 C_8H_{18} + 0.850 C_8H_{16} + 0.019 C_9H_{12}$	2.466×10^{14}	225.8	Zhang et al. (2018)
n-dodecane	$C_8H_{18} \rightarrow 0.058 H_2 + 0.530 CH_4 + 0.755 C_2H_4 + 0.546 C_2H_6 + 0.552 C_3H_6 + 0.286 C_3H_8 + 0.155 C_4H_8 + 0.067 C_4H_{10} + 0.163 C_9H_{12}$	7.385×10^{14}	209.6	
	$C_8H_{16} \rightarrow 0.045 H_2 + 0.413 CH_4 + 0.622 C_2H_4 + 0.429 C_2H_6 + 0.433 C_3H_6 + 0.226 C_3H_8 + 0.146 C_4H_8 + 0.053 C_4H_{10} + 0.204 C_9H_{12} + 0.061 C_7H_8 + 0.064 C_7H_{12}$	2.631×10^{14}	217.8	
n-heptane	$C_7H_{16} \rightarrow 0.36 H_2 + 0.75 CH_4 + 0.46 C_2H_6 + 0.25 C_3H_8 + 0.24 C_4H_{10} + 0.51 C_2H_4 + 0.29 C_3H_6 + 0.18 C_4H_8 + 0.05 C_6H_{12} + 0.05 C_6H_{14} + 0.02 C_7H_8$	7.1×10^{12}	219	Chakraborty et al. (2009), Konda et al. (2022)
RP-3, EHF-1, HCF-1	$C_{12}H_{23} \rightarrow 0.16 H_2 + CH_4 + 0.58 C_2H_6 + 0.43 C_2H_4 + 0.42 C_3H_6 + 0.28 C_3H_8 + 0.25 C_4H_8 + 0.84 C_7H_8$	2.1×10^{15}	263.6	Hou et al. (2013)
MCH	$C_7H_{14} \rightarrow 0.47 H_2 + 0.64 CH_4 + 0.38 C_2H_6 + 0.2 C_3H_8 + 0.18 C_4H_{10} + 0.34 C_2H_4 + 0.25 C_3H_6 + 0.13 C_4H_8 + 0.01 C_6H_{14} + 0.01 C_7H_{16} + 0.02 C_7H_8$	2×10^{14}	213	Konda et al. (2022), Kamal et al. (1997)

7.2.4. Experimental details for validation of simulation results

Thermal cracking studies of n-heptane ($n\text{-C}_7\text{H}_{16}$) were conducted in an electrically heated tubular reactor setup. A schematic of the experimental setup is shown in Fig. 7.3. The experimental setup and procedure details are given in Chapter-3. A multi-channel gas chromatography coupled with TCD detectors was used to find the composition of cracked-gas products. The composition of feed and liquid products was obtained using a GC analyzer fitted with an HP-5 column and FID detector. The concentration of CO_2 in the flue gas was measured using a non-dispersive infrared CO_2 analyzer.

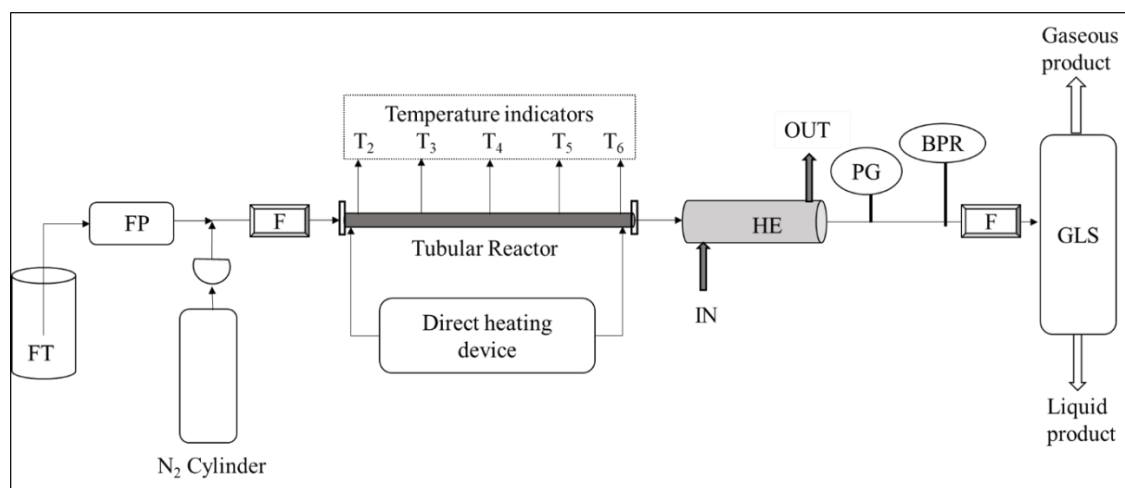


Fig. 7.3: Schematic of experimental setup used in present work.

7.3. Results and Discussion

7.3.1. Numerical analysis

The CFD simulation was performed to obtain the flow behavior, temperature, and product distribution along the length of the reactor tubes. To develop a coke model, the required distributions of coke-forming precursors across the length of the reactor are obtained from the CFD simulation. The work simulated ten cases (as mentioned in Table 7.1) to examine the temperature and product distribution patterns for different fuels and operating conditions. A representative case (Case-3 in Table 7.1) of the simulation studies is demonstrated below.

Fig. 7.4. shows the variation in thermo-physical properties of n-dodecane along the length of the reactor. The conditions used for the simulation are fluid inlet temperature 250 °C, reactor pressure 40 bar, n-dodecane mass flowrate 2.25 g/min, space-time 57 s, and input heat flux 68.1 kW/m². The SST k- ω turbulence model is used in the CFD simulation. Fig 7.4a shows the variation in wall and fluid temperatures along the reactor length. It is noted that the fuel temperature is about 20 to 30 °C less than the corresponding wall temperature. The results (Fig. 7.4b-e) show that the fluid density, viscosity, thermal conductivity, and heat capacity are greatly influenced near the pseudo-critical temperature. The pseudo-critical temperature is a temperature at which the specific heat capacity becomes maximum at a given pressure. In most scenarios, the reactor inlet temperature is lower than the pseudo-critical temperature of a fuel. When a fuel reaches nearer to its pseudo-critical temperature on absorbing heat, the thermo-physical properties undergo extreme variations. The decrease in viscosity can enhance heat transfer due to the decreasing effect of viscous boundary layer thickness. A sharp increase in the specific heat capacity of the fluid improves the convective heat transfer. The plots show an increasing trend in fluid thermal conductivity above 400 °C and a ratio of x/D greater than 100 (where 'x' is the distance from the leading edge and D is the inner diameter). The possible reason could be the onset of cracking of the fuel to smaller hydrocarbons (e.g., C₁ to C₄). The smaller hydrocarbons possess higher thermal conductivities and viscosities beyond 400 °C and 40 bar.

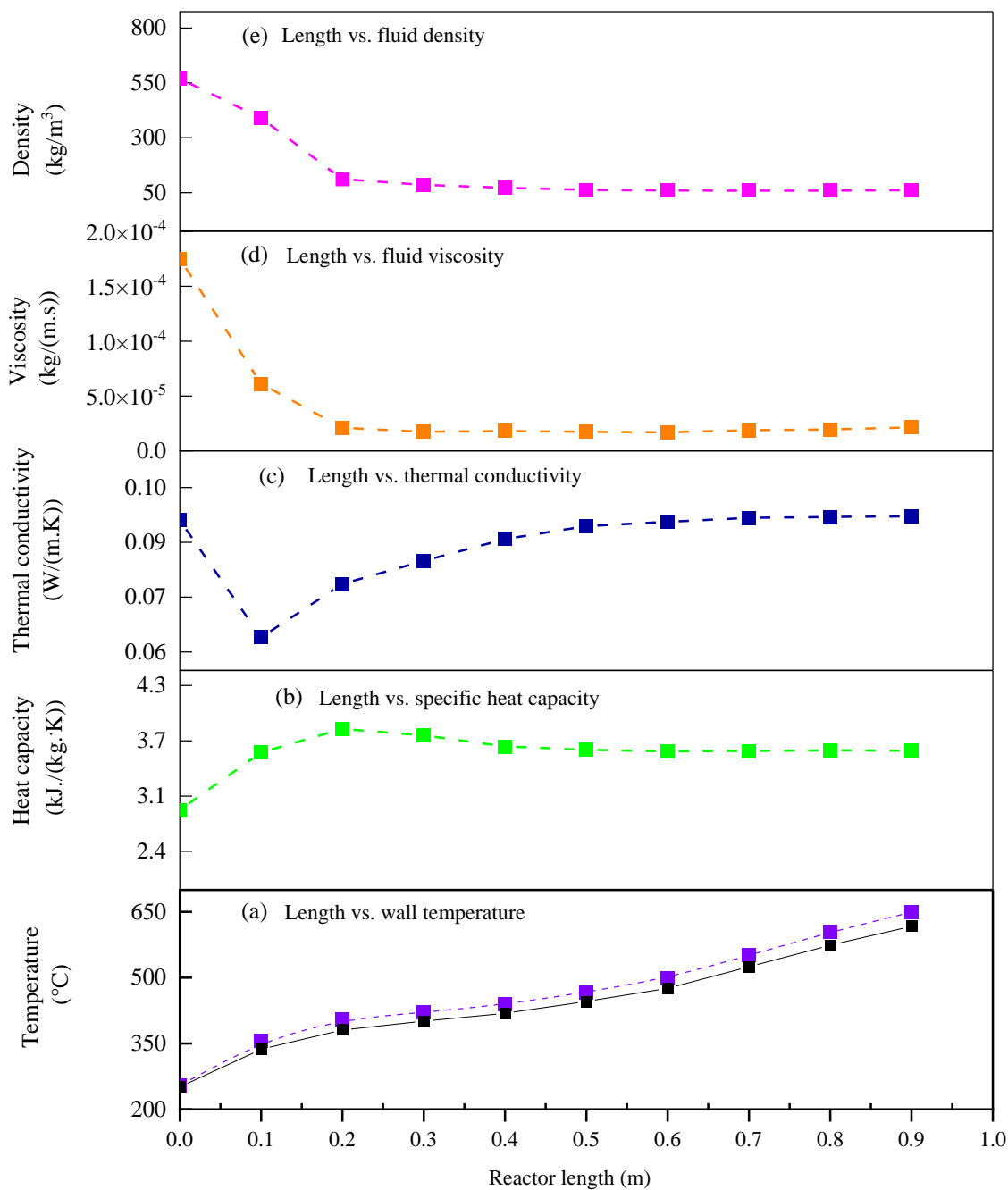


Fig. 7.4: Variation in a) wall and fluid temperature, b) specific heat capacity, c) thermal conductivity, d) fluid viscosity, and e) fluid density, along reactor length for n-dodecane at 650 °C and 40 bar.

=====

Fig. 7.5 shows the variation in mole fraction composition of lighter hydrocarbons and some critical species formed from the cracking of n-dodecane along the length of the reactor at 40 bar pressure and for a fuel exit temperature of 650 °C. The thermal cracking reaction generally follows a free radical mechanism. Fig. 7.5a shows the concentration profile of lighter alkanes (C₂, C₃, and C₄) with reactor length. Lighter alkanes are formed due to the cracking of larger alkyl radicals, followed by a bimolecular hydrogen abstraction reaction. The profile shows that the cracking reaction starts above 400 °C for the n-dodecane and the extent of cracking increases with reactor length or wall temperature. Beyond a temperature of about 600 °C, the minor variation in concentration profiles indicates the possibilities of secondary cracking reactions. Fig. 7.5b shows the variation in olefin (ethylene, propylene, and butene) concentration with reactor length. β -scission is the main mechanism for olefin formation from alkyl radicals. Dehydrogenation of alkane can be the other route for olefin production. The dominance of low molecular weight olefins (i.e., C₂ and C₃) in the product indicates the possibilities of dehydrogenation reaction at higher temperatures. A representative scenario of the concentration profile of a few cycloalkanes and aromatics is shown in Fig. 7.5c. At a temperature range between 550 °C to 650 °C, several secondary reactions, such as secondary cracking (i.e., breaking of the primary cracking products), dehydrogenation, dehydro-cyclization, a combination of alkenes, etc., reactions can occur. The dehydro-cyclization reaction of alkane or alkenes can lead to cycloalkenes and aromatic hydrocarbons in the liquid products. Hence, the concentration of cyclooctene initially increased with reactor length. However, at higher temperatures (or higher length because of temperature increase with length) or with longer residence time, the cycloalkanes/cycloalkenes can further crack to form lighter hydrocarbons, resulting in a reduction in cyclooctene (a cycloalkene) concentration along the reactor length. The cyclooctene can undergo dehydrogenation reactions to form aromatic hydrocarbons, which can further undergo condensation reactions, leading to the formation of polyaromatic hydrocarbons (PAHs). The probable mechanisms of thermal cracking reactions are detailed in previous works (Konda et al. (2022), Vuchuru et al. (2022)). Fig 7.5d depicts the variation in n-dodecane (feed) concentration with reactor length. As obvious, the concentration of n-dodecane decreased with reactor length and above 400 °C due to the cracking of feed.

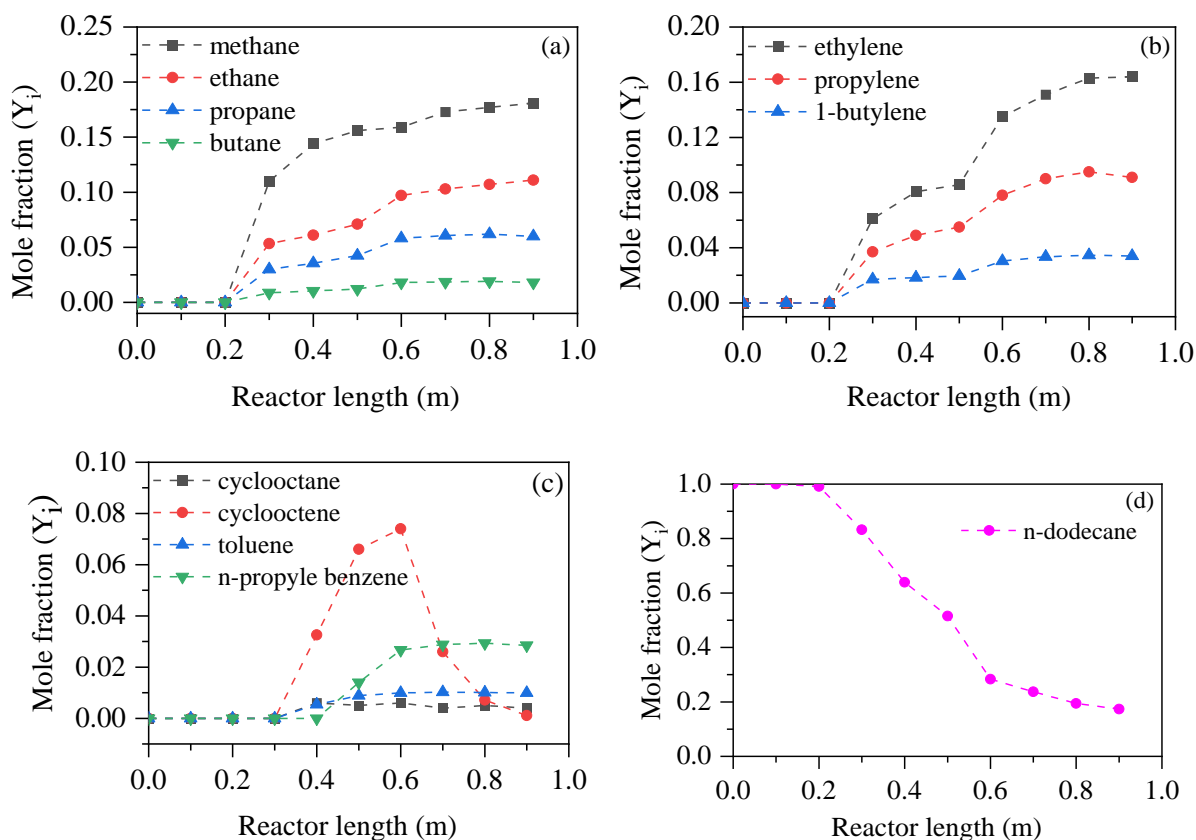
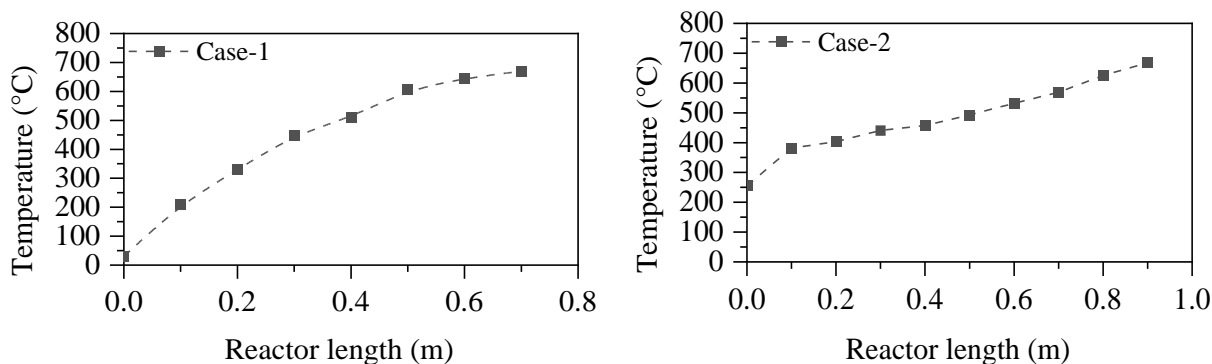


Fig. 7.5: Variation of various components along reactor length obtained from numerical simulation a) H₂ and lighter paraffins, b) lighter olefins, c) cyclo-compounds, d) n-dodecane

The temperature profile of the ten different cases mentioned in Table 7.1 is shown in Fig 7.6. The variation of different components along the reactor length are tabulated in Table 7.4.



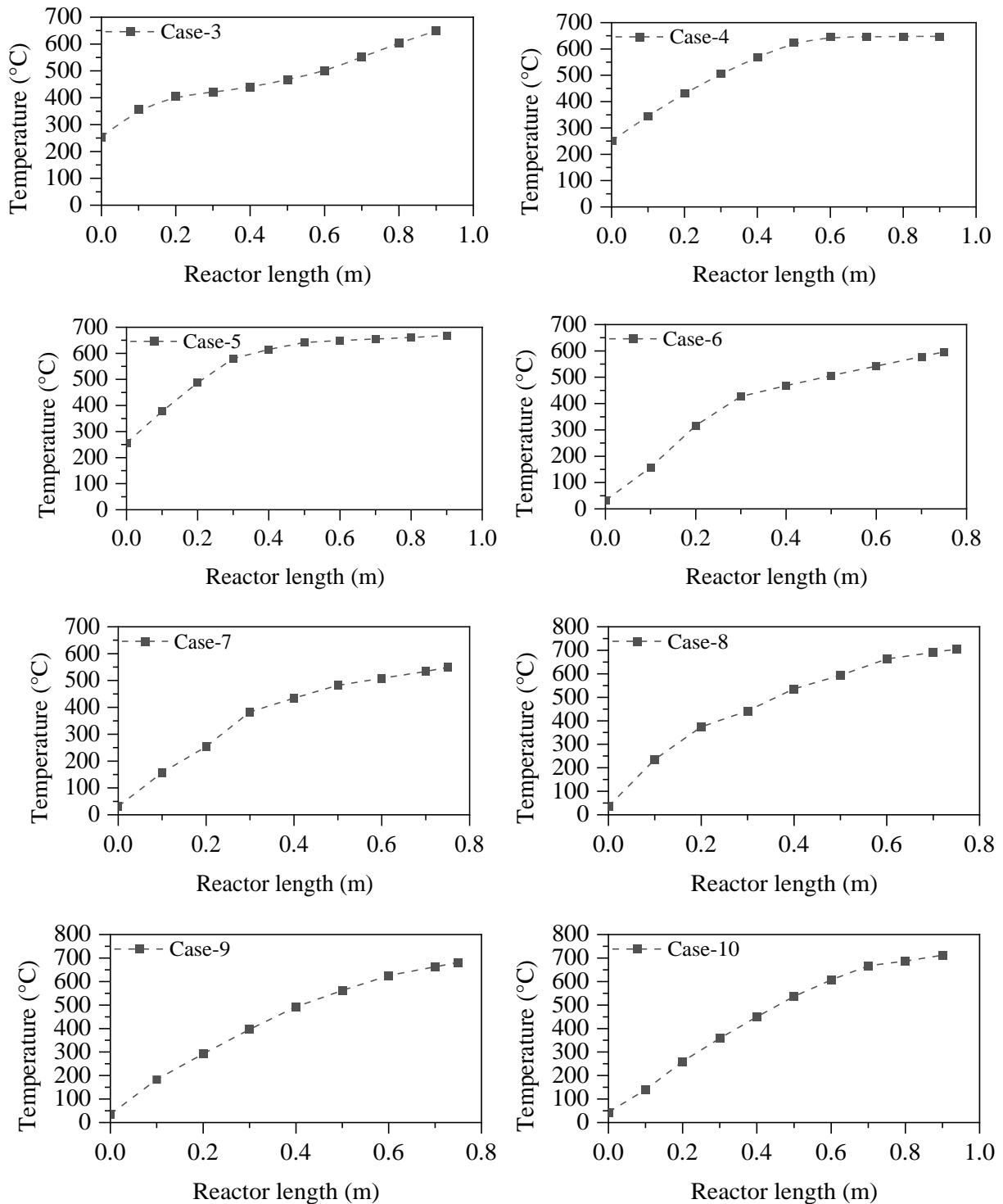


Fig. 7.6: Temperature profiles for all ten different cases.

Table:7.4: Variation in composition of various species along the reactor length for nine different cases.

Cases	Reactor length (m)	H ₂	C ₁	C ₂	C ₃	C ₄	C ₂ ⁼	C ₃ ⁼	C ₄ ⁼	C ₇ H ₈	C ₇ H ₁₂	C ₈ ⁼	C ₉ H ₁₂	feed
Case-1	0.1	0	0	0	0	0	0	0	0	0	0	0	0	1
	0.2	0	0	0	0	0	0	0	0	0	0	0	0	1
	0.3	0	0	0	0	0	0	0	0	0	0	0	0	1
	0.4	0.081	0.098	0.049	0.049	0.007	0.082	0.053	0.009	0.009	0.005	0.001	0.048	0.509
	0.5	0.111	0.128	0.062	0.079	0.014	0.104	0.084	0.017	0.011	0.053	0.046	0.048	0.243
	0.6	0.111	0.158	0.104	0.098	0.024	0.173	0.103	0.029	0.013	0.014	0.006	0.049	0.118
	0.7	0.113	0.155	0.104	0.096	0.024	0.173	0.1	0.028	0.013	0.014	0.007	0.052	0.122
Case-2	0.1	0	0	0	0	0	0	0	0	0	0	0	0	1
	0.2	0	0	0	0	0	0	0	0	0	0	0	0	1
	0.3	0.053	0.118	0.057	0.032	0.009	0.071	0.023	0.018	0	0.005	0	0	0.612
	0.4	0.062	0.155	0.066	0.038	0.011	0.081	0.031	0.021	0.006	0.006	0.035	0	0.482
	0.5	0.056	0.168	0.076	0.046	0.013	0.085	0.026	0.020	0.010	0.006	0.071	0.015	0.404
	0.6	0.105	0.171	0.106	0.062	0.019	0.125	0.063	0.035	0.011	0.012	0.080	0.029	0.176
	0.7	0.107	0.186	0.111	0.065	0.02	0.159	0.069	0.036	0.011	0.012	0.028	0.031	0.161
	0.8	0.11	0.190	0.115	0.068	0.02	0.164	0.071	0.037	0.011	0.012	0.008	0.031	0.158
	0.9	0.129	0.197	0.109	0.064	0.019	0.164	0.093	0.043	0.011	0.013	0.001	0.031	0.122



Cases	Reactor length (m)	H ₂	C ₁	C ₂	C ₃	C ₂ ⁻	C ₃ ⁻	C ₄ ⁻	C ₇ H ₈	feed
Case-4	0.1	0	0	0	0	0	0	0	0	1
	0.2	0	0	0	0	0	0	0	0	1
	0.3	0.006	0.039	0.02	0.01	0.021	0.012	0	0.028	0.865
	0.4	0.01	0.062	0.034	0.017	0.032	0.022	0.002	0.05	0.772
	0.5	0.012	0.078	0.044	0.021	0.039	0.029	0.003	0.064	0.710
	0.6	0.013	0.087	0.048	0.024	0.043	0.032	0	0.065	0.688
	0.7	0.014	0.091	0.051	0.025	0.044	0.034	0	0.068	0.673
	0.8	0.016	0.097	0.054	0.027	0.047	0.037	0	0.07	0.653
	0.9	0.016	0.103	0.058	0.028	0.05	0.039	0	0.071	0.635
Case-5	0.1	0	0	0	0	0	0	0	0	1
	0.2	0.003	0.021	0.015	0.006	0.018	0.008	0	0.019	0.911
	0.3	0.009	0.065	0.039	0.02	0.036	0.026	0.004	0.056	0.745
	0.4	0.015	0.106	0.061	0.03	0.052	0.044	0.009	0.087	0.596
	0.5	0.018	0.128	0.072	0.036	0.061	0.053	0	0.104	0.528
	0.6	0.019	0.136	0.076	0.038	0.064	0.056	0	0.112	0.499
	0.7	0.02	0.139	0.078	0.039	0.065	0.057	0	0.114	0.488
	0.8	0.02	0.143	0.08	0.04	0.067	0.059	0	0.118	0.473
	0.9	0.021	0.146	0.083	0.041	0.069	0.061	0	0.121	0.459

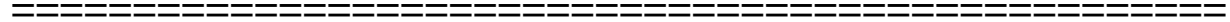


	Reactor length (m)	H ₂	C ₁	C ₂	C ₃	C ₄	C ₂ ⁻	C ₃ ⁻	C ₄ ⁻	C ₇ H ₈	C ₆ H ₁₂	C ₆ H ₁₄	feed
Case 6	0.1	0	0	0	0	0	0	0	0	0	0	0	1
	0.2	0	0	0	0	0	0	0	0	0	0	0	1
	0.3	0.033	0.26	0.017	0.009	0.009	0.019	0.012	0.009	0.006	0.006	0.054	0.566
	0.4	0.033	0.27	0.018	0.009	0.009	0.019	0.013	0.01	0.006	0.006	0.055	0.558
	0.5	0.034	0.27	0.018	0.009	0.009	0.019	0.013	0.01	0.006	0.006	0.056	0.552
	0.6	0.035	0.273	0.019	0.01	0.001	0.02	0.013	0.01	0.006	0.007	0.056	0.543
	0.7	0.035	0.274	0.018	0.01	0.001	0.02	0.013	0.01	0.006	0.007	0.056	0.543
	0.75	0.034	0.272	0.018	0.009	0.009	0.02	0.013	0.01	0.006	0.007	0.056	0.546
Case-7	0.1	0	0	0	0	0	0	0	0	0	0	0	1
	0.2	0	0	0	0	0	0	0	0	0	0	0	1
	0.3	0.028	0.207	0.015	0.01	0.007	0.017	0.009	0.0063	0.004	0.0048	0.044	0.648
	0.4	0.028	0.212	0.016	0.01	0.0071	0.017	0.0096	0.0065	0.0042	0.0049	0.045	0.639
	0.5	0.029	0.215	0.016	0.01	0.0073	0.017	0.0098	0.0066	0.0043	0.005	0.046	0.634
	0.6	0.03	0.22	0.017	0.01	0.0075	0.018	0.0101	0.0068	0.0043	0.0051	0.0467	0.625
	0.7	0.03	0.22	0.016	0.01	0.0075	0.018	0.0101	0.0068	0.0043	0.0051	0.0467	0.625
	0.75	0.03	0.22	0.016	0.01	0.0074	0.018	0.01	0.0068	0.0043	0.0051	0.0467	0.627



	Reactor length (m)	H ₂	C ₁	C ₂	C ₃	C ₄	C ₂ ⁻	C ₃ ⁻	C ₄ ⁻	feed
Case 8	0.1	0	0	0	0	0	0	0	0	1
	0.2	0	0	0	0	0	0	0	0	1
	0.3	0.027	0.187	0.013	0.008	0.006	0.0146	0.0084	0.0053	0.731
	0.4	0.026	0.192	0.0137	0.009	0.0061	0.0147	0.0086	0.0055	0.724
	0.5	0.027	0.195	0.0139	0.093	0.0063	0.0142	0.0088	0.0055	0.636
	0.6	0.028	0.2	0.0145	0.095	0.0065	0.0158	0.0091	0.0584	0.573
	0.7	0.028	0.2	0.0144	0.095	0.0065	0.0166	0.0091	0.0058	0.625
	0.75	0.027	0.207	0.0143	0.094	0.0064	0.0167	0.0101	0.0058	0.618

	Reactor length (m)	H ₂	C ₁	C ₂	C ₃	C ₂ ⁻	C ₃ ⁻	C ₄ ⁻	C ₇ H ₈	feed
Case-9	0.1	0	0	0	0	0	0	0	0	1
	0.2	0	0	0	0	0	0	0	0	1
	0.3	0	0	0	0	0	0	0	0	0.99
	0.4	0.091	0.102	0.047	0.031	0.088	0.021	0.0284	0.012	0.432
	0.5	0.125	0.168	0.076	0.049	0.108	0.049	0.043	0.072	0.234
	0.6	0.151	0.206	0.09	0.0596	0.117	0.065	0.0488	0.101	0.131
	0.7	0.176	0.220	0.092	0.0631	0.119	0.072	0.0455	0.112	0.101
	0.75	0.176	0.22	0.091	0.0629	0.1193	0.071	0.0459	0.112	0.101



	Reactor length (m)	H ₂	C ₁	C ₂	C ₃	C ₂ ⁻	C ₃ ⁻	C ₄ ⁻	C ₇ H ₈	feed
Case-10	0.1	0	0	0	0	0	0	0	0	1
	0.2	0	0	0	0	0	0	0	0	1
	0.3	0.011	0.031	0.0087	0.0111	0.069	0.0303	0.004	0	0.697
	0.4	0.082	0.104	0.0418	0.0347	0.104	0.0496	0.003	0.026	0.437
	0.5	0.155	0.289	0.0857	0.054	0.182	0.062	0.009	0.123	0.040
	0.6	0.155	0.295	0.087	0.0503	0.184	0.057	0	0.125	0.047
	0.7	0.148	0.328	0.0885	0.0425	0.187	0.052	0	0.136	0.018
	0.8	0.15	0.341	0.0862	0.0392	0.183	0.051	0	0.127	0.023
	0.9	0.154	0.338	0.0842	0.0382	0.18	0.05	0	0.119	0.037

Fig. 7.7 shows a variation in the mole fraction composition of ethylene, propylene, toluene, and n-propyl benzene along the reactor length for different cases, as mentioned in Table 7.1. The analysis revealed that the concentration profile of the lighter olefins and aromatics is a strong function of operating temperature, pressure, feed space-time, and feed composition. The composition of ethylene (C_2H_4) and propylene (C_3H_6) is relatively more for the n-dodecane than the RP-3 fuel for similar values of operating temperature and space-time (e.g., case-3 and case-5 in Fig. 7.7a and 7.7b). The primary reason for the variation could be due to fuel structure rather than operating conditions. The n-dodecane is straight-chain paraffin, whereas the paraffin content in RP-3 is about 59 vol%. Generally, the thermal cracking of hydrocarbons follows a free radical mechanism. According to the free-radical mechanism, hydrocarbon molecule undergoes C-C and C-H bond cleavage to release hydrogen radical and alkyl radical. The hydrocarbon radicals having carbon atoms > 5 can undergo an isomerization reaction. The alkyl radicals (normal and isomerized forms) undergo a unimolecular decomposition reaction to form lower alkyl radicals and lower olefins. The n-dodecane being straight-chain paraffin, the unimolecular decomposition reactions dominants to release lower olefins than the RP-3. A higher value of the olefin-to-paraffin can lead to a better heat sink capacity, but the coke-forming tendency also increases. Liu et al. (2013) also reported a similar phenomenon for n-decane and RP-3 fuels. The olefin concentration for the n-heptane (case-6 and case-7) fuel is significantly lower than n-dodecane (case-2), which may be due to several reasons, such as the difference in operating temperature, pressure, and space-time, in addition to the carbon chain length. For a particular temperature and pressure, the impact of the residence-time (equivalent to space-time) on olefin composition can be two ways. Higher residence time can lead to more olefin formation due to enhanced cracking. Again, a longer residence time may reduce the olefin yield due to bi-molecular hydrogenation reactions. Hence, the ultimate impact can be the resultant effect of the two phenomena. Fig. 7.7c shows that the concentration of toluene is significantly higher for kerosene-based fuels like RP-3, HCF-1, and EHF-1 (i.e., case-4, case-5, case-9, and case-10) than n-dodecane (case-1 to case-3), which is due to the higher weightage of the toluene product in the cracking scheme of the kerosene-based fuels, as reported by Hou et al. (2013) in Table 7.3. The higher weightage may be due to the possible dehydrogenation reaction of feed containing methylcyclohexane and freshly formed (as a result

of cracking) cycloalkanes to toluene. Fig. 7.7d shows the concentration profile of n-propyl benzene for n-dodecane cracking. The higher concentration of n-propyl benzene for case-1 is due to the higher (nearly 3.3 times) mass flow rate of n-dodecane than the other two cases. Between case-2 and case-3, the exit temperature is slightly higher for case-2, resulting in a higher concentration of n-propyl benzene, possibly due to the enhanced rate of aromatization reaction.

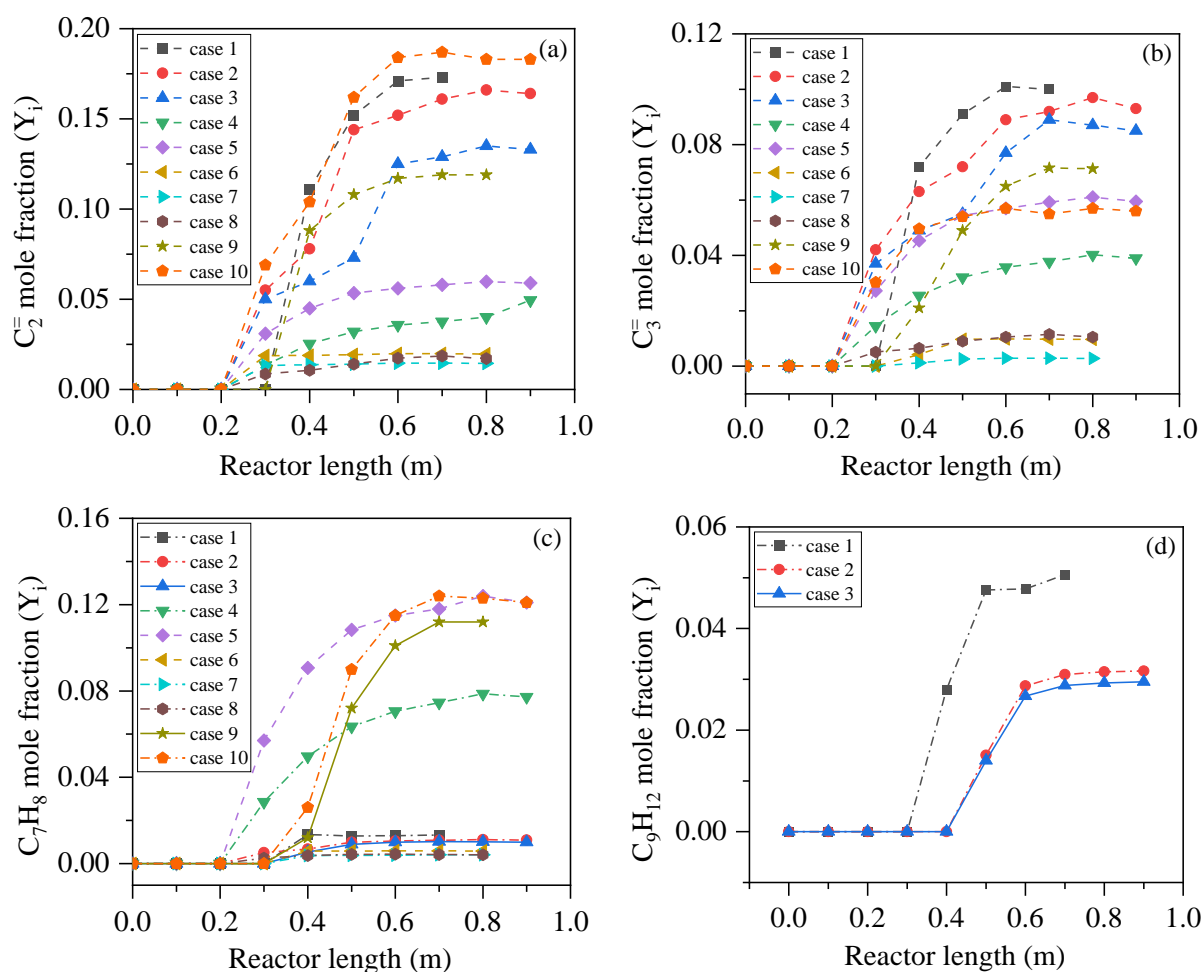


Fig. 7.7: Concentration profile of a) ethylene, b) propylene, c) toluene d) n-propyl benzene for different cases (shown in Table 7.1) for different hydrocarbons.

7.3.2. Analysis of experimental results for n-heptane cracking

7.3.2.1. Effect of temperature on cracking percentage, coke, and product distribution

The cracking study was performed at a temperature range between 550 °C to 650 °C under 40 bar reactor pressure in a tubular flow reactor, as described in the experimental section. The feed flow rate was maintained at 14 ± 0.1 g/min in all cases. Eq. 7.8 was used to estimate the n-heptane cracking percentage at experimental temperatures. To find the mass flow rate of liquid products above the n-heptane boiling point, the ASTM D86 distillation curves, as shown in Fig. 7.8a, were used in the work. The cracking percentage of n-heptane at different temperatures under 40 bar pressure is presented in Fig. 7.8b. The cracking percentage of n-heptane increased almost linearly with temperature, and the fuel cracking percentage improved by about 12% with the increase in temperature from 600 °C to 650 °C.

n-heptane cracking percentage (wt.%) =

$$\left(1 - \frac{\text{mass flow rate of liquid product } (\geq \text{feed boiling point})}{\text{mass flow rate of } n\text{-heptane}} \right) \times 100 \quad \text{Eq. (7.8)}$$

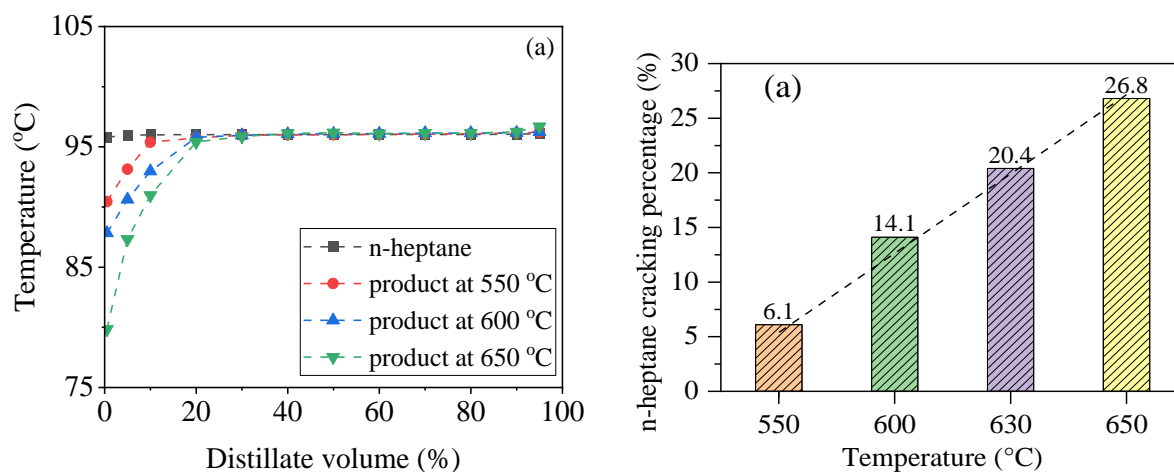


Fig. 7.8: Effect of temperature on a) ASTM D86 distillation characteristics of cracked products, b) n-heptane cracking percentage.

To estimate the coke deposition rate on the reactor surface, the reactor was flushed with nitrogen gas to remove the hydrocarbon from the reactor line after the cracking experiment. Then the reactor temperature was raised to about 700 °C in the presence of O₂ flow to convert the deposited carbonaceous materials into CO₂. The CO₂-containing gas stream was passed through a gas flow meter followed by a non-dispersive infrared analyzer to measure the CO₂ concentration in the exit gas. Eq. 3.3 was used to estimate the amount of reactor coke.

The coke deposition rate at four different temperatures is shown in Fig. 7.9a. Though the cracking percentage increased almost linearly, the coke deposition rate increased exponentially with reactor temperature. The increased rate of coke formation at higher temperatures may be due to either a secondary cracking reaction at higher temperatures or an enhanced polymerization reaction rate (Li et al. (2022), Chen et al. (2007)). Fig. 7.9b shows the distribution of cracked gas components with reactor temperature. The figure shows an increase in hydrogen (H₂), methane (CH₄), ethylene (C₂H₄), and propylene (C₃H₆) concentrations with temperature due to the enhanced rate of cracking reaction and β -scission of C-C bonds. The marginal decrease in ethane and propane species in the cracked gas with temperature may be due to the dehydrogenation reaction of ethane and propane molecules. No significant change is noted for the C₄ hydrocarbons. The analysis further reveals that the olefin-to-paraffin ratio marginally increased from 0.76 to 0.97 as the reactor temperature increased from 600 °C to 650 °C (Fig. 7.9c). The marginal increase in the olefin-to-paraffin ratio may be due to enhanced rate dehydrogenation reactions of lighter alkanes. Fig. 7.9d shows the GC analysis results of liquid products obtained at 600, 630, and 650 °C temperatures. Though we performed GC analysis for the 550 °C product sample, the results are not included in the figure because the feed (i.e., n-heptane) concentration is more than 99.5%, and the contribution of any individual components is less than 0.2 %. The result shows an increasing trend in C₅ and C₆ hydrocarbon concentration with the increase in reactor temperature from 600 °C to 650 °C. The increase in lighter components (< C₇) in the liquid products is in accordance with the fuel cracking percentage results. It is also noted that dehydro-cyclization reaction that leads to the formation of naphthenic and aromatic (e.g., toluene) compounds occurs mostly above 600 °C.

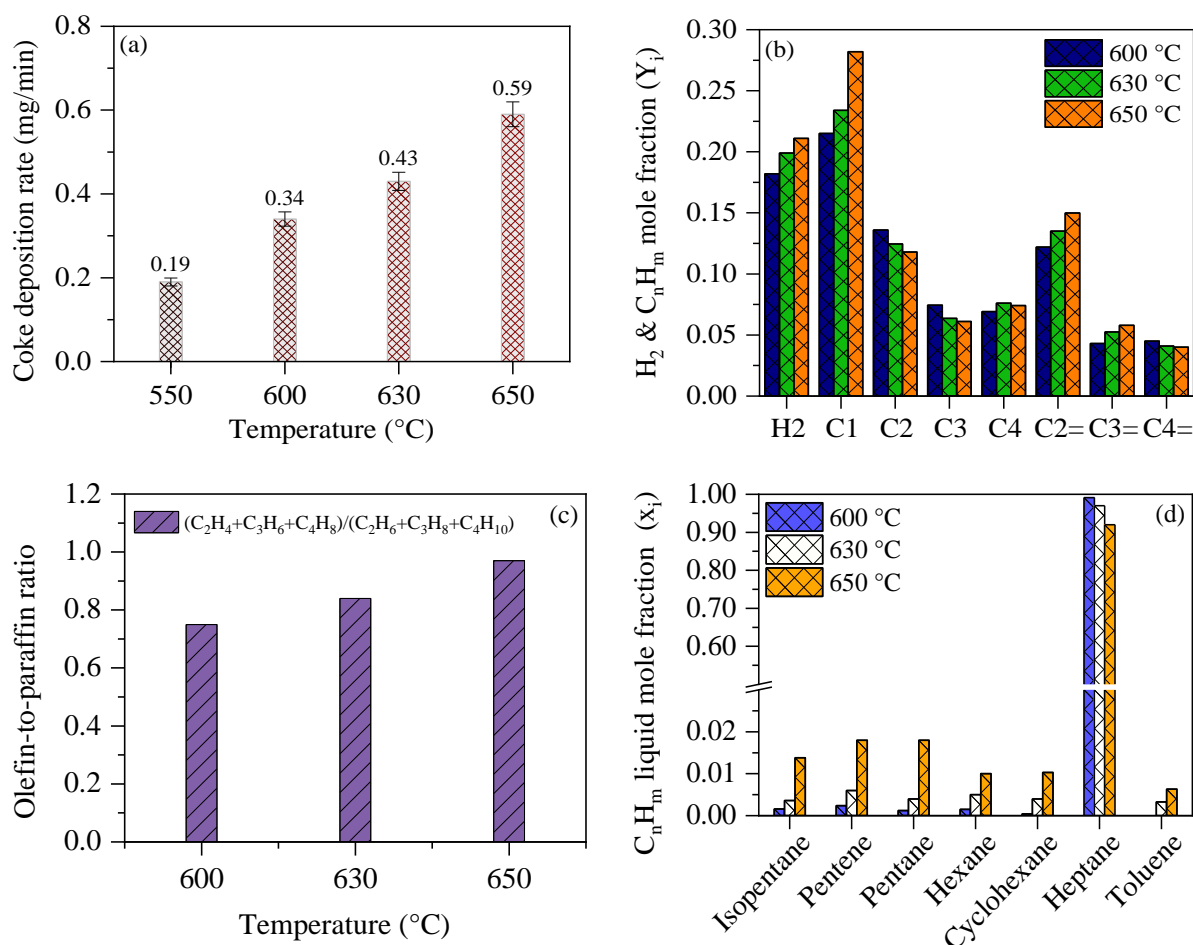


Fig. 7.9: Effect of temperature on a) coke deposition rate, b) components distribution in gaseous products, c) olefin-to-paraffin ratio, d) components distribution in liquid products.

7.3.2.2. Heat sink capacities of *n*-heptane

Thermal cracking reactions are heat-absorbing endothermic reactions, and the amount of heat sink or heat absorption depends on the extent of the endothermic cracking reactions. Before starting the cracking reaction, the fuel absorbs heat to increase its sensible temperature, and the heat sink is generally referred to ‘sensible’ or ‘physical’ heat sink. Once the cracking reaction starts, the heat sink includes physical and chemical heat sinks. The amount of endothermicity depends on various factors, such as operating temperature and pressure conditions, fuel flow rate,

fuel composition, and extent of cracking. Eq. 4.11 and 4.12 are used for calculating the total heat sink and Eq. 4.14 is used for estimating the endothermic sink capabilities of n-heptane.

The energy loss due to heat transfer to the surroundings was estimated by performing dry heating experiments under 40 bar pressure at different temperatures with an airflow rate of 100 mL/min. The variation in energy loss quantity at different temperatures is shown in Fig. 7.10a. The energy loss quantity was subtracted from the total input energy in estimating the total heat sink by the fuel. The enthalpy of fluid at the reactor inlet and exit conditions were obtained from the NIST database. Fig. 7.10b shows the variation in total heat sink and chemical heat sink capacity of n-heptane at different temperatures. The higher value of heat sinks at 650 °C could be due to increased cyclohexane and toluene concentration in the cracked products.

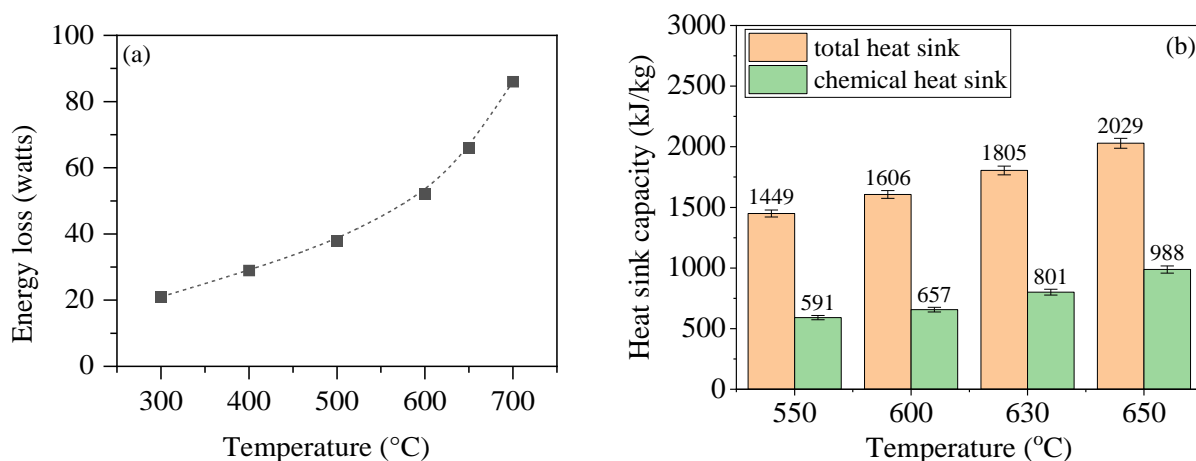


Fig. 7.10: Effect of temperature on a) energy loss, b) heat sink capacity of n-heptane.

The simulation results of the temperature profile and variation of different major species along the reactor length for n-heptane at 600 °C and 40 bar are shown in Fig. 7.11.

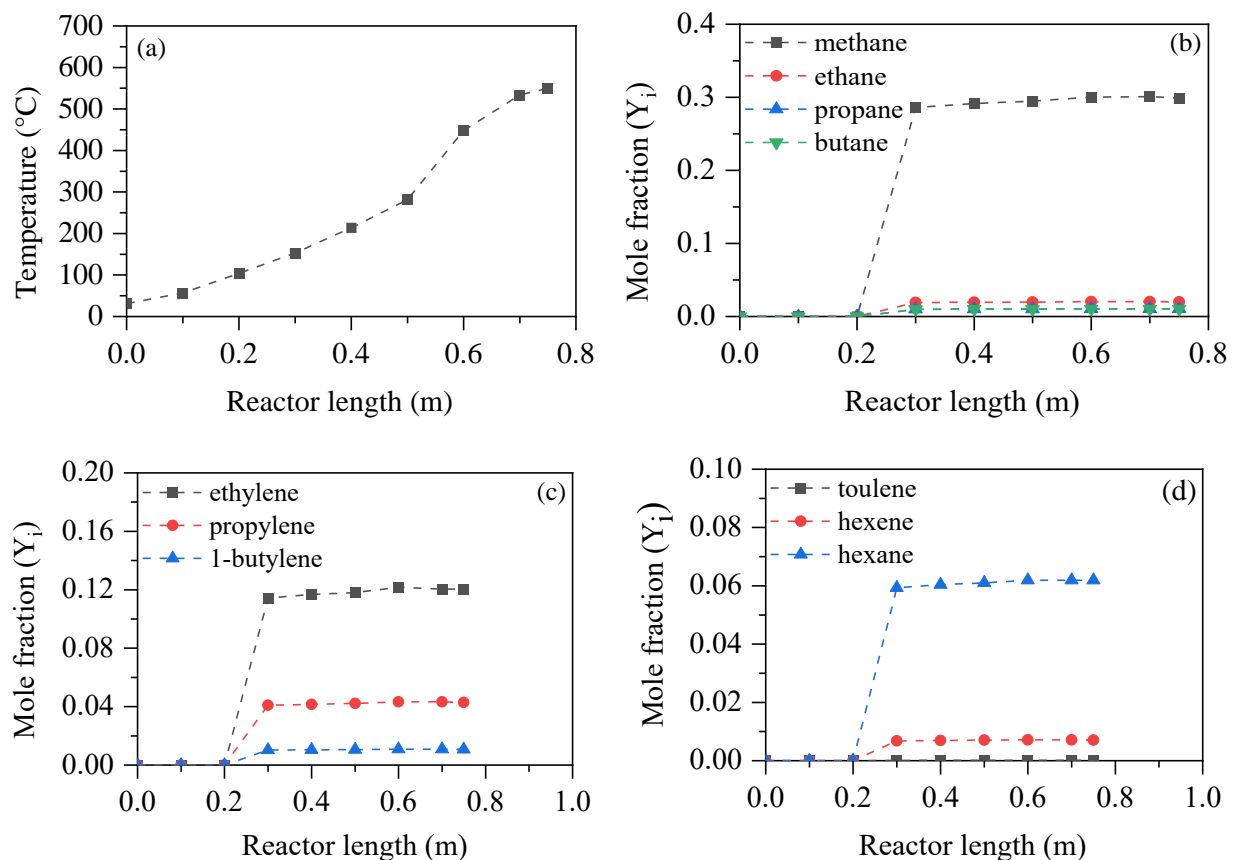


Fig. 7.11: Variation in a) reactor temperature, b) H_2 and lighter paraffins, c) lighter olefins, d) major components in liquid fractions, along reactor length.

7.3.3. Development of predictive coke model and its validation

In the work, a coke model is developed to predict the coke deposition rate for a thermal cracking process. From literature data and our experimental evidence, it is clear that the coke deposition rate depends on factors like operating parameters, feed characteristics, reactor dimension, orientation of reactor, and method of analysis. In developing the coke model, the critical variables, such as the feed property, operating parameters, and concentration of coke precursors, are included in the model as presented in Eq. 7.9. The temperature, pressure, and residence time parameters value are varied in the range of 550-710 °C, 35-55 bar, and 1.1-41 s, respectively. The density of fuels varied between 678 kg/m³ to 800 kg/m³. In developing the coke model, ethylene, propylene, and aromatics mole fraction are considered the major coke precursors.

While most researchers have used a horizontal reactor for cracking studies, Liu et al. (2009) used a vertical reactor for coke deposition studies. It is noted that the coke deposition rate on the reactor surface for vertical arrangement is significantly (nearly 30-40%) lower than a horizontal arrangement under a similar operating condition. The majority of literature data on coke deposition rate are related to the reactor surface coke, while Konda et al. (2022) and Vuchuru et al. (2022) reported the total coke (a combination of surface deposition coke and carry-away coke). The experimental evidence shows that the contribution of surface coke may be about 20% to 30 % of the total coke amount under similar conditions depending on operating temperature. Hence, developing a ‘Coke predictive model’ from the literature data is challenging. The experimental data mentioned in Table 7.5 was used to form a set of linear equations (Eq 7.10). A matrix method was adopted to solve the algebraic equations for estimating the coefficient values.

$$C = a_1T + a_2P + a_3\rho + a_4t + a_5C_2^- + a_6C_3^- + a_7A \quad \text{Eq. (7.9)}$$

where, C = coke deposition rate in mg/min, T = temperature in °C, P = pressure in bar, ρ = density of fuel in kg/m³, t = residence time in second, C_2^- = ethylene mol. fraction, C_3^- = propylene mol. fraction, A = aromatic mol. fraction, and a_i (i =1,2,3...) are the constant coefficients of different variables.

$$\begin{bmatrix} T_1 & P_1 & t_1 & \rho_1 & (C_2^-)_1 & (C_3^-)_1 & A_1 \\ - & - & - & - & - & - & - \\ - & - & - & - & - & - & - \\ - & - & - & - & - & - & - \\ T_{10} & P_{10} & t_{10} & \rho_{10} & (C_2^-)_{10} & (C_3^-)_{10} & A_{10} \end{bmatrix} \times \begin{bmatrix} a_1 \\ - \\ - \\ - \\ a_7 \end{bmatrix} = \begin{bmatrix} C_1 \\ - \\ - \\ - \\ C_{10} \end{bmatrix} \quad \text{Eq. (7.10)}$$

The estimated value of the constant coefficients are $a_1 = 9 \times 10^{-3} (\text{mg} / ^\circ\text{C} \cdot \text{min})$, $a_2 = 2.2 \times 10^{-2} (\text{mg} / \text{bar} \cdot \text{min})$, $a_3 = -9 \times 10^{-3} (\text{mg} / \text{s} \cdot \text{min})$, $a_4 = 9 \times 10^{-3} (\text{mg} \cdot \text{m}^3 / (\text{min} \cdot \text{kg}))$, $a_5 = 5.59 (\text{mg} / \text{min})$, $a_6 = -13.32 (\text{mg} / \text{min})$, and $a_7 = 2.75 (\text{mg} / \text{min})$.

Therefore, the obtained form of the coke deposition model after substituting the constant coefficients is as follows (Eq. 7.11).

$$C = 9 \times 10^{-3} T + 2.2 \times 10^{-2} P - 9 \times 10^{-3} \rho + 9 \times 10^{-3} t + 5.59 C_2^= - 13.3 C_3^= + 2.75 A \quad \text{Eq. (7.11)}$$

Table 7.5: Fuels and parameters used in developing coke model

Fuel	T (°C)	P (bar)	D (kg/m ³)	t (s)	C ₂ ⁼ (y _i)	C ₃ ⁼ (y _i)	A (y _i)	Coke (mg/min)	Reference
n-dodecane	675	37	750	14.4	0.173	0.100	0.013	0.33	Jiang et al. (2011)
n-dodecane	670	40	750	40.3	0.164	0.093	0.011	0.60	Liu et al. (2009)
n-dodecane	648	40	750	40.9	0.133	0.085	0.010	0.41	Liu et al. (2009)
RP-3	651	40	796	40.9	0.050	0.039	0.071	0.24	Liu et al. (2009)
RP-3	662	40	796	40.5	0.069	0.060	0.121	0.34	Liu et al. (2009)
n-heptane	600	55	678	2.10	0.020	0.013	0.006	0.67	Konda et al. (2022)
n-heptane	550	55	678	2.20	0.018	0.010	0.004	0.42	Konda et al. (2022)
MCH	700	55	761	2.10	0.017	0.010	0.004	1.15	Konda et al. (2022)
HCF-1	680	55	800	1.40	0.12	0.07	0.11	0.62	Vuchuru et al. (2002)
EHF-1	710	35	791	1.10	0.18	0.05	0.12	1.13	Li et al. (2018)

7.3.3.1. Validation of coke model

To validate the developed coke model, a Pareto plot of the experimentally obtained coke deposition rate ($C_{\text{expt.}}$) from literature data and the model-predicted coke deposition rate ($C_{\text{pred.}}$) is plotted as shown in Fig. 7.12a. The plot shows that the model-predicted coke deposition rates are in good agreement with the experimentally measured coke deposition rates (the R^2 value of linear fitting is 0.94). The developed Coke model was also validated with literature results which are not considered for estimating the values of the constant coefficient of the model parameters in the present work. The model was further tested for the present experimental results for n-heptane. It is noted that the predicted value of coke deposition rates lies within $\pm 25\%$ of the experimental rates. Though we have included the density parameter in the present model, the influence of cycloparaffin and aromatic content in a feed on coking rate cannot be ignored. Previous studies show that the coking rate of aromatic hydrocarbon is relatively higher than a paraffinic compound for a similar value of fuel cracking percentage (Konda et al. (2022)). The details of the operating conditions and coke deposition values are tabulated in Table 7.6. Further, the results of the predictive coke model are compared with an Arrhenius equation-based coke model (Eq. 7.12), as reported by Tian et al. (2023) and Liu et al. (2013). Fig. 7.12b shows a comparison of the predictive coke model (present work) and the Arrhenius equation-based Coke model for five different cases (cases 2, 3, 4, 5, and 9). The values of different parameters were obtained from the literature to estimate the coking rate using the Arrhenius equation-based coke model (Liu et al. (2013)). The plot shows that both models are reasonably good at predicting the coke deposition rate for the cracking of hydrocarbons. However, the Arrhenius equation-based coke model shows relatively larger deviation for the RP-3 fuels.

$$r_c = k_{co} e^{-\frac{E_1}{RT_w}} e^{-\gamma t} C_o^n + k_{lo} e^{-\frac{E_2}{RT_w}} C_A^m \quad \text{Eq. (7.12)}$$

where, r_c is coke formation rate, k_{co} and k_{lo} , are pre-exponential factor, E_1 and E_2 are activation energy, n and m are order of coke growth reactions, C_o is olefin concentration, C_A is aromatic concentration, and γ is decay constant for catalytic coke activity.

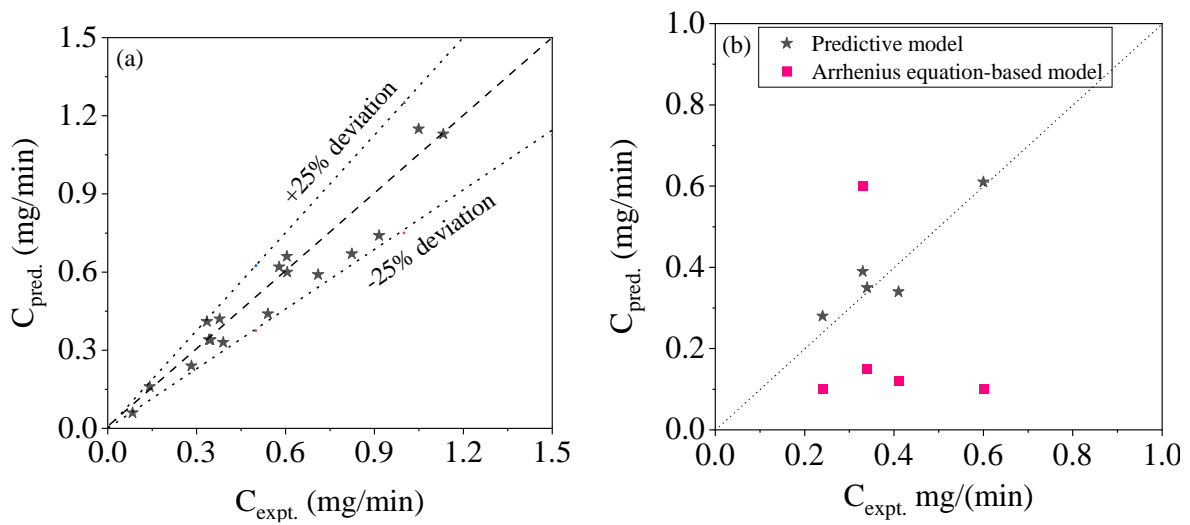


Fig. 7.12: a) Pareto plot of experimental and model predicted coking rates, b) comparison of present predictive model and Arrhenius equation-based coke model.

Table 7.6: Validation of Coke model with experimental results

Fuel	T _{exit.} (°C)	Pressure (bar)	Density (kg/m ³)	Residence time (s)	C ₂ ⁼ (y _i)	C ₃ ⁼ (y _i)	A (y _i)	C _{expt.} (mg/min)	C _{pred.} (mg/min)	References
n-dodecane	675	37	750	14.4	0.173	0.100	0.013	0.33	0.39	Jiang et al. (2011)
n-dodecane	670	40	750	40.3	0.164	0.093	0.011	0.60	0.61	Liu et al. (2009)
n-dodecane	648	40	750	40.9	0.133	0.085	0.010	0.41	0.34	Liu et al. (2009)
RP-3	651	40	796	40.9	0.050	0.039	0.071	0.24	0.28	Liu et al. (2009)
RP-3	662	40	796	40.5	0.069	0.060	0.121	0.34	0.35	Liu et al. (2009)
n-heptane	600	55	678	2.10	0.020	0.013	0.006	0.67	0.82	Konda et al. (2022)
n-heptane	550	55	678	2.20	0.018	0.010	0.004	0.42	0.38	Konda et al. (2022)
MCH	700	55	761	2.10	0.017	0.010	0.004	1.15	1.05	Konda et al. (2022)
HCF-1	680	55	800	1.40	0.120	0.070	0.110	0.62	0.58	Vuchuru et al. (2022)
EHF-1	710	35	791	1.10	0.180	0.050	0.120	1.13	1.13	Li et al. (2018)
RP-3	700	40	791	1.5	0.150	0.053	0.110	0.74	0.92	Wang et al. (2022)
n-heptane	600	41	678	9.8	0.020	0.050	0.002	0.06	0.08	Xie et al. (2008)
cyclohexane	600	42	774	9.8	0.015	0.008	0.130	0.16	0.14	Xie et al. (2008)
HCF-1	650	55	800	1.4	0.101	0.040	0.092	0.44	0.54	Vuchuru et al. (2022)
MCH	650	55	761	2.2	0.016	0.009	0.010	0.66	0.60	Konda et al. (2022)
n-heptane	600	40	678	3.6	0.122	0.043	0.000	0.34	0.42	Present work
n-heptane	650	40	678	3.5	0.150	0.058	0.006	0.59	0.71	Present work

7.4. Conclusion

Coke deposition characteristics of hydrocarbons are investigated using a flow reactor under supercritical temperature and pressure conditions. The CFD analysis was performed to understand the variations in thermophysical properties, such as density, specific heat, viscosity, and thermal conductivity of different hydrocarbon fuels. Numerical simulation was performed to generate the concentration profiles of coking precursors like light olefins and aromatics along the length of the reactor. Product species distribution from thermal cracking reaction and transport properties were estimated using the shear stress transport $k-\omega$ turbulence model. Further, a coke prediction model is developed using the simulation results of coke precursors and fuel properties under different temperature and pressure conditions. In most cases, literature-reported coke data and operating conditions are used to develop the predictive coke model. Furthermore, the predictive Coke model is validated with experimental results for different hydrocarbons and a wide range of operating conditions. It is noted that the predicted coke lies within $\pm 25\%$ of the experimental coke for a temperature range of 550 °C to 700 °C and a pressure range of 35 bar to 55 bar. Further, to verify the suitability of the developed model, thermal cracking of n-heptane was performed experimentally using a flow reactor for a temperature range of 550 to 650 °C under 40 bar pressure. It has been found that the coke deposition rate increased almost exponentially with reactor temperature. At 650 °C and 40 bar pressure, the experimental value of the coke deposition rate is about 0.6 mg/min vis-a-vis the model-predicted coking rate is 0.7 mg/min. Therefore, the developed Coke model agrees well with the experimental findings. The cracking percentage of n-heptane at 650 °C under 40 bar pressure is 26.8%. The present investigation would be useful in obtaining a quick estimation of the coking rate for the thermal cracking of hydrocarbon fuels under supercritical conditions.

The outcome of Chapter 7 bridges the following objective mentioned in Chapter 1.

- Understanding the influence of coke precursors and operating conditions on coke deposition rate.

Chapter-8
Summary and Conclusions of Present Research

Summary and Conclusions of Present Research

8.1. Summary and Conclusions

Supersonic vehicles above Mach-3 speeds encompass heavy thermal loads on their engine structure due to the exothermic combustion of onboard fuel. The magnitude of heat loads can't be compensated by the sensible heat of the fuel alone. Fuel needs to undergo endothermic cracking reactions in order to meet the cooling requirements. In the present work, the thermal cracking characteristics of hydrocarbon fuels were investigated to examine various aspects, such as cracking percentage, heat sink possibility, and coke deposition rate, of the fuels under supercritical conditions. In this regard, the selection of an appropriate test setup and operating parameters to perform laboratory experiments that closely resemble an actual scenario is challenging. The selection of methodology/techniques in calculating cracking parameters like cracking percentage, coke deposition rate, and heat sinks, is the other crucial aspect of this research. Though a good number of investigations have been reported by researchers on the cracking behavior of various fuels, the primary emphasis was on improving the fuel conversion and heat sinks. The information on coke deposition and chemical heat sink aspects of hydrocarbon fuels is inadequate in the literature. As the heat sink capability of a fuel depends on many factors, like type of hydrocarbon fuel, operating temperature, pressure, space velocity, etc., the study needs careful consideration of these parameters. Based on the exhaustive literature review, as mentioned in Chapter-2 of this thesis, the major gaps have been identified and attempted to address some of them.

In the present research, an appropriate flow reactor was designed and fabricated to conduct thermal cracking experiments for a wide range of temperature and pressure conditions. The flow reactor was externally heated by a direct power source. The details of the experimental setup and procedures adopted are explained in Chapter-3. The methodology/techniques considered in analyzing cracking conversion, coking rate, heat sink, and endothermicity are also elaborated in Chapter-3 of this thesis. Firstly, we selected a few single-component hydrocarbons, namely n-heptane, methylcyclohexane, and toluene, to standardize the experimental and analysis techniques and also to examine the impact of hydrocarbon structure on the cracking behavior of hydrocarbons under supercritical conditions. After establishing standard protocols, the cracking behavior of a multi-component fuel (namely HCF-1) was investigated to find the heat sink

characteristics of the fuels. We have also examined the efficacy of homogeneous initiators on the cracking characteristics and endothermicity of hydrocarbon fuels. Further, the kinetics of the supercritical cracking reactions were examined to find the kinetic rate constant and apparent activation energy. Furthermore, a coke model was developed, and simulation studies were performed to predict the coke deposition rate. A summary of the investigation is presented below.

- The cracking of three hydrocarbons with identical carbon numbers was examined to understand the effect of molecular structure on cracking characteristics under supercritical environments. A straight-chain alkane namely n-heptane, a cycloalkane namely methylcyclohexane (MCH), and an aromatic molecule namely toluene, compounds of C₇ carbon numbers were chosen for the study. The cracking experiments were conducted at a temperature range of 500-700 °C and 55 bar pressure to determine the cracking percentage, coke deposition rate, and heat sinks of the hydrocarbons. The heat loss quantity associated with thermal cracking experiments by direct heating method is estimated to be about 8-12% of the total energy input for a particular operating condition. The loss percentage is less for lower temperatures. At a temperature of 700 °C, the cracking percentage of n-heptane, MCH, and toluene is 31%, 20%, and 2.5%. In the work, a new methodology is established for estimating the cracking percentage. The coke deposition rate was estimated considering both 'Carry away' coke and 'Reactor-containing' coke. The estimated value of the coke deposition rate of n-heptane, MCH, and toluene at 700 °C is 19.1, 12.9, and 4.5 mg/min respectively. The chemical heat sink capacity of n-heptane is 987 kJ/kg, 18% higher than the MCH at 700 °C and 55 bar pressure. The kinetic study revealed that the first-order kinetic model fit well with the experimental results and the rate constant is in the range of 0.05 - 0.6 (1/s) for n-heptane fuel, and 0.01 to 0.3 (1/s) for MCH. The apparent activation energy of the n-heptane and MCH cracking reaction is about 62 kJ/mol and 93 kJ/mol, respectively.
- A multi-component hydrocarbon fuel (namely HCF-1) of kerosene range with a boiling range of 168-220 °C is examined. The effects of reactor temperature, pressure, and space-time on fuel cracking percentage, coke deposition, heat sinks, and product distributions were studied in detail. The range of various operating parameters considered for the cracking studies are: temperature 550-680 °C, pressure 25-55 bar, and space-time 2.8 to 8.5 s. The

fuel cracking percentage, coking deposition, and heat sinks increased with an increase in reactor temperature. The estimated value of fuel cracking conversion, coke deposition, and chemical heat sink of the fuel at 680 °C and 55 bar are 10.3 wt.%, 7 mg/min, and 805 kJ/kg, respectively. A decreasing trend in the olefin-to-alkane ratio was noted with the increase in cracking temperatures and pressures. The increase of space-time from 2.8 s to 8.5 s enhanced the fuel conversion by 2.4 times, and heat sink by 1.8 times from (634 to 1144 kJ/kg) at 650 °C and 55 bar. The first-order rate constant value lies in the range of 0.01 - 0.15 (1/s), and the apparent activation energy is about 125 kJ/mol.

- The suitability of homogeneous initiators in improving the cracking characteristics of hydrocarbon fuel was investigated using a hydrocarbon fuel (namely HCF-2) of boiling range 172-219 °C. Two initiators, namely triethyl amine (TEA) and di-tert-butyl-peroxide (DTBP) were chosen to examine the efficacy of the initiators on cracking conversion and heat sink characteristics of the fuel. The experiments were carried out at a temperature of 650 °C and 55 bar pressure with a fuel flow rate of 50 mL/min. The concentration of initiators was varied between 0.1 wt.% and 1 wt.% with respect to fuel. The fuel conversion increased by 8.6% (from 8.1% to 16.7%) and 6.1% (from 8.1% to 14.2%) in the presence of 1 wt.% of TEA and DTBP, respectively. However, for the 0.5 wt.% loadings, the fuel conversion increased by 4.4% and 2.6% with TEA and DTBP, respectively. The coke deposition rate increased by about 10% and 19% with 0.5% loading of TEA and DTBP, respectively. The contribution of alkyl benzenes (C₁-C₅ alkyl benzenes) was evident in promoting the coke depositions. The chemical heat sink capacity of the fuel improved by about 7% (from 586 kJ/kg to 627kJ/kg) and 13% (from 586 kJ/kg to 664 kJ/kg) with 0.5% loading of TEA and DTBP, respectively. Between the two initiators, the nitrogen-based TEA initiator showed somewhat better performance in terms of fuel cracking percentage and coke deposition rate, and the DTBP offered better heat sink capacity. The study also revealed that, though the initiators are useful in enhancing fuel conversion and endothermicity, a higher loading of the initiators is not beneficial because of more coke deposition.
- To estimate the coke deposition rate for a thermal cracking process, a Coke predictive model was developed using numerical simulation. Different properties, such as density, specific

heat, viscosity, and thermal conductivity, of various hydrocarbon fuels were studied to understand fluid behavior. The concentration profiles of coke precursors along the length of the reactor were analyzed. The shear stress transport model (SST k- ω) was implemented to predict the wall temperatures in the analysis. The coke model was developed based on the coke precursor concentration and fuel properties at different temperatures and pressures. The developed model was validated with experimental results for various hydrocarbon fuels. The model predicted coke value showed a good agreement (< 25% deviation) with the experimental results.

A summary of fuel cracking percentage, coke deposition rate, and heat sinks of the five hydrocarbons/fuels at different operating conditions is presented in Tables 8.1, 8.2, 8.3, and 8.4 along with the physicochemical properties of the fuels.

Table 8.1: Properties of various hydrocarbon fuels

Parameter	n-heptane	MCH	Toluene	HCF-1	HCF-2
Specific gravity at 28 °C	0.67	0.76	0.86	0.79	0.795
Boiling range (°C)	95.8-96.1	98.2-98.8	108-109	168-220	172-219
Average boiling point (°C)	98.4	101	110.6	187	191
Aniline point (°C)	68 ± 1	39 ± 1	< 20	66 ± 1	68 ± 1
Critical temperature (°C)	267 ± 1	299 ± 1	318 ± 1	381.6	379 ± 0.5
Critical pressure (bar)	27.3 ± 1	34.7 ± 1	41 ± 1	23.2 ± 0.1	23 ± 0.1
Calorific value (MJ/kg)	46.9 ± 0.5	45.5 ± 0.3	41.8 ± 0.2	45.7 ± 0.2	45 ± 0.2
Paraffin (P) (vol.%)	> 99.5	-	-	54 ± 1	51.1 ± 1
Naphthenes (N) (vol.%)	-	> 99.5	-	36 ± 1	40.4 ± 1
Aromatic (A) (vol.%)	-	-	> 99.5	9.6 ± 0.5	8.3 ± 0.2

Table 8.2: Cracking percentage, heat sink, and coke deposition for various fuels

Parameter	n-heptane	MCH	Toluene	HCF-1	HCF-2
Temperature (°C)	550-650	550-650	550-650	550-680	650
Pressure (bar)	55 ± 1	55 ± 1	55 ± 1	55 ± 1	55 ± 1
Residence time (s)	0.95-1.14	0.95-1.17	0.95-1.14	0.94-1.17	0.97
Cracking percentage (wt.%)	11.4-22.8	4.4-13.5	< 1.5	1.2-10.5	8.1
Total heat sink (kJ/kg)	1527-1857	1434-1718	1387-1664	1170-1824	1632
Chemical heat sink (kJ/kg)	675-822	60-722	-	321-804	586
Coke (mg/min)	4.7-12.2	1.7-7.4	0.92-2.5	1.9-6.98	4.1

Table 8.3: Effect of pressure on conversion, coke deposition, and heat sinks

Parameter	650	650	650	650
Temperature (°C)	650	650	650	650
Pressure (bar)	25	35	45	55
Fuel conversion (wt.%)	2.6	4.2	5.8	7.6
Total heat sink (kJ/kg)	1729	1752	1780	1814
Chemical heat sink (kJ/kg)	368	418	487	634
Coke deposition (mg/min)	2	2.56	3.45	4.1

Table 8.4: Effect of initiator loading on cracking percentage, coke, and heat sinks

	HCF-2	HCF-2 + TEA			HCF-2 + DTBP		
Temperature (°C)	650	650	650	650	650	650	650
Pressure (bar)	55	55	55	55	55	55	55
Initiator loading (wt.%)	-	0.1%	0.5%	1%	0.1%	0.5%	1%
Residence time (s)	0.97	0.97	0.97	0.97	0.97	0.97	0.97
Cracking percentage (wt.%)	8.1	8.9	12.5	16.7	8.3	10.7	14.2
Total heat sink (kJ/kg)	1632	1640	1670	1706	1643	1705	1723
Chemical heat sink (kJ/kg)	586	593	627	667	596	664	689
Coke deposition (mg/min)	4.1	4.2	4.5	6.4	4.2	4.9	6.8

From the comprehensive investigation, it can be said that thermal management of hypersonic vehicles can be achieved by employing hydrocarbon fuels with about 15-30% cracking percentage. A multi-component fuel may be more desirable than a single-component fuel because of distributed cracking over a long range of fuel transfer lines. For a single-component fuel, fuel may crack within a short length of the fuel transfer line and not throughout the entire passage. The investigation revealed that the cyclic structures showed a greater degree of thermal stability than a straight-chain hydrocarbon. Kerosene range multi-component fuel (HCF-1) under a supercritical environment showed sufficient chemical heat sink capability. Though an initiator is helpful in enhancing the heat sink capability of a fuel, coke formation can be a critical issue in selecting an appropriate fuel. A suitable coke additive may be useful to decelerate the coke formation rate during the pyrolysis process. Therefore, the present research will be helpful in understanding the cracking phenomena under a supercritical environment and in identifying an appropriate fuel for hypersonic applications.

Scope for Further Studies

The thesis presents the applicability of various hydrocarbon fuels for regenerative cooling in high-speed supersonic engines. The cracking characteristics of a few hydrocarbon fuels under supercritical conditions have been examined in detail. The influence of hydrocarbon structure, operating temperature, and pressure on cracking characteristics, heat sink, and coke formation rate was examined and presented in tabular or graphical form. The influence of homogeneous initiators on fuel conversion and heat sink properties of hydrocarbon fuels are also studied in the work. Considering the impact of this applied research, we feel that in certain areas, a further and detailed investigation is required. Further investigation could be conducted in the following direction:

- Pyrolysis characteristics of kerosene/ATF-derived narrow-cut fuels need to be investigated for their suitability for futuristic high-speed aircraft.
- Kinetic modeling coupled with a coke model needs thorough investigation for the thermal cracking of hydrocarbon fuels.
- Improvement in the Coke model considering more number of fuel properties.
- Morphological studies of solid deposits/coke produced due to the cracking of hydrocarbons with various analytical techniques, like XRD, SEM, TEM, etc.
- Studies to reduce coke deposition rate with homogenous coke inhibitors.
- Influence of coke inhibitors on the ignition delay characteristics of the cracked product needs to be examined.

Bibliography

- Balster L M., Corporan E., DeWitt M J., Edwards J T., Ervin J S., Graham J L., Lee S., Pal S., Phelps D K., Rudnick L R., Santoro R J., Schobert H H., Shafer L M., Striebich R C., West Z J., Wilson G R., Woodward R., Zabarnick S, Development of an advanced, thermally stable, coal-based jet fuel. *Fuel Process. Technol.* 89, 364–378, **2008**.
- Balster L M., Zabarnick S., Striebich R C., Predicting the fouling tendency of a thermally stressed jet fuel using high performance liquid chromatography (HPLC). *Prepr. Am. Chem. Soc., Div. Pet. Chem.* 47, 161–164, **2002**.
- Bao W., Li X., Qin J., Zhou W., Yu D., Efficient utilization of heat sink of hydrocarbon fuel for regeneratively cooled scramjet, *Appl. Therm. Eng.*, 33, 208-218, **2012**.
- Bishop G J., Elvers B., Aviation Fuels, *Ullmann's Encyclopedia of Industrial Chemistry*, ACS Omega, 26741–26755 26753, **2021**.
- Bruno T J., Smith B L., Improvements in the Measurement of Distillation Curves. 2. Application to Aerospace/Aviation Fuels RP-1 and S-8, *Ind. Eng. Chem. Res.*, 45,4381-4388. **2006**.
- Burdette G W., Lander H R., McCoy J R., High-Energy Fuels for Cruise Missiles, 2, 289-292, **2012**.
- Chakraborty J P., Kunzru D., High pressure pyrolysis of n-heptane, *J. Anal. Appl. Pyrolysis*, 86, 44–52. **2009**.
- Chakraborty J.P., Kunzru D., High pressure pyrolysis of n-heptane: effect of initiators, *J. Anal. Appl. Pyrol.*, 95, 48–55, **2012**.
- Chang. J., Fujimoto. K., Tsubaki N., Effect of initiative additives on hydro-thermal cracking of heavy oils and model compound, *Energ. Fuel.*, 17, 457–461, **2003**.
- Chen G M., Zhang X W., Mi Z T., Effects of pressure on coke and formation of its precursors during catalytic cracking of toluene over USY catalyst, *J. Fuel Chem. Technol.* 35, 211-216, **2007**.
- Chen T., Zhang J., Wang L., Jiao Y., Zhang Q., Wang J., Chen Y., Li X., A study of methylcyclohexane cracking in a micro-channel reactor coated with M/SiO₂ (M=Fe, Co, Ni) catalysts under supercritical condition. *J. Anal. Appl. Pyrolysis*, 141,104642, **2019**.
- Cheng Y., Wang Y., Jiang P-X., Zhu Y., Oxidative and pyrolytic coking characteristics of supercritical-pressure n-decane and its influence mechanism on heat transfer, *Fuel*, 130874, **2024**.

- =====
- Feng X T., Zhang L., Wang F., Zhang X., Zou J., Synthesis of aluminum nanoparticles as additive to enhance ignition and combustion of high energy density fuels, *Front. Chem. Sci. Eng.*, 12, 358–366, **2018**.
- Feng Y., Zhang H., Zhang D., Chen F., Xinhai X., Qin J., Jiao Y., The mechanism of ethanol blending on the variation of chemical heat sink in n-decane thermal cracking process, *Fuel*, 129204, **2023**.
- Fortin T.J., Bruno T.J., Assessment of the thermophysical properties of thermally stressed RP-1 and RP-2, *Energ. Fuel*, 27, 2506–2514, **2013**.
- Gao, M., Hou, L., Zhang, X., Zhang, D., Coke deposition inhibition for endothermic hydrocarbon fuels in a reforming catalyst coated reactor. *Energ. Fuels*, 33, 6126–6133, **2019**.
- Gascoin N., Abraham G., Gillard P., Synthetic and jet fuels pyrolysis for cooling and combustion applications, *J. Anal. Appl. Pyrolysis* 89, 294–306, **2010**.
- Gascoin N., Gillard P., Bernard S., Bouchez M., Characterization of coking activity during supercritical hydrocarbon pyrolysis. *Fuel Process. Technol.*, 89, 1416–1428, **2008**.
- Goel P., Boehman A L., Numerical simulation of jet fuel degradation in flow reactors. *Energ. Fuels*, 14, 953–962, **2000**.
- Gong T., Hui L., Zhang J., Sun D., Qin L., Du Y., Li C., Lu J., Hu S., Feng H., Atomic layer deposition of alumina passivation layers in high-aspect-ratio tubular reactors for coke suppression during thermal cracking of hydrocarbon fuels. *Ind. Eng. Chem. Res.*, 54, 3746–3753, **2015**.
- Guan Y., Lou J., Liu R., Ma H., Song J., Jirong Song Reactive molecular dynamics simulation on thermal decomposition of n-heptane and methylcyclohexane initiated by nitroethane, *Fuel*, 162, 116447, **2020**.
- Haowei, L., Jiang, Q., Yuguang, J., Weixing, Z., Wen, B., Hongyan, H. Experimental study on the thermodynamic characteristics of the high temperature hydrocarbon fuel in the cooling channel of the hypersonic vehicle. *Acta Astronautica*, 155, 63–79, **2019**.
- Heinrich B., Luc Bouhali A., Ser F., Vigot C., Endothermic liquid fuels-some chemical considerations on the cooling process. *Proceeding of the 10th AIAA/NAL–NASDA–ISAS*, **2001**.
- Hou L Y., Dong N., Sun D P., Heat transfer and thermal cracking behavior of hydrocarbon fuel, *Fuel*, 103, 1132-1137, **2013**.

- =====
- Hou L.Y., Dong N., Ren Z.Y., Zhang B., Hu S.L., Cooling and coke deposition of hydrocarbon fuel with catalytic steam reforming, *Fuel Process. Technol.*, 128, 128-133, **2014**.
<https://www.grc.nasa.gov/WWW/K-12/airplane/rampart.html>
<https://www.isro.gov.in/ScramjetEngineTechnology.html>
- Huang B., Shrestha U., Davis R J., Chelliah H K., Endothermic pyrolysis of JP-10 with and without zeolite catalyst for hypersonic applications, *AIAA*, 56, 1616–1626, **2018**.
- Huang H., Sobel D., Spadaccini L J., Endothermic heat-sink of hydrocarbon fuels for scramjet cooling. *Proceedings of the 38th AIAA/ ASME/SAE/ASEE*, **2002**.
- Huang H., Spadaccini L J., Sobel D R., Fuel-cooled thermal management for advanced aeroengines. *J. Eng. Gas Turbines Power* 126, 284–293, **2004**.
- Huang H., Spadaccini L.J., Coke removal in fuel-cooled thermal management systems, *Ind. Eng. Chem. Res.*, 44, 267–278, **2005**.
- Huber M L., Lemmon E W., Bruno T J., Effect of RP-1 compositional variability on thermophysical properties, *Energ. Fuels*, 23, 5550–5555, **2009**.
- Jackson T.A., Eklund D.R., Fink A.J., High speed propulsion: performance advantage of advanced materials, *J. Mater. Sci.*, 39, 5905–5913, **2004**.
- Jia Z., Wang Z., Cheng Z., Zhou W., Experimental and modeling study on pyrolysis of n-decane initiated by nitromethane. *Combust. Flame*, 165, 246–258, **2016**.
- Jia Z., Zhou W., Yu W., Han Z., Experimental investigation on pyrolysis of n-decane initiated by nitropropane under supercritical pressure in a miniature tube, *Energ. Fuel*, 33 5529-5537, **2019**.
- Jian Y., Semih E., Thermal decomposition of c10–c14 normal alkanes in near-critical and supercritical regions: product distributions and reaction mechanisms, *Ind. Eng. Chem. Res.*, 36, 574-584, **1997**.
- Jiang P. X., Wang Y., Zhu Y., Differential global reaction model with variable stoichiometric coefficients for thermal cracking of n-decane at supercritical pressures, *Energ. Fuel*, 33 7244-7256, **2019**.
- Jiang R., Liu G., Guozhu X., He C., Yang L., Wang X., Zhang Z., Supercritical thermal decompositions of normal–and iso–dodecane in tubular reactor, *J. Anal. Appl. Pyrolysis*, 92, 292–306, **2011**.
- Jiang R., Liu G., Zhang X., Thermal cracking of hydrocarbon aviation fuels in regenerative cooling microchannels. *Energ. Fuels*, 27, 2563–2577, **2013**.

-
- Jiao S., Li S., Pu H., Dong M., Shang Y., Experimental investigation on thermal cracking and convective heat transfer characteristics of aviation kerosene RP-3 in a vertical tube under supercritical pressures, *Int. J. Therm. Sci.*, 146, 106092, **2019**.
- Jiao Y., Zhang H., Li S.S., Guo C., Yao P., Wang J., Impact of acidity in ZrO₂-TiO₂-Al₂O₃ composite oxides on the catalytic activity and coking behaviours during n-decane cracking, *Fuel*, 233, 724–731, **2018**.
- Jin B., Jing K., Liu J., Zhang X., Liu G., Pyrolysis and coking of endothermic hydrocarbon fuel in regenerative cooling channel under different pressures, *J. Anal. Appl. Pyrolysis*, 125, 117–126, **2017**.
- Keke X., Hua M., Model validation and parametric study of fluid flows and heat transfer of aviation kerosene with endothermic pyrolysis at supercritical pressure, *Propuls. Power Res.*, 4, 202-211, **2015**.
- Keke X., Hua M., Modeling and simulation of supercritical-pressure turbulent heat transfer of aviation kerosene with detailed pyrolytic chemical reactions, *Energ. Fuel*, 29, 4137-4149, **2015**.
- Kim S., Sasmaz E., Pogaku R., Lauterbach J., Effects of reaction conditions and organic sulfur compounds on coke formation and HZSM-5 catalyst performance during jet propellant fuel (JP-8) cracking, *Fuel*, 259, 116240, **2020**.
- Konda S., Dinda S., Regenerative cooling capacity of hydrogenated carene under supercritical environment, *Int. J. Energy Research*, 46, 18256-18268, **2022**.
- Lander H., Endothermic fuels for hypersonic vehicles, *J. Aircraft*, 8, 4, **2012**.
- Lei Y., Guangqian Li., Guijin He., Yongsheng G., Li X., Wenjun F., Impacts of hydrogen to carbon ratio (H/C) on fundamental properties and supercritical cracking performance of hydrocarbon fuels, *Chem. Eng. J.*, 283, 1216-1223, **2016**.
- Li G., Hou B., Wang A., Xin X., Cong Y., Wang X., Li N., Zhang T., Making JP-10 super fuel affordable with a lignocellulosic platform compound. *Angew. Chem. Int. Ed.* 131, 12282–12286, **2019**.
- Li H., Wang Y, Wang L, Zhang X, Liu G, Pyrolysis and Coke Deposition of JP-10 with Decalin in Regenerative Cooling Channels, *Energ. & Fuel.*, 6096-6108, **2022**.
- Li H., Wang X., Song Q., Yang Z., Qi W., Experimental investigation of n-Heptane unsteady-state pyrolysis coking characteristics in microchannel. *J. Anal. Appl. Pyrolysis*, 161, 105384, **2022**.
-

-
- Li H., Wu Y., Yang Z., Song Q., Zhang J., Wang X., Effect of molecular structure on pyrolysis coking performances of hydrocarbons at different temperatures. *Fuel*, 326, 125095, **2022**.
- Li X., Huai X., Cai J., Zhong F., Fan X., Guo Z., Convective heat transfer characteristics of China RP-3 aviation kerosene at supercritical pressure, *Appl. Therm. Eng.*, 31, 2360–2366, **2011**.
- Li Y., Jin B., Zhang X., Liu G., Pyrolysis and heat sink of an endothermic hydrocarbon fuel EHF-851, *J. Anal. Appl. Pyrol.*, 155, 105084, **2021**.
- Li Z., Wang H., Jing K., Wang L., Li Y., Zhang X., Liu G., Kinetics and modeling of supercritical pyrolysis of endothermic hydrocarbon fuels in regenerative cooling channels, *Chem. Eng. Sci.*, 207, 202-214, **2019**.
- Li, F., Li, Z., Jing, K., Wang, L., Zhang, X., Liu, G. Thermal cracking of endothermic hydrocarbon fuel in regenerative cooling channels with different geometric structures. *Energ. Fuels*, 32, 6524–6534, **2018**.
- Li, H., Jiang, Q., Jiang, Y., Zhang, D., Cheng, K., Bao, W., Huang, H. Experimental and theoretical investigation of power generation scheme driven by thermal cracked gaseous hydrocarbon fuel for hypersonic vehicle. *Energy Convers. Manage.*, 165, 334– 343, **2018**.
- Liang C., Wang Y., Jiang S., Zhang Q., Li X., The comprehensive study on hydrocarbon fuel pyrolysis and heat transfer characteristics, *Appl. Therm. Eng.*, 117, 652-658, **2017**.
- Lisa S O., Hadler A B., Bruno T J., Variability of the rocket propellants RP-1, RP-2, and TS-5: application of a composition and enthalpy explicit distillation curve method. *Ind. Eng. Chem. Res.* 47, 9225–9233, **2008**.
- Liu B., Zhu Q., Qin L X., Li X J., Li X Y., Tang S Y., Wang J. L., Heat-Sink Enhancement of Supercritical Methylcyclohexane Cracking over Lanthanum-Modified Beta Zeolite, *J. Propuls. Power.*, 801-809, **2016**.
- Liu G., Han Y., Wang L., Zhang X., Mi Z., Supercritical thermal cracking of n-dodecane in presence of several initiative additives: products distribution and kinetics, *Energ. Fuels*, 22, 3960–3969, **2008**.
- Liu G., Han Y., Wang Li., Zhang X., Mi Z., Solid deposits from thermal stressing of n-dodecane and chinese RP-3 jet fuel in the presence of several initiators, *Energ. Fuels*, 23, 356-365, **2009**.
- Liu G., Wang X., Zhang X., Pyrolytic depositions of hydrocarbon aviation fuels in regenerative cooling channels, *J. Anal. Appl. Pyrolysis*, 104, 384-395, **2013**.
-

- =====
- Liu Y., Gong S., Wang H., Wang L., Zhang X., Liu G., Pyrolysis of C8-C16 hydrocarbons with different molecular structures using high-pressure micro-reactor with GC-MS/FID, *J. Anal. Appl. Pyrolysis*, 149, 104864, **2020**.
- Liu Z., Bi Q., Feng J., Evaluation of heat sink capability and deposition propensity of supercritical endothermic fuels in a minichannel, *Fuel*, 158, 388-398, **2015**.
- Liu, Y., Chen, R., Liu, J., Zhang, X., Research progress of catalysts and initiators for promoting the cracking of endothermic hydrocarbon fuels. *Trans. Tianjin Univ.* 28, 199–213, **2022**.
- Lovestead T M., Bruno T J., A comparison of the hypersonic vehicle fuel JP-7 to the rocket propellants RP-1 and RP-2 with the advanced distillation curve method. *Energ. Fuels*, 23, 3637– 3644, **2009**.
- Ma, H., Xie, M., Zeng, W., Chen, B., Experimental study on combustion characteristics of Chinese RP-3 kerosene, *Chin. J. Aeronaut.* 29, 375–385, **2016**.
- Mahapatra D., Jagadeesh G., Shock tunnel studies on cowl/ ramp shock interactions in a generic scramjet inlet, *J. Aerosp. Eng.*, 222, 1183-1191, **2008**.
- Mi J., Ye D., Dai Y., Xie H., Wu D., Sun H., Guo Y., Fang W., Strategically designed macromolecules as additives for high energy-density hydrocarbon fuels, *Fuel*, 270, 117433, **2020**.
- Mohamadalizadeh A., Towfighi J., Karimzadeh R., Modeling of catalytic coke formation in thermal cracking reactors, *J. Anal. Appl. Pyrolysis*, 82 134-139, **2008**.
- Mun J., Kim N., Jeong B., Jung J., Endothermic Cracking of n-Dodecane in a Flow Reactor using Washcoated Activated Carbon on Metal Foam, *ACS Omega*, 7, 8518-8525, **2022**.
- Nalabala M., Dinda S., Supercritical pyrolysis of in-house developed endothermic fuel and estimation of coke and endothermicity, *Energ. J.*, 129993, **2024**.
- Ning W., Yu P., Jin Z., Research status of active cooling of endothermic hydrocarbon fueled scramjet engine. *J. Aerosp. Eng.* 227, 1780–1794, **2012**.
- Pan Y., Zhang H., Zhang C., Wang H., Jing K., Wang L., Zhang X., Liu G., Supercritical pyrolysis and coking of jp-10 in regenerative cooling channels. *Energ. Fuels*, 34, 1627–1638, **2020**.
- Petley D H., Jones S C., Thermal management for a Mach-5 cruise aircraft using endothermic fuel, *J. Aircr.*, 29, 384-389, **1992**.
- Puri P., Ma F., Choi J Y., Yang V., Ignition characteristics of cracked JP-7 fuel, *Combust. Flame*, 142, 454-457, **2005**.

- =====
- Qin J., Zhang S.L., Bao W., Yu W.L., Yu B., Zhou W., Yu D., Experimental study on chemical recuperation process of endothermic hydrocarbon fuel, *Fuel*, 108, 445-450, **2013**.
- Qu S.D., Liu G.Z., Meng F., Wang L., Zhang X., Catalytic cracking of supercritical n-dodecane over wall-coated HZSM-5 with different Si/Al ratios, *Energ. Fuel*, 25, 2808–2814, **2011**.
- Roohollahi G., Kazemeini M., Mohammadrezaee A., Golhoseini R., Application of a simple lumped kinetic model for the catalytic cracking reaction of n-butane over the HZSM-5 zeolite, *Procedia Eng.*, 42, 140-147, **2012**.
- Saggese C., Singh A V., Xue X., Chu C., Kholghy M R., Zhang T., Camacho J., Giaccai J., Miller J H., Thomson M J., Sung C J., Wang H. The distillation curve and sooting propensity of a typical jet fuel. *Fuel*, 235, 350–362, **2019**.
- Smith B L., Bruno T J., Composition–explicit distillation curves of aviation fuel JP–8 and a coal–based jet fuel. *Energ. Fuels*, 21, 2853–2862, **2007**.
- Smith J H., Harper J C., Jabber H., Analysis and environmental fate of air force distillate and high density fuels, Engineering & services laboratory air force engineering & services centre, Tyndall air force base, ESL-TR-81-54, **1981**.
- Sobel D.R., Spadaccini L.J., Hydrocarbon Fuel Cooling Technologies for Advance Propulssion, *J. Eng. Gas Turbines Power.*, 119, 344-351, **1997**.
- Song C., Eser S., Schobert H H., Hatcher P G., Pyrolytic degradation studies of a coal–derived and a petroleum–derived aviation jet fuel. *Energ. Fuels*, 7, 234–243. **1993**.
- Stashkiv M.S., Yanovsky L.S., Shevchenko I.V., Study of the combustion characteristics of endothermic fuel thermal decomposition products in a subsonic airflow, *J. Phys. Conf. Ser.*, 1399, 044091, **2019**.
- Sun D., Du Y., Zhang J., Jiao Y., Li Y., Wang Z., Li C., Feng H., Lu J., Effects of molecular structures on the pyrolysis and anti-coking performance of alkanes for thermal management, *Fuel*, 194, 266-273, **2017**.
- Sun D., Li C., Du Y., Kou L., Zhang J., Li Y., Wang Z., Li J., Feng H., Lu J., Effects of endothermic hydrocarbon fuel composition on the pyrolysis and anti-coking performance under supercritical conditions, *Fuel*, 239, 659-666, **2019**.
- Tang S., Wang J., Zhu Q., Chen Y., Li X., Preparation of rutile TiO₂ coating by thermal chemical vapor deposition for anticoking applications, *ACS Appl. Mater. Interfaces*, 6, 17157–17165, **2014**.

-
- Tian K., Yang P., Klemeš J. J., Ma T., Zeng M., Wang Q., Effect of pressure on regenerative cooling process of endothermic hydrocarbon fuel at severe pyrolysis conditions, *Aerosp. Sci. Technol.*, 138, 108357, **2023**.
- Tian Y., Qiu Y., Hou X., Wang L., Liu G., Catalytic cracking of JP-10 over HZSM-5 nanosheets. *Energ. Fuels*, 31, 11987–11994, **2017**.
- Tianhao Y., Chen P., Liu L., Zhou Q., Zhu J., Wang X., Investigation on the thermal cracking of n -decane under supercritical pressure by a developed online-sampling experimental method, *Pet. Chem.* 60, 39–44, **2020**.
- Venkataraman R., Eser S., Characterization of solid deposits formed from short durations of jet fuel degradation: Carbonaceous solids, *Ind. Eng. Chem. Res.*, 47, 9337–9350, **2008**.
- Vuchuru K., Konda S., Vipin K B., Dinda S., In-situ cooling capacity of a hydrocarbon fuel under supercritical conditions: Heat sink, coke deposition, and impact of initiator, *Fuel Communications*, 12 100075, **2022**.
- Wang C., Du C., Shang J., Zhu Y., Yao H., Xu M., Shan S., Han W., Du Z., Yang Z., Li D., A comprehensive review of the thermal cracking stability of endothermic hydrocarbon fuels, *J. Anal. Appl. Pyrolysis*, 169, 105867, **2023**.
- Wang F., Wei Q., Li K., Biney B.W., Liu H., Chen K., Wang Z., Guo A., Coke formation of heavy oil during thermal cracking: New insights into the effect of olefinic-bond-containing aromatics, *Fuel*, 336, 127138, **2023**.
- Wang H., Yang Z., Liu J., Li G., Zhang X., Activating ABO₃-type coating by additive for coke inhibition in supercritical thermal cracking of endothermic hydrocarbon fuel, *Fuel Process. Technol.*, 198, 106229, **2020**.
- Wang R., Zhao J., Bao Z., Thermal cracking and coke deposition characteristics of aviation kerosene RP-3 in an S-bend tube. *Fuel*, 313 122673, **2022**.
- Wang Y., Jiang P., Zhu Y. H., A novel global reaction modeling approach considering the effects of pressure on pyrolysis of n-decane at supercritical pressures, *Fuel*, 287, 119416, **2020**.
- Wang Z., Guo Y., Lin R., Effect of triethylamine on the cracking of heptane under a supercritical condition and the kinetic study on the cracking of heptane, *Energy Convers. Manage.*, 49, 2095–2099, **2008**.
- Wang Z., Lin R., Fang W., Li G., Guo Y., Qin Z., Triethylamine as an initiator for cracking of heptane. *Energ.*, 31, 2773–2790, **2006**.

-
- Wang Z., Lin R., Guo Y., Li G., Fang W., Qin Z., Tributylamine as an initiator for cracking of heptane, *Energy Convers. Manag.*, 49, 1584–1594, **2008**.
- Ward T A., Ervin J S., Zabarnick S., Shafer L., Pressure effects on flowing mildly-cracked n-decane. *J. Propuls. Power*, 21, 344–355, **2005**.
- Ward T.A., Ervin J.S., Striebich R.C., Zabarnick S., Simulations of flowing mildly cracked normal alkanes incorporating proportional product distributions. *J. Propul. Power*, 20, 394–402, **2004**.
- Wen B., Jiang Q., Zhou W., Duo Z., Daren Y., Power generation and heat sink improvement characteristics of recooling cycle for thermal cracked hydrocarbon fueled scramjet. *Sci. China Technol. Sci.*, 54, 955-963, **2011**.
- Wickham D T., Engel J R., Hitch B D., Additives to increase fuel heat sink capacity, *Proceedings of the 38th AIAA/ASME/SAE/ ASEE*, **2002**.
- Wickham D T., Engel J R., Hitch B D., Karpuk M E., Initiators for endothermic fuels, *J. Propul. Power*, 17, 1253–1257, **2001**.
- Wickham D T., Engel J R., Rooney S., Hitch B D., Additives to improve fuel heat sink capacity in air/fuel heat exchangers. *J. Propul. Power*, 24, 55–63, **2008**.
- Wilcox D C., Formulation of the $k-\omega$ Turbulence Model Revisited, *AIAA JOURNAL*, **2008**.
- Wu Z., Mao Y., Raza M., Zhu J., Feng Y., Wang S., Qian Y., Yu L., Lu X., Surrogate fuels for RP-3 kerosene formulated by emulating molecular structures, functional groups, physical and chemical properties. *Combust. Flame* 208, 388–401, **2019**.
- Wu, Y., Wang, X., Song, Q., Zhao, L., Su, H., Li, H., Zeng, X., Zhao, D., Xu, J. The effect of temperature and pressure on n-heptane thermal cracking in regenerative cooling channel. *Combust. Flame*, 194, 233–244, **2018**.
- Xian X., Liu G., Zhang X., Wang L., Mi Z., Catalytic cracking of n-dodecane over HZSM-5 zeolite under supercritical conditions: experiments and kinetics, *Chem. Eng. Sci.*, 65, 5588–5604, **2010**.
- Xiao J., Zhang J.X., Pan L., Shi C., Zhang X., Zou J.J., Photocatalytic synthesis of high-energy-density fuel: catalysts, mechanisms, and challenges, *Trans. Tianjin. Univ.*, 27, 280–294, **2021**.
- Xie W., Fang W., Li D., Xing Y., Guo Y., Lin R., Coking of model hydrocarbon fuels under supercritical condition, *Energ. Fuels*, 23, 2997–3001, **2009**.

- =====
- Xing Y., Fang W., Xie W., Guo Y., Lin R., Thermal cracking of JP-10 under pressure. *Ind. Eng. Chem. Res.*, 47, 10034–10040, **2008**.
- Xu, K., Meng, H. Model validation and parametric study of fluid flows and heat transfer of aviation kerosene with endothermic pyrolysis at supercritical pressure. *Propul. Power Res.*, 4, 202–211, **2015**.
- Yang C., Liu G., Wang X., Jiang R., Wang Li., Zhang X., Preparation and anticoking performance of mocvd alumina coatings for thermal cracking of hydrocarbon fuels under supercritical conditions, *Ind. Eng. Chem. Res.*, 51, 1256-1263, **2012**.
- Ye D., Mi J., Bai S., Zhang L., Guo Y., Fang W, Thermal cracking of jet propellant-10 with the addition of a core-shell macroinitiator, *Fuel*, 254, 115667, **2019**.
- Yeh Y H., Tsai C E., Wang C., Gorte R J., Heat-flow measurements for n-hexane reactions on H-ZSM-5 and H(Zn)-ZSM5: Implications for endothermic reforming in hypersonic aircraft, *Ind. Eng. Chem. Res.*, 56, 6198–6203, **2017**.
- Yeh Y H., Yu J., Luo J., Gorte R J., Endothermic reforming of n-hexane on metal (Pt, Ga) containing HZSM-5 at high pressures, *Ind. Eng. Chem. Res.*, 54, 10675–10683. **2015**.
- Yu J., Eser S., Determination of critical properties (Tc, Pc) of some jet fuels, *Ind. Eng. Chem. Res.*, 34, 404-409, **1995**.
- Yue L., Lu X.X., Chi H., Guo Y., Li Xu., Fang W., Yu Li., Hu S., Heat-sink enhancement of decalin and aviation kerosene prepared as nanofluids with palladium nanoparticles. *Fuel*, 121, 149–156, **2014**.
- Yue L., Wu J., Gong Y., Hou J., Xiong L., Xiao C., Fang W., Heat transfer and cracking performance of endothermic hydrocarbon fuel when it cools a high temperature channel, *Fuel Process. Technol.* 149, 112-120, **2016**.
- Zhang B., Lin R S., Wang B C., Xian C J L., Study of cracking catalysts of mixed zeolites modified by Ag and La to endothermic hydrocarbon fuels, *Acta Chim. Sin.*, 60, 1754–1759, **2002**.
- Zhang D., Hou L., Gao M., Zhang X., Experiment and Modeling on Thermal Cracking of n-Dodecane at Supercritical Pressure, *Energy Fuel*, 32, 12426–12434, **2018**.
- Zhang D., Hou L., Liu J., Gao M., Surrogate models of thermally cracked hydrocarbon fuels at typical pyrolysis temperatures, *Fuel*, 293, 120393, **2021**.

- =====
- Zhang L.K, Qu S.D., Wang L., Zhang X., Liu G., Preparation and performance of hierarchical HZSM-5 coatings on stainless-steel microchannels for catalytic cracking of hydrocarbons, *Catal. Today*, 216, 64–70, **2013**.
- Zhang T., Chen Y., Liu P., Zhou L., Zhu Q., Wang J., Li X., Investigation on the thermal cracking of n-decane under supercritical pressure by a developed online-sampling experimental method, *Pet. Chem.*, 60, 39-44, **2020**.
- Zhong F., Fan X., Yu G., Li J., Heat transfer of aviation kerosene at supercritical conditions, *J. Thermophys. Heat Transf.*, 23, 543-550, **2009**.
- Zhong F., Fan X., Yu G., Li J., Thermal cracking and heat sink capacity of aviation kerosene under supercritical conditions, *J. Thermophys. Heat Transf.*, 25, 3, **2011**.
- Zhou H., Gao X.K., Liu P.H., Q. Zhu., J.L. Wang., X.Y. Li., Energy absorption and reaction mechanism for thermal pyrolysis of n-decane under supercritical pressure, *Appl. Therm. Eng.*, 112, 403–412, **2017**.
- Zhou W., Jia Z., Qin J., Bao W., Yu B., Experimental study on effect of pressure on heat sink of n-decane, *Chem. Eng. J.*, 243, 127–136, **2014**.
- Zhou, H., Gao, X., Liu, P., Zhu, Q., Wang, J., Li, X., An experimental and simulated investigation on pyrolysis of blended cyclohexane and benzene under supercritical Pressure. *Pet. Chem.*, 57, 71–78, **2017**.
- Zhou, W., Bao, W., Qin, J., Qu, Y. Deterioration in heat transfer of endothermal hydrocarbon fuel. *J. Therm. Sci.*, 20, 173–180, **2011**.
- Zhu Y., Liu B., Jiang P., Experimental and numerical investigations on n-decane thermal cracking at supercritical pressures in a vertical tube, *Energ. Fuel*, 28, 466–474, **2014**.
- Zhu Y., Yu C., Li Z., Mi Z., Zhang X., Formation of coke in thermal cracking of jet fuel under supercritical conditions, *Front. Chem. Eng.*, 2, 17–21, **2008**.
- Zuo J., Zhang S., Qin J., Bao W., Cui N., Liu X., Effects of cracking reaction on supersonic film cooling using gaseous hydrocarbon fuel as coolant, *Appl. Therm. Eng.*, 171, 115134, **2020**.

Biography of Student and Supervisor

Biography of Student:

Mr. Vuchuru Kalyan completed B.Tech. in Chemical Engineering from Sri Venkateshwara University, Tirupati, India in 2009, and M.Tech. in Chemical Engineering from Osmania University, Hyderabad, India in 2012. After his post-graduation, he worked as Lecturer in the DVR College of engineering and technology (June 2012 - June 2013), Anurag University (July 2013 - August 2016), and Bule Hora University, Ethiopia (October 2016 - July 2018). He registered in Doctor of Philosophy (Ph.D.) program in Chemical Engineering Department at BITS Pilani-Hyderabad Campus in August 2018. Mr. Kalyan has published his works in reputed journals, such as the Journal of Analytical and Applied Pyrolysis, Fuel Communications, and The Journal of Supercritical Fluids.

Biography of Supervisor:

Dr. Srikanta Dinda is working as a Professor in Chemical Engineering Department at BITS Pilani-Hyderabad Campus. He joined the department as an assistant professor in July 2011. Prior to joining BITS Pilani, he worked at Reliance Jamnagar Refinery from September 2007 to July 2011. He completed his Doctor of Philosophy (Ph.D.) degree in Chemical Engineering from IIT-Kharagpur in 2008. He completed his B.Tech. and M.Tech. from the University of Calcutta, in 2001 and 2003, respectively. Prof. Dinda also finished his Bachelor of Science (B.Sc.) degree in Chemistry (Hons) from Vidyasagar University in 1998. His research activities include studies on heterogeneous kinetics, development of refining catalysts, synthetic resins, biomaterials from non-edible plant oils, and CO₂ capture, endothermic fuel development which resulted in more than 65 publications in peer-reviewed journals and 57 presentations/proceedings in national and international conferences. He has received ten patents in the area of the catalytic cracking process. He has completed a few research projects funded by DST-SERB, CSIR, BITS Pilani, and DRDO, and currently working on three ongoing projects funded by DBT, DRDO, and DST-SERB. He has supervised three Ph.D. students and currently supervising four Ph.D. students.
